

PEOPLE'S DEMOCRATIC REPUBLIC OF ALGERIA
MINISTRY OF HIGHER EDUCATION AND SCIENTIFIC RESEARCH



IBN KHALDOUN UNIVERSITY OF TIARET
FACULTY OF APPLIED SCIENCES
ELECTRICAL ENGINEERING DEPARTMENT



THESIS

Presented by:

BOURADI Sarah

Thesis submitted in fulfillment of the requirements for:

Degree of DOCTORATE (L.M.D) in Electrical Control

THEME

**Intelligent Control of New Static Converter
Structures for Vehicular Applications**

Presented on

under board of examiners composed of:

Pr. ALLAOUI Tayeb	University of Tiaret	President
Dr. BERKANI Abderrahmane	University of Tiaret	Examiner
Dr. LARIBI Souad	University of Tiaret	Examiner
Pr. NEGADI Karim	University of Tiaret	Supervisor
Pr. TALEB Rachid	University of Chlef	Examiner
Pr. GUETTAF Yacine	University of El Bayadh	Examiner

2022/2023

Declaration of Authorship

I, Sarah BOURADI, declare that this thesis titled, "Intelligent Control of New Static Converter Structures for Vehicular Applications" and the work presented in it are my own. I confirm that:

- This work was done wholly or mainly while in candidature for a research degree at this University.
- Where any part of this thesis has previously been submitted for a degree or any other qualification at this University or any other institution, this has been clearly stated.
- Where I have consulted the published work of others, this is always clearly attributed.
- Where I have quoted from the work of others, the source is always given. With the exception of such quotations, this thesis is entirely my own work.
- I have acknowledged all main sources of help.
- Where the thesis is based on work done by myself jointly with others, I have made clear exactly what was done by others and what I have contributed myself.

Signed:

Date:

"It is not knowledge, but the act of learning, not possession but the act of getting there, which grants the greatest enjoyment."

Carl Friedrich Gauss

Acknowledgements

First of all, I thank *ALLAH* the Almighty for giving me courage, patience and health during all these years of study. I would like, first of all, to express my gratitude and my sincere thanks to *Mr. NEGADI Karim* Professor at the University of Tiaret for having supervised and followed this work. His precious advice, his scientific rigor and his criticisms have greatly contributed to the realization of this work. I express my sincere thanks to *Mr. ALLAOUI Tayeb* professor at the University of Tiaret for having done me the honor of chairing the jury. I also address my best feelings of gratitude to the honorable members of the Jury who did me the honor to accept to examine and to evaluate this work; starting with *Mr. BERKANI Abderrahmane*, lecturer at the University of Tiaret, *Mr. TALEB Rachid* professor at the University of Chlef, *Mr. GUETTAF Yacine* professor at the University of El Bayadh and *Mrs. LARIBI Souad* lecturer at the University of Tiaret. Finally, my thanks go to all those who helped me in any way to achieve this work.

Contents

Declaration of Authorship	ii
Acknowledgements	iv
General Introduction	1
1 State of Art of Electric Vehicles	9
1.1 Overview	9
1.2 Definition of an electric vehicle	10
1.3 Types of electric vehicles	11
1.3.1 Battery Electric Vehicle (BEV)	12
1.3.2 Hybrid Electric Vehicle (HEV)	12
1.3.3 Plug-In Hybrid Electric Vehicle (PHEV)	13
1.3.4 Fuel Cell Electric Vehicle (FCEV)	13
1.4 Technical components of electric vehicles	14
1.4.1 Electric engines	14
1.4.2 Energy Sources and Energy Storage Systems	16
Energy Storage Devices	16
Energy Generation systems	22
1.4.3 Power Converters	24
DC-AC converters	24
DC-DC converters	27
1.4.4 Gear Box	33
1.4.5 Glider	34
1.4.6 Charging of the Electric Vehicle	35
AC Charging	35
DC Charging	35
Wireless charging	36
1.5 Barriers of EV adoption	37
1.5.1 Technical barriers	37
Range anxiety	37
Long charging period	37
Safety concerns	38
1.5.2 Social barriers	38
Social acceptance	38
1.5.3 Economic barriers	38
1.5.4 Infrastructure barriers	38

Charging stations	38
1.5.5 Policy barriers	39
2 Mathematical Modeling of the Traction System Components	40
2.1 DESCRIPTION OF THE TRACTION SYSTEM OF THE ELECTRIC VEHICLE	40
2.2 DYNAMIC MODELING OF THE EV	41
2.2.1 Rolling Resistance Force	41
2.2.2 Aerodynamic Drag	42
2.2.3 Slope resistance force	42
2.2.4 Stokes or viscous friction force	42
2.3 ENERGY SOURCES AND ENERGY STORAGE SYSTEMS MODEL	43
2.3.1 Fuel Cell Modeling	43
2.3.2 Battery Modelling and Control	46
2.3.3 Supercapacitor Modeling and Control	48
2.4 ELECTRIC ENGINES MODELING	48
2.4.1 Permanent Magnet DC Motor (PMDC) Modeling	48
2.4.2 Permanent Magnet Synchronous Motor Modeling (PMSM)	49
Simplifying hypotheses	49
PMSM equations in the reference frame (a, b, c)	50
2.5 POWER CONVERTERS MODELING	54
2.5.1 DC-DC Boost Converter Modeling	54
2.5.2 Bidirectional DC-DC Buck Boost Converter Modeling	57
2.5.3 Modeling of the Two-Level Voltage Inverter	57
Pulse Width Modulation (PWM) control	59
2.5.4 Description and Modeling of the Z-Source Inverter	60
Operating modes	63
2.6 POWER MANAGEMENT	64
3 Control of the Four-quadrant DC-DC converter	71
3.1 FOUR-QUADRANT DC-DC CONVERTER	71
3.1.1 General description	71
3.1.2 Operation and modeling of the 4-Q DC-DC converter	72
3.2 PWM CONTROL OF THE FOUR-QUADRANT DC-DC CHOPPER	75
3.3 PI CONTROL of the 4-Q DRIVING a DC-DC CONVERTER	76
3.4 GENETIC ALGORITHMS based OPTIMIZED PI CONTROL of the 4-Q CHOPPER DRIVING a PMDC MOTOR	79
3.4.1 Optimization problem (generality)	79
Continuous versus discrete optimization problems	79
Constrained and unconstrained optimization problems	79
Single-objective or multi-objective optimization problems	79
Deterministic and stochastic optimization problems	79
3.4.2 Heuristic methods	80
3.4.3 Metaheuristic methods	80
3.4.4 Classification of Metaheuristics	81
3.4.5 Genetic Algorithm	81
Operating principle of genetic algorithms	82
Detailed description of genetic algorithms	84
Advantages and disadvantages of genetic algorithms	87
3.4.6 Optimization criteria for a PID controller	87
3.5 SIMULATION RESULTS AND DISCUSSIONS	88

4	Experimental design of a four-quadrant chopper for vehicular applications	94
4.1	Main Diagram	94
4.2	Synoptic Diagram	94
4.3	CONTROL BLOCK	95
4.3.1	Arduino Board	95
	Why Arduino Uno?	95
	Constitution of the Arduino Uno board	97
4.3.2	Programming Framework	98
	Arduino software	98
	Program download steps	98
	Code injection	99
4.3.3	Galvanic isolation	99
	Isolation principle	99
	4N25 integrated circuit	99
4.3.4	MOSFET Driver	100
4.4	POWER BLOCK	101
4.4.1	Static Solid State Switch	101
4.4.2	Other Accessories	101
4.5	PRACTICAL IMPLEMENTATION OF THE TEST BENCH	102
4.5.1	Speed Sensor Output Conditioning	102
4.5.2	Software Implementation	102
4.5.3	Global experimental bench	103
	Detailed test bench	104
	Experimental results	104
	General conclusion and perspectives	114
A	Appendix A	119
B	Appendix B	120
C	Appendix C	121
D	Appendix D	122
	Bibliography	123

List of Figures

1	La jamais contente (English: The Never Contented)	2
2	The Tesla Roadster	2
3	Annual oil price from 1960 to 2020	3
4	Oil production in Algeria from 1998 to 2021. (in a 1000 barrel per day)	4
5	Total CO2 emissions in year 2019. (CO2 equivalent kiloton kt)	4
6	CO2 emissions in Algeria from 1959 to 2019.	5
1.1	Publication on electric vehicles extracted from SCOPUS	10
1.2	An electric vehicle	11
1.3	Types of electric vehicles	12
1.4	Lithium-Ion battery of the Nissan electric car	17
1.5	Supercapacitor	20
1.6	Flywheel	20
1.7	Hydraulic accumulator	21
1.8	Hydrogen fuel cell	22
1.9	Photovoltaic systems	24
1.10	Voltage source inverter	26
1.11	Current source inverter	27
1.12	Impedance source inverter	27
1.13	Inverters types	28
1.14	(a) Buck converter. (b) Boost converter. (c) Buck–boost converter. (d) Cuk converter. (e) SEPIC converter. (f) Zeta converter	30
1.15	Non-isolated bidirectional DC-DC converter topologies	31
1.16	Flyback converter	31
1.17	Forward converter	32
1.18	Half bridge bidirectional DC-DC converter	32
1.19	Full bridge converter	33
1.20	Four-quadrant DC-DC converter	33
1.21	Gear box	34
2.1	EV components	41
2.2	Elementary forces applied on an electric vehicle	42
2.3	Fuel cell characteristics	46
2.4	Battery model	46
2.5	Battery control	47
2.6	Supercapacitor electrical model	48
2.7	Schematic of PMDC motor	49

2.8	Bloc diagram of the PMDC motor	49
2.9	PMSM Graphical representation	50
2.10	Graphical representation of Park transformation	52
2.11	Boost converter scheme	55
2.12	Boost circuit when the MOSFET is closed	55
2.13	Boost circuit when the MOSFET is open	56
2.14	DC-DC Buck-Boost model	57
2.15	Buck-Boost model in two transfer directions (a) From v_{bat} to v_{dc} (forward mode), (b) From v_{dc} to v_{bat} (reverse mode)	58
2.16	Schematic of the two-level voltage inverter	58
2.17	Principle diagram of the PWM	60
2.18	PWM technique	60
2.19	Equivalent circuit of the impedance network	61
2.20	The difference between a traditional carrier-based PWM and a ST PWM	62
2.21	Operating modes of the Z-source inverter	63
2.22	The different modes of energy flow	65
2.23	The flowchart of the energy management controller	66
2.24	The acceleration pedal positions	66
2.25	The DC bus voltage	67
2.26	The fuel cell voltage	67
2.27	The Fuel cell current	67
2.28	The battery voltage	68
2.29	The battery current	68
2.30	The State of charge of the battery	68
2.31	The Electromagnetic torque response	69
2.32	The stator current in d-q coordinates	69
2.33	The stator current of the PMSM	69
2.34	The motor speed responses	70
2.35	The motor power response	70
2.36	The power management under different driving modes	70
3.1	Four-quadrant DC-DC chopper model	71
3.2	Schematic diagram show the switching type of triggering in all quadrants. (a) First quadrant (b) Second quadrant (c) Third quadrant (d) Fourth quadrant.	75
3.3	PWM control applied on the 4-Q chopper.	77
3.4	PID controller scheme	78
3.5	PI Controller with the PMDC motor	78
3.6	General principle of Metaheuristics	81
3.7	Classification of metaheuristics	82
3.8	Schematic of the Genetic Algorithm principle.	83
3.9	Structure of a canonical genetic algorithm [102].	83
3.10	Crossing at a breakpoint	86
3.11	Crossing at two breakpoints	86
3.12	Example of a mutation in a binary string	86
3.13	Global diagram of the simulation of a 4Q chopper driving a PMDC motor	88
3.14	Block diagram of a four-quadrant chopper simulation	89
3.15	Control signal for the 4-Q chopper	89
3.16	Battery voltage responses to the reference variation	90
3.17	Armature current responses	90
3.18	Electrical torque responses to load variations	90
3.19	Field current of the PMDC motor	91

3.20	Four-quadrant control signals with genetic algorithms	91
3.21	Battery Voltage in case of optimization with GA	92
3.22	Armature current of the DC motor	92
3.23	Electrical torque responses to the reference variations	92
3.24	Field current of the PMDC motor	93
3.25	Comparison of the speed responses to the references in case of PI control and GA based optimized PI control	93
4.1	The drive train of an electric vehicle	95
4.2	Synoptic scheme of the studied system	95
4.3	Control Block of the four-quadrant chopper	96
4.4	Arduino UNO board	96
4.5	Constituents of the Arduino Uno board	97
4.6	Communication with Arduino	98
4.7	The internal structure of an opto-coupler	99
4.8	Mounting of optocoupler under ISIS Proteus	100
4.9	Driver implementation on Proteus software	101
4.10	MOSFET Transistor IRFP460	101
4.11	Speed sensor conditioning and calibration circuit	103
4.12	Conditioning scale	103
4.13	System tested on Proteus	104
4.14	Control of the switches in forward motoring movement	104
4.15	Control of the switches in backward motoring movement	104
4.16	Output signals of the Arduino in forward motoring movement for duty cycle=0.8	105
4.17	Output signals of the Arduino in backward motoring movement for duty cycle=0.8	105
4.18	Output signals of the Arduino in forward motoring movement for duty cycle=0.15	105
4.19	Output signals of the Arduino in backward motoring movement for duty cycle=0.15	106
4.20	Output signals of the Arduino in forward motoring movement for duty cycle=0.5	106
4.21	Output signals of the Arduino in backward motoring movement for duty cycle=0.5	106
4.22	Output signals of the driver IR2112 in forward motoring movement (S1 and S2)	107
4.23	Output signals of the driver IR2112 in backward motoring movement (S2 and S3)	107
4.24	Motor speed response to a reference equivalent to 50rpm	107
4.25	Motor speed response to a reference equivalent to 100rpm	108
4.26	Experimental test bench	108
4.27	Experimental test bench	109
4.28	Motor speed response and DC voltage response. $v_{bat} = 7V$ (without regulation).	109
4.29	Motor speed response and DC voltage response in case of energy recovery.	110
4.30	Speed response in case of backwards.	110
4.31	DC voltage regulation response with electric braking applied	111
4.32	Performance tracking of motor speed regulation response for benchmark referenced	111
4.33	Speed response in the case of applied torque	112
4.34	Speed response and DC voltage regulation with the DC-DC buck-Boost converter	112
4.35	PMDC motor speed variation with sudden changes in the reference speed	113
4.36	Motor speed regulation and voltage responses.	113

List of Tables

1.1	Market share of EVs	11
1.2	Typical electric vehicles and their main characteristics	14
1.3	Types of electric engines used in EVS	16
1.4	Commonly used battery types	18
1.5	Overview of battery costs at pack level for different BEVs	18
1.6	Overview on the existing EVs in the industry with their battery technology	19
1.7	Characteristics of different materials used for flywheels	21
1.8	Different Types of FCs with their characteristics	23
1.9	Types of inverters with their advantages and disadvantages	26
1.10	Cost of standard components of a glider based on reference [20]	35
1.11	Comparison of wireless charging systems	37
2.1	Switching states of three phase ZSI. (!S1, !S2 and !S3 are the complements of S1, S2 and S3 respectively)	62
3.1	4Q DC-DC converter operating modes	76
4.1	Other accessories	102
A.1	PMSM and IM parameters	119
A.2	Battery parameters	119
B.1	Parameters of the components used in the simulation	120
D.1	Parameters of the components used in the experimental part	122

To my parents, whose constant support made this possible, to my family and friends, and to everyone who contributed to my development both academically and personally

General Introduction

The introductory section of the thesis presents the background, main motives and objectives of the research. Accordingly, the scientific contributions of this study project are highlighted and the plan of the thesis is briefly detailed.

Historical Background

ALTHOUGH the global transition to electric vehicles is rapidly gaining momentum, the existing research and policies are ill-suited to the Algerian context. Nonetheless, Algerian lawmakers now dispose of the required data to make educated investments and policies in this field, which can in turn help create the necessary environment that would allow the nascent ecosystem of electric vehicle startups to thrive in the country. Historically, and on a global scale, EV development has known five major eras: the pre-electric car era (1830 - 1880), the glory days (1880–1914), the dark age (1914–1970), the renaissance (1970–2003), and the electric vehicle movement (2003–present). The first electric vehicle was introduced in the 1830s at an industrial conference by a Scottish businessman named Robert Anderson. It resembled a motorized cart powered by a battery that used crude oil. Subsequently, two model EVs were created simultaneously by the Dutch scholar Sibrandus Stratingh and the Hungarian scientist Nyos Jedlik. On the opposite side of the Atlantic, Thomas Davenport, a former farrier who later became an inventor, is credited with creating essential parts of the electric motor that gave rise to the first electric vehicle [1].

The previously mentioned vehicles consisted of prototypes with speeds of 7 mph with bulky steering and small driving range. The development of electric vehicles stagnated until the introduction of rechargeable lead acid battery in 1859 by Gaston Planté. The latter were subsequently refined by Camille Faure in 1881 and later on used together with an electric motor by William Morrison in the late 1880s to form an electric car with a maximum speed of 20 mph [1]. In 1899, a Belgian company created “La Jamais Contente”, the first electric car to exceed 100 km/h (it achieved 105 km/h). Camille Jenatton, a Belgian, drove the car, which had Michelin tires and was fashioned like a torpedo [2]. This was followed by a considerable increase in the population of electric vehicles in the onset of the 20th century, where it is estimated that one third of the vehicles on the road were electric.

The short range of electric vehicles, their poor speed, lack of power, the availability of oil, and their price which was roughly twice that of a gasoline-powered Ford all contributed to their demise in the 1920s. In the 1970s the oil prices reached a high levels and the noise and air pollution caused by internal combustion engine vehicles made car manufacturers search for other solutions such as electric vehicles.



FIGURE 1: La jamais contente (English: The Never Contented)

Thus, Victor Wouk, the hybrid vehicle's godfather, constructed the first hybrid car, the Buick Skylark from GM, in 1972. (General Motors). Roger Smith, GM's president, sponsored a research fund in 1988 to build a new electric automobile, which became the EV 1 and was built between 1996 and 1998 [2].

Even though people's interest in electric vehicles was at its lowest, vehicle manufacturers continued to invest more in electric vehicles. Among these manufacturers was Toyota, which introduced the Toyota Prius, the first series-produced hybrid vehicle in 1997. In the first year, 18,000 units were sold in Japan, and by 2006, Toyota had sold 500,000 units globally. Many manufacturers introduced hybrid electric cars between 1997 and 2000, including the Honda EV Plus, G.M. EV1, Ford Ranger truck EV, Nissan Altra EV, Chevy S-10 EV, and Toyota RAV4 EV [2].

The year 2003 was the turning point in the EV story, when two Silicon Valley engineers named Martin Eberhand and Mark Tarpinning founded Tesla motors. The start-up company announced the production of luxury sports cars that could run 198 miles on a single charge. In 2008, Elon Musk revealed that the initial product of Tesla motors would be the Tesla Roadster, which was brought to production by the CEO at the time Ze'ev Drori in 2012.



FIGURE 2: The Tesla Roadster

The favorable results achieved by Tesla motors inspired many vehicle producers to raise the bar and develop their own electric vehicles. Furthermore, Nissan launched the Nissan Leaf, Zero emission car to become the world's best-selling vehicle. In addition, Toyota and EDF started testing a new hybrid car derived from the Prius in 2010 and 2011, in preparation for future commercialization. The experimentation took place in the city of Strasbourg. This hybrid petrol car can be recharged from a domestic electrical socket, which means that for short journeys it can run exclusively on electricity, with petrol propulsion being reserved for longer journeys.

At the 2012 Geneva Motor Show, the latest hybrid car concept with PAC was exhibited. It's the Toyota FCV-R. This concept's marketing is scheduled for 2015. Manufacturers such as the Renault Zoe Corporation developed pure electric automobiles in the same year [3], [4].

Motivation

The shift to electric vehicles (EVs) for transportation is a necessity to achieve global net zero. The latter has three main axes that all attract our attention to begin this research project in the form of a doctoral thesis:

Energy conception

Every feature of civilized life was altered in the 18th century by the discovery and industrialization of oil production, particularly transportation. As we enter the twenty-first century, oil is the most financially significant natural resource since it serves as the foundation of every country's socio-economic and political system. However, there are market discussions about peak oil, which suggests that oil output in the majority of oil wells has peaked and will now await a reduction in oil supplies. Given that creating an artificial low in supply raises the demand and subsequently the price of oil [5]. Figure 3 shows the annual OPEP oil prices from year 1960 to 2020, it can be seen that oil prices kept increasing over the years which validates the before mentioned hypothesis [6].

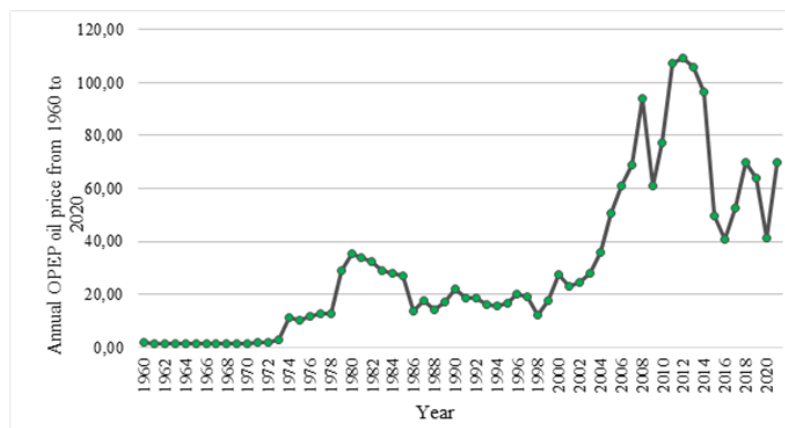


FIGURE 3: Annual oil price from 1960 to 2020

Following this, a number of analysts forecast a global oil peak in the early 21st century, which led to predictions of an oil crisis or possibly the end of the oil economy within the next 50 years. On the other hand, the expected rise in world oil demand from now until 2030 is 38%. The European Commission created an action plan in 2006 with the goal of reducing energy usage by 20% by the year 2020 [5]. In Algeria, oil production is still considered high, however it can be seen in Figure 4 that it reached its peak value around the period 2005 and 2008. Since then, the oil production started to get lower over the years [7].

In such a scenario, it is only essential that the purportedly remaining oil to be used wisely and as efficiently as possible, while also looking for alternate sources of energy

Air pollution

Over the past centuries, the global energy consumption has increased with a significant growth. The growing requirements has also led to an increase in energy related carbon dioxide emissions in the world, which is a strong cause of climate change [8]. Figure 5 illustrates the total CO₂ emissions in year 2019 showing that Algeria is one of the major contributors of CO₂ emissions causing air pollution [9].

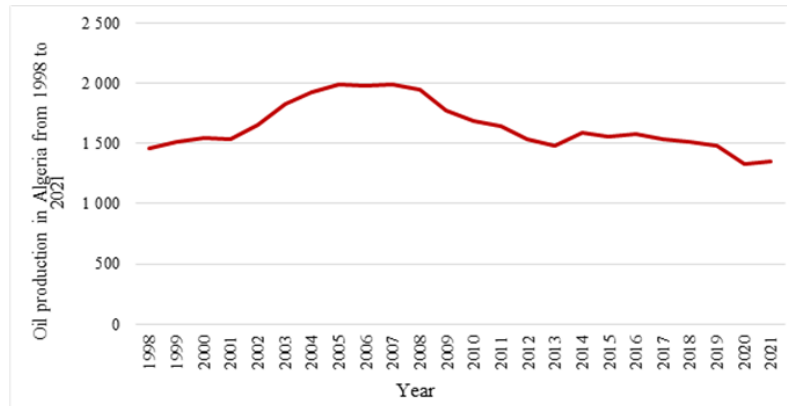


FIGURE 4: Oil production in Algeria from 1998 to 2021. (in a 1000 barrel per day)

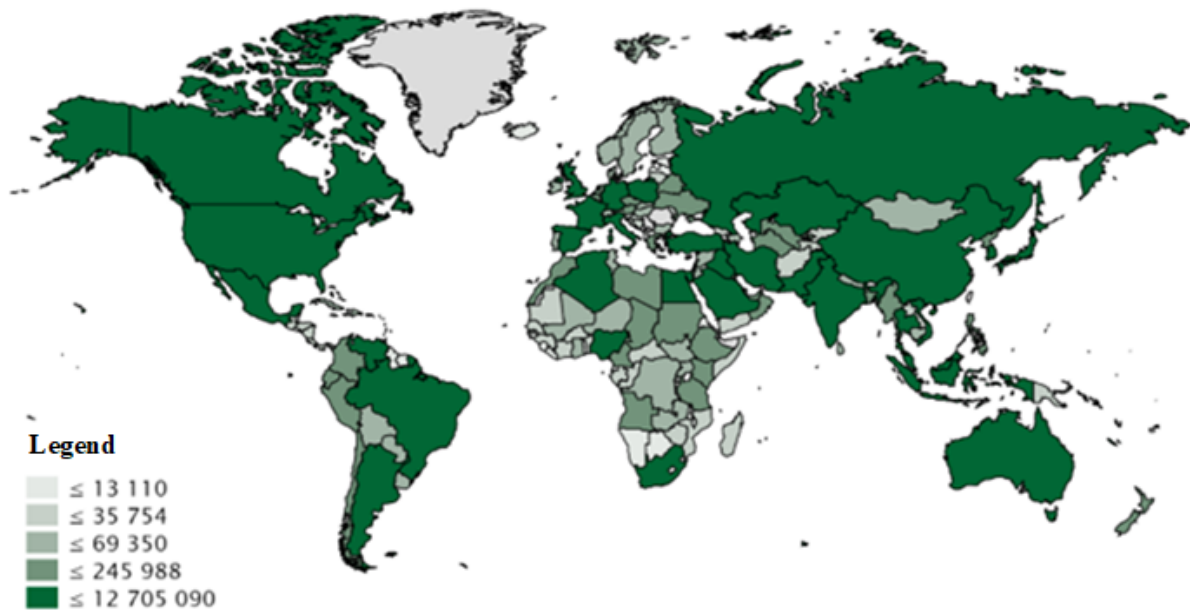


FIGURE 5: Total CO2 emissions in year 2019. (CO2 equivalent kiloton kt)

Algerian experts confirmed that the reason for "about 2,500 deaths annually in Algeria due to air pollution" is the emission of toxic gases by urban traffic, explaining that air pollution in Algeria has become a "reality". After power plants, diesel engines are among the largest sources of pollutants that scientists have linked to premature death, lung cancer, asthma and other serious respiratory illnesses. The diesel fuel used in these engines has a high concentration of sulphur, amounting to several thousand parts per million, which hinders the work of the innovative anti-pollution devices within the diesel combustion mechanism in the engines and contributes to increasing pollution by harmful particles [10]. Figure 6 illustrates the CO2 emissions in Algeria from year 1959 to 2019, showing the alarming growth in CO2 levels in the country [11].

In September 2021, Algiers was going through a period of "Moderate" air quality with a US AQI reading of 55. This United States Air Quality Index figure is calculated by measuring the levels of six of the most prolific air pollutants. It is then used as a metric when comparing air pollution in other cities. Sometimes records are non-existent for all six pollutants so the level is calculated by using what figures are available. In Algiers, the only recorded figure was that of PM_{2.5} which was 14 $\mu\text{g}/\text{m}^3$. This level is just under one and a half times higher than the recommended level of 10 $\mu\text{g}/\text{m}^3$, which is the suggested maximum figure by the World Health Organization (WHO), although no amount of air pollution is considered to be safe [12].

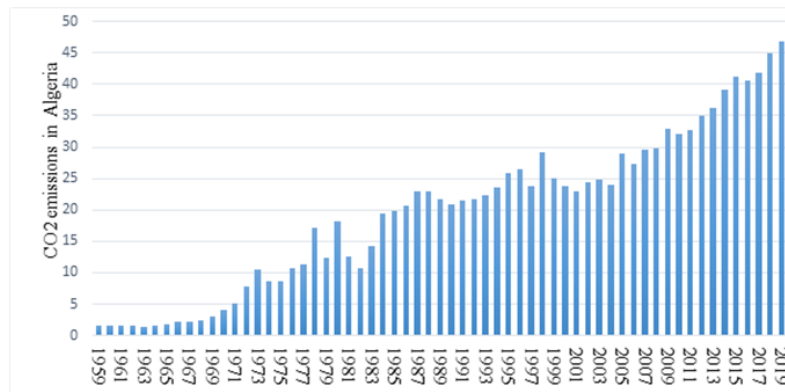


FIGURE 6: CO2 emissions in Algeria from 1959 to 2019.

With the level of air pollution of this size, the advice would be to stay indoors and close windows and doors to prevent more polluted air from entering. Those who are sensitive to poor quality air should avoid undue outdoor journeys. However, if this cannot be avoided, then a good quality mask should be worn at all times. There is a downloadable app available for most mobile devices which is free of charge and gives up-to-date information as to the state of the air in real-time.

Looking back at the 2020 figures released by [IQAir.com](https://www.iqair.com) it can be easily seen that Algiers air quality remained in the “Moderate” category for the full twelve months. Readings between 12.1 and 35.4 qualify for this moniker. Looking more closely though, it can be seen that the best month for air quality was December with a $16.9 \mu\text{g}/\text{m}^3$. Yet the following month of January provided the worst with its figure of $29.3 \mu\text{g}/\text{m}^3$. The remaining months fell in between

Historically, records pertaining to air quality were kept since 2019 when the recorded annual average was $21.2 \mu\text{g}/\text{m}^3$. A slight improvement was registered in 2020 with its figure of $20.2 \mu\text{g}/\text{m}^3$. This 2020 figure could be skewed because of the COVID-19 pandemic. Due to various periods of “lockdown”, many vehicles were no longer used on a daily basis as their drivers were not required to drive to the office. This cut a considerable amount of pollution from the air. Some factories and small production units were also temporarily closed so their emissions were no longer present in the atmosphere.

In Algeria, the quantity ranges between 10 and $35 \mu\text{g}/\text{m}^3$, which is a rate that exceeds the rates recorded in the European Union and the Balkans. It is noteworthy that the southern regions of the country are considered the most polluted because of sandstorms and flying dust. Reducing vehicle emissions is an important intervention to improve air quality, especially in urban areas. Policies and standards that require cleaner fuels and advanced vehicle emissions standards can reduce vehicle emissions by 90 per cent or more.

Towards EVs in Algerian roads

Due to its environmental benefits, the government established a plan in 2020 to encourage the introduction of electric vehicles. Redha Tir, the chairman of the National Economic, Social and Environmental Council (CNESE), stated that the council is exploring producing an electric automobile that is entirely built in Algeria and emphasized that Algeria has the resources required to carry out environmental projects. Under the “Le Programme Nationale de Maitrise de l’Energie pour le secteur du transport à l’horizon 2030” program, Algeria aims to convert ICE vehicles into 1.1 million LPG vehicles and 11,000 CNG buses and trucks by 2030. There are no special incentives for electric vehicles listed, however by the end of 2023, roughly 100 Naftal service stations will include electric vehicle recharging stations [13]

The president of Algeria urges his nation to promote electric vehicles. Abdelmadjid Tebboune advocated the implementation of an energy transition at the Council of Ministers on March 22, 2020, in Algiers at

the Palace of Nations, particularly through the purchase of electric vehicles. Several speeches, including one by the minister of industry and mines, served as inspiration for this presidential directive. On February 16, 2020, Ferhat Ait Ali Braham spoke to the media outside of a government meeting and declared that Algeria will soon start producing electric vehicles [13].

The strategy for importing used cars, the major points of which were revealed on April 7, 2020, by the Minister of Industry and Mines while speaking on the country's radio stations, contains additional methods of promoting electric cars in Algeria. Thus, he stated that the importation of used automobiles will need to abide by the vehicle's hybrid nature in addition to the age requirement (less than 3 years). Vehicles fueled by diesel are strictly forbidden. The preference for electric vehicles in Algeria is intended to lessen the carbon footprint of this North African nation, where more than 99% of all energy production and consumption, including in the electrical sector, is dependent on hydrocarbons[14]

A further confirmation was provided by the president that energy transition is indeed the goal for the next five years. Furthermore, it is essential to increase energy efficiency and develop renewable energy sources to meet the growing needs of the population. Thus, it is crucial to emphasize the industrial context that drives and guides the thesis's research focus.

Aims and scopes

The electric vehicle technology is thought to be the answer to many urgent public concerns, being a solution for the automotive industry after years of crises, a way to address the growing ecological consequences of the transportation system and a key to minimize the world's energy reliance on oil. This technology is a chance for the struggling energy sector, it is a practical, affordable substitute for conventional vehicles that meets consumers' changing needs.

Although this technology has a great potential, its current lack of economic viability in comparison to well-established conventional vehicles and its restricted operating range raise severe concerns. Many studies in the past have a history of making overly optimistic predictions. Two significant barriers to the use of electric vehicles, which have been thoroughly researched, are their short range and increased prices. Studies that combine these two variables are less common, despite the fact that they encourage behavior that is incongruent: the less you drive, the less a vehicle's restricted range is a hindrance, but the more you drive, the more you gain from an electric vehicle's reduced operating expenses. These studies frequently utilize longitudinal data, or data from prolonged observation periods. The limited driving range of an electric vehicle can be a real problem especially in a country like Algeria, with a distance only from east to west is of 1216 km, and links all the main cities in the north of the country. Thus making is impossible to use electric vehicles to travel in this immense country, unless we think about other solutions in order to improve the driving mileage. The aim of this thesis is to develop a control strategy in order to extend the limited driving range of an electric vehicle, which is primarily due to the use of the battery alone as an energy storage device.

Objectives and Limitation of the Study

Objectives

The broad objective was to study about the EVs energy consumption and management with more reliability and efficiency, the specific objectives of the study were:

- To examine the effect of existed power converter devices integrated on the actual EVs.
- To determine the efficiency of the EVs storage system.
- To determine time and distance required for such hybrid EVs on the Algerian road.

- To study the behavior of the EVs on the network grid.

Limitation of the study

Like all research projects, some constraints were found such as:

- No real EVs existed on the Algerian road and also there was no possibility to visit other countries due to time and budget limitation.
- In the case of our project, applying of our achievement on a real EVs not taken, because of the time constriction.
- Some converter structures and management algorithms could not be analyzed due to budget limitation.

Contribution and Hypothesis set to achieve the objective

One of the best possible solutions is integrating new vehicle architectures that include the battery electric, fuel cell electric, supercapacitors, and hybrid vehicles. Generally, hybrid vehicles are considered more fuel-efficient because the drive train allows us to recover kinetic energy when braking. Moreover, due to the presence of a second power source, the engine can be turned off or shifted to a more efficient operating point. With electric vehicles, the source of energy is flexible; any energy source can be used to generate the required electricity. This drive train allows us to work with renewable energy sources, such as wind or solar energy as a power supply for the auxiliary system of the electric car (air conditioning, heating systems, lights, etc.).

The aforementioned energy storage system that is based on a battery only can have many drawbacks such as the limited life-cycle, the limited power density as well as high cost. Unlike batteries, supercapacitors offer many advantages namely high power density, long life cycle along with a wide operating range. These complementary features can be combined in one storage system, which will eventually increase the driving range by supporting the battery during high power demands, as well as prolonging its lifetime.

The first contribution of this work lays in adopting a sufficient power management strategy using artificial intelligence in order to assure the optimal power flow in all of the electric vehicle's components.

The second contribution consists of using advanced power electronics, namely the Z-source three level inverter, the four-quadrant DC-DC converter, the bidirectional buck-boost converter along with other converters in an effort to upgrade the traction system of the electric vehicle.

The third contribution is the energy recovery from the regenerative braking, allowing the bidirectional power flow from the motor to the storage systems and the other way around. The last contribution involves advanced control methods used to control the traction system with the aim of achieving the reference speed in an optimum time.

Outline of the thesis

The manuscript is structured into four chapters. As presented in the first part the motivation and contribution of this thesis focus on the control of a traction system of an electric vehicle along with an artificial intelligence based power management strategy.

- Chapter 1 describes the state-of-the-art and related works of Electric vehicles. The power sources as well as energy storage system are presented, and then the static converter systems are introduced.

- Chapter 2 is dedicated to the modeling of the traction system components namely the storage systems, the power electronic devices and the electric motors. Simulations results of the classic control methods are presented as well using Z-source three level inverter along with the power management strategy in order to assure the proper power flow in the electric vehicle's components .
- Chapter 3 proposes a conventional PI control strategy for the four-quadrant DC-DC chopper along with the Genetic algorithms based PI controller including simulation results and discussions.
- Chapter 4 proposes an experimental bench using a four-quadrant DC-DC converter along with a permanent magnet DC-DC motor. This chapter includes simulation results followed by experimental results.

The contributions of this work are summarized, and the possible future works and perspectives are proposed.

Chapter 1

State of Art of Electric Vehicles

The purpose of this chapter is to present the state of the art of the drive train of an electric vehicle. This chapter begins with an overview the definition of electric vehicles in a general way, their different configurations, their advantages and disadvantages as well as the general description of the traction chain (energy sources, static converters, DC motors and asynchronous motors). Then, we are interested in the static converter (four-quadrant chopper) and its operating principle to control a DC motor. Followed by presentation of the charging modes of an electric vehicle.

1.1 Overview

Published work on electric vehicle engineering dates back to the late 1970s, coinciding with the energy crises of that period. Since then, electric vehicles have been considered the domain of automotive and mechanical engineers and thus were not a popular research topic for electrical engineers until the mid-1990s. The long-held view that electric vehicles were simply vehicles with an electric propulsion system as a replacement for an internal combustion engine has gradually changed. As shown in the histogram in [Figure 1.1](#), the last decade has seen an increase in publications from the electrical engineering community in this research area, indicating that there is a growing research interest in electric vehicles and the related issue of power and energy management.

Electric vehicles are now being classed as a new category of electrical equipment with unique features [15]. As such, there are various opportunities for research and development contributions in the scope of electrical engineering as there is a still some fluidity in industrial standards [16]. Power and energy management of energy storage systems within the vehicle is one such area of growing interest. As shown in the histogram above, evident work in the area of electric vehicles reached its highest levels in the last years.

Previous studies have examined EV technology from different perspectives. Un-Noor et al [17] reviewed all available useful data on EV configurations, battery energy sources, electrical machines, charging techniques, optimization techniques, impacts, trends, and possible directions for future developments.

Its objective is to provide a comprehensive picture of current EV technology and future development capabilities to aid future research in the EV sector. However, development challenges were not analyzed. Julio A. Sanguesa et al [18] reviewed the progress of EVs with respect to trends in battery technology, charging methods, as well as new research challenges and opportunities opened with the different standards that are available for the EV charging process, as well as power control and battery energy management proposals. Kumar et al. [19] emphasized understudied aspects such as dealer experience, charging infrastructure resilience, and marketing methods, as well as well-studied ones such as charging infrastructure development, total cost of ownership, and purchase incentive policies. Kumar et al. [19] also shed light on the dynamics underlying electric vehicle adoption by highlighting key mediators and modifiers. König et al [20] did a thorough analysis of the literature, offering a comprehensive overview of key metrics and costs for battery electric vehicles in the categories of vehicle, infrastructure, mobility, and energy. Sharma et al described the basic concepts of electric vehicles (EVs) and explained the developments made from ancient times to the present day to improve the performance of electric vehicles. Sharma et al also reviewed the various energy storage systems (ESS) and components used in electric vehicles.

Liu et al [21] presented a review of advanced electric machines and control strategies for electric vehicles, which clarifies the development trends of electric machines and enables the integration of these ideas into EV applications. Acharige et al. [22] presented an overview of different charging systems in terms of embedded and non-embedded chargers, AC-DC and DC-DC converter topologies, and AC and DC based charging station architectures. In addition, recent charging systems, which are integrated with renewable energy sources, are presented to identify the powertrain of modern charging stations. Finally, future trends and challenges in EV charging and grid integration are summarized for the future direction of EV charging system researchers [23].

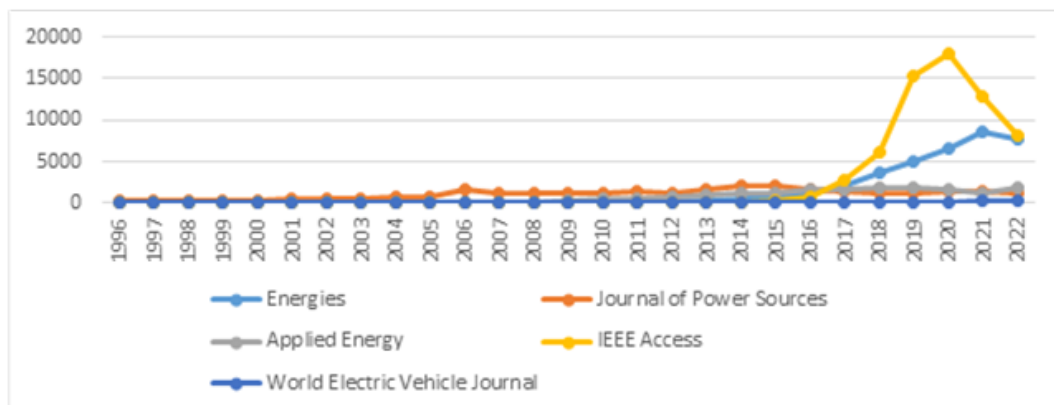


FIGURE 1.1: Publication on electric vehicles extracted from SCOPUS

1.2 Definition of an electric vehicle

As the name implies, the primary energy source for an electric vehicle is electricity. The battery packs underneath its floor provide this electricity, which the motor then transforms into mechanical motion. As a result, electric vehicles are an environmentally friendly alternative to combustion-engine vehicles considering that they do not produce any pollutants because there is no internal combustion. They differ from cars that run on gasoline in that they can get their energy from a variety of sources, including nuclear power, fossil fuels, and renewable sources like tidal, solar, and wind power, or any combination of these [24]. The energy is then sent to the car either directly through an electrical cable, wirelessly through inductive charging, or across overhead power lines. The power can then be kept onboard using a battery or a fuel cell. Typically, the energy used by combustion-based engines in vehicles can only come from one or a very limited number of sources, primarily non-renewable fossil fuels. The

ability of electric or hybrid electric vehicles to recover braking energy as electricity to be sent back to the grid (V2G) or restored to the on-board battery (regenerative braking) gives these types of engines an efficiency of 80%, compared to the thermodynamic engines' efficiency of just 25% [25]. The growth of EV sales and market share was a result of the automotive industry's transformation, battery technological advancements, and environmental concerns [18].



FIGURE 1.2: An electric vehicle

Country	2013	2014	2015	2016	2017	2018	2019	2020
Norway	6.10 %	13.84%	22.39%	27.40%	29.00%	39.20%	49.10%	55.90%
Iceland	0.94 %	2.71%	3.98%	6.28%	8.70%	19.00%	22.60%	45.00%
Sweden	0.71 %	1.53%	2.52%	3.20%	3.40%	6.30%	11.40%	32.20%
The Netherlands	5.55 %	3.87%	9.74%	6.70%	2.60%	5.40%	14.90%	24.60%
China	0.08 %	0.23%	0.84%	1.31%	2.10%	4.20%	4.90%	5.40%
Canada	0.18 %	0.28%	0.35%	0.58%	0.92%	2.16%	3.00%	3.30%
France	0.83 %	0.70%	1.19%	1.45%	1.98%	2.11%	2.80%	11.20%
Denmark	0.29 %	0.88%	2.29%	0.63%	0.40%	2.00%	4.20%	16.40%
USA	0.62 %	0.75%	0.66%	0.90%	1.16%	1.93%	2.00%	1.90%
United Kingdom	0.16 %	0.59%	1.07%	1.25%	1.40%	1.90%	22.60%	45.00%
Japan	0.91 %	1.06%	0.68%	0.59%	1.10%	1.00%	0.90%	0.77%

TABLE 1.1: Market share of EVs

1.3 Types of electric vehicles

The most basic type of EV uses simply batteries as its energy source, however there are others that can use various energy source forms. These are known as hybrid EVs (HEVs). The International Electrotechnical Commission's Technical Committee 69 (Electric Road Cars) advocated that vehicles that use two or more types of energy sources, storage, or converters be classified as HEVs as long as at least one of them provides electrical energy [26]. This description allows for a wide range of HEV pairings, such as ICE and battery, battery and flywheel, battery and capacitor, battery and fuel cell, among others. As a result, both the public and professionals began referring to cars with an ICE and an electric motor as HEVs, those with a battery and a capacitor as ultra-capacitor-assisted EVs, and those with a battery and a fuel cell as FCEVs. This terminology have gained widespread acceptance, and EVs may now be classified as follows:

1. Battery Electric Vehicle (BEV)
2. Hybrid Electric Vehicle (HEV)

3. Plug-in Hybrid Electric Vehicle (PHEV)
4. Fuel Cell Electric Vehicle (FCEV)

1.3.1 Battery Electric Vehicle (BEV)

These vehicles use batteries as primary energy which are recharged by the electrical grid or other renewable energies, such as solar and wind power. The range of these vehicles depends directly on the capacity of the battery. In general, they can travel 100 to 250 km on a single charge, while high-end models can go much further, from 300 to 500 km [27]. These ranges depend on driving conditions and style, vehicle configuration, road conditions, climate, battery type and age. Once depleted, recharging the battery takes a long time compared to refueling a conventional ICE vehicle. Batteries can take up to 36 hours to fully recharge [28]. There are others that take much less time, but none that compare to the short time it takes to fill a fuel tank.

The charging time depends on the charger configuration, its infrastructure, and the operating power level. The advantages of BEVs are their simplicity of construction, operation and convenience. They do not produce greenhouse gases (GHGs) or noise and are therefore beneficial to the environment. Electric propulsion provides instantaneous and high torque, even at low speeds. These advantages, combined with their limited range, make them ideal for use in urban areas. The Nissan Leaf and Tesla are popular BEVs today, as are some Chinese vehicles. Figure 1.3 shows the basic configuration of BEVs: the wheels are driven by one or more electric motors, which are powered by batteries via a power converter circuit.

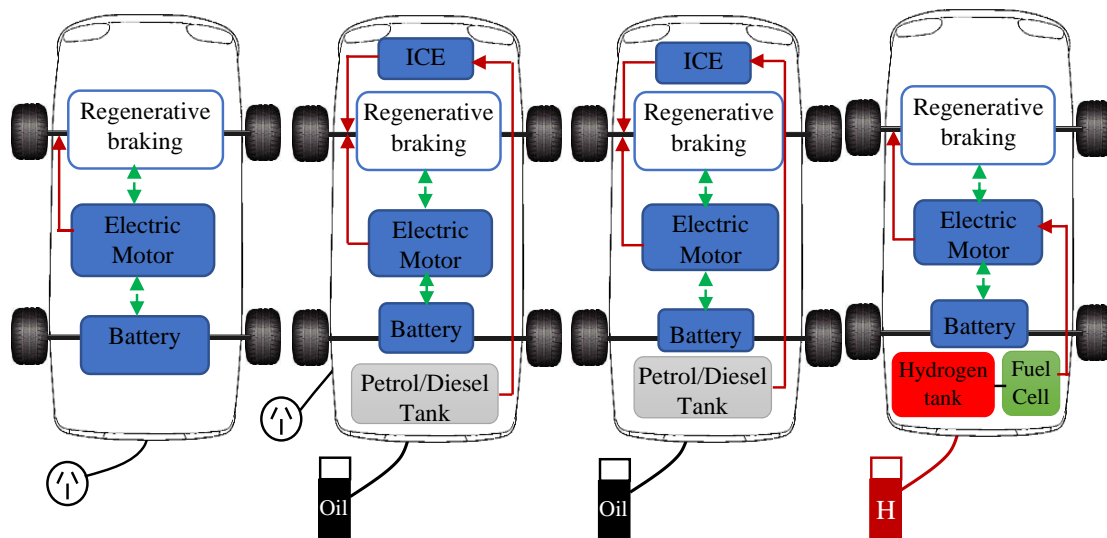


FIGURE 1.3: Types of electric vehicles

1.3.2 Hybrid Electric Vehicle (HEV)

HEVs are powered by a traditional internal combustion engine as well as an electric propulsion system. The primary engine is an internal combustion engine, with the electric motor's primary purpose being to boost fuel efficiency. In order to recharge their propulsion vehicle batteries, batteries must utilize their internal combustion engines and regenerative braking systems as they cannot plug in and recharge from the grid [29].

An HEV uses the electric drive system when the power demand is low. This is a great advantage in low-speed conditions such as urban areas; it also reduces fuel consumption because the engine remains

completely off during idling periods, such as in traffic jams, which will also reduce greenhouse gas emissions. When higher speeds are required, the HEV switches to the internal combustion engine. The two powertrains can also work together to improve performance by bridging shift gaps and increasing speed when needed, additionally improving driving mileage. To achieve these characteristics, power management strategies are utilized. For instance, when the vehicle is started, the internal combustion engine can run the engine as a generator to produce energy and store it in the battery. Overtaking requires an increase in speed, so both the internal combustion engine and the engine drive the powertrain. When braking, the powertrain turns the engine like a generator to charge the battery through regenerative braking. At cruising speed, the internal combustion engine runs the vehicle and engine as a generator, charging the battery. The energy flow is stopped when the vehicle comes to a stop [30].

1.3.3 Plug-In Hybrid Electric Vehicle (PHEV)

The PHEV concept emerged to extend the all-electric range of HEVs [31]. It uses both an internal combustion engine and an electric powertrain, like an HEV, but the difference between the two is that PHEV uses electric propulsion as the primary driving force, so these vehicles require a larger capacity battery than HEVs. PHEVs start in "all-electric" mode, run on electricity, and when the batteries are low, they rely on the internal combustion engine to give a boost or recharge the battery pack. The internal combustion engine is used here to increase range. PHEVs can recharge their batteries directly from the electrical grid (which HEVs cannot); they also have the ability to use regenerative braking [32]. The ability of PHEVs to run solely on electricity most of the time makes their carbon footprint smaller than that of HEVs. They also consume less fuel and therefore reduce the associated cost. The vehicle market is now quite populated with these vehicles, with sales of the Chevrolet Volt and Toyota Prius being testament to their popularity.

1.3.4 Fuel Cell Electric Vehicle (FCEV)

FCEVs are also known as fuel cell vehicles (FCVs). The term derives from the fact that the heart of these cars are fuel cells that create power through chemical processes [33], [34], [35]. Since hydrogen is the preferred fuel for fuel cell cars to execute this reaction, they are sometimes referred to as "hydrogen fuel cell vehicles". Hydrogen is transported in special high-pressure tanks by fuel cell trucks. Another component of the power generating process is oxygen, which is taken from the environment's air. The fuel cells generate energy, which powers an electric motor that drives the wheels. Excess energy is stored in devices like batteries or supercapacitors [36]. FCVs only emit water as a byproduct of their power generation process, which is discharged from the vehicle via the tailpipes. Figure 1.3 depicts the configuration of an FCV. One advantage of such cars is that they can generate their own power that produces no carbon, allowing them to minimize their carbon footprint more than any other EV. Another significant advantage, and maybe the most crucial for now, is that recharging these cars takes the same amount of time as filling a traditional vehicle at a gas station. This increases the likelihood of these cars being adopted in the near future [37]. The shortage of hydrogen fuel stations is a key present barrier to the adoption of this technology, yet BEV or PHEV charging facilities were not prevalent until a few years ago. Another drawback, according to a study to the United States Department of Energy (DOE), is the high cost of fuel cells, which cost more than \$200 per kW, significantly more than ICE (less than \$50 per kW) [38]. There are also safety considerations in the event that explosive hydrogen leaks from the tanks. If these impediments were removed, FCVs may really represent the future of automobiles. Table 1.2 represents the typical vehicles in the industry along with their main characteristics [26].

Vehicle Model	Peugeot e208	Citroen Ami	Toyota Prius	Mitsubishi Outlander	Toyota Mirai
Release year	2022	2020	2018	2018	2018
Type	BEV	BEV	HEV	PHEV	FCEV
Entry price (€)	33000	7000	32300	37000	78900
Battery size (kWh)	46	5.5	1.3	13.8	1.6
Fossil-fuel autonomy (km)	0	0	500	550	650
Electric autonomy (km)	450	75	0	55	0
CO ₂ emissions (g/km)	0	0	106	46	0

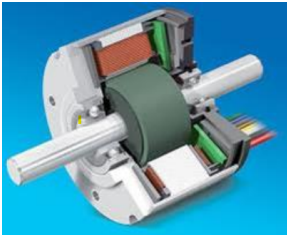
TABLE 1.2: Typical electric vehicles and their main characteristics

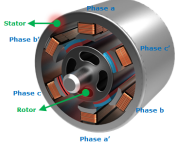
1.4 Technical components of electric vehicles

1.4.1 Electric engines

The electric motor sits right in the core of the propulsion system of the electric vehicle, it is the key element that enables the vehicle to move by converting the electric energy into a mechanical energy. In addition, the motor acts as a generator during regenerative braking. There are specific requirements of EV's motor according to [21], such as high power, high torque, wide speed range, high efficiency, reliability, robustness, reasonable price, low noise and small size [39], [40].

Different motors can be used to drive electric vehicles namely DC motors, which were the most widely used since they have less maintenance and cost compared to other drives. These motors are suitable only for small power applications as in electric wheelchairs, microcars (etc.). Table 1.3 summarizes the most important characteristics of each engine, its drawbacks, and the type of vehicle used in it [17].

Motor type	Advantage	Disadvantage	Vehicles used in
Brushed DC Motor 	<ul style="list-style-type: none"> • Maximum torque at low speed 	<ul style="list-style-type: none"> • Bulky structure • Low efficiency • Heat generation at brushes 	<ul style="list-style-type: none"> • Fiat Panda Elettra (Series DC motor) • Conceptor G-Van (Separately excited DC motor)
Permanent Magnet Brushless DC Motor (BLDC) 	<ul style="list-style-type: none"> • No rotor copper loss • More efficiency than induction motors • Lighter • Smaller • Better heat dissipation • More reliability • More torque density • More specific power 	<ul style="list-style-type: none"> • Short constant power range • Decreased torque with increase in speed • High cost because of PM 	<ul style="list-style-type: none"> • Toyota Prius (2005)

Motor type	Advantage	Disadvantage	Vehicles used in
<p>Permanent Magnet Synchronous Motor (PMSM)</p> 	<ul style="list-style-type: none"> • Operable in different speed ranges without using gear systems • Efficient • Compact • Suitable for in-wheel application • High torque even at very low speeds 	<ul style="list-style-type: none"> • Huge iron loss at high speeds during in-wheel operation 	<ul style="list-style-type: none"> • Toyota Prius • Nissan Leaf • Soul EV
<p>Induction Motor (IM)</p> 	<ul style="list-style-type: none"> • The most mature commutator less motor drive system • Can be operated like a separately excited DC motor by employing field orientation control 		<ul style="list-style-type: none"> • Tesla Model S • Tesla Model X • Toyota RAV4 • GM EVI
<p>Switched Reluctance Motor (SRM)</p>  <p>Synchronous Reluctance Motor (SynRM)</p> 	<ul style="list-style-type: none"> • Simple and robust construction • Low cost • High speed • Less chance of hazard • Long constant power range • High power density • Robust • Fault tolerant • Efficient • Small 	<ul style="list-style-type: none"> • Very noisy • Low efficiency • Larger and heavier than PM machines • Complex design and control • Problems in controllability and manufacturing • Low power factor 	<ul style="list-style-type: none"> • Chloride Lucas
<p>PM assisted Synchronous Reluctance Motor</p> 	<ul style="list-style-type: none"> • Greater power factor than SynRMs • Free from demagnetizing problems observed in IPM 		<ul style="list-style-type: none"> • BMW i3

Motor type	Advantage	Disadvantage	Vehicles used in
<p style="text-align: center;">Axial Flux Ironless Permanent Magnet Motor</p> 	<ul style="list-style-type: none"> • No iron used in outer rotor • No stator core • Lightweight • Better power density • Minimized copper loss • Better efficiency • Variable speed machine • Rotor is capable of being fitted to the lateral side of the wheel 		<ul style="list-style-type: none"> • Renovo Coupe

TABLE 1.3: Types of electric engines used in EVS

1.4.2 Energy Sources and Energy Storage Systems

Energy Storage Devices

- *Battery:*

The traction batteries are used to power the propulsion systems of EVs, hence the advances in traction battery technology have a significant influence on the EV industry. When a rechargeable lead-acid battery became commercially available, it was installed in an EV. As battery technology has evolved, the battery industry has seen an increase in the number of different types of traction batteries. In spite of the advances in battery technology, the requirements for traction batteries have not changed significantly. EV batteries, unlike starter, lighting and ignition batteries, must provide continuous power. Therefore, increased energy capacity is essential. In addition, high specific power, specific energy and energy density are essential [40]. Several battery technologies have emerged with the development of EVs, including lead-acid, nickel-cadmium (Ni-Cd), lithium-ion (Li-Ion), lithium iron phosphate (Li-phosphate), lithium polymer (Li-Polymer), nickel metal hydride (Ni-MH), zebras, and zinc-air batteries [41]. The Li-Ion battery is the most popular battery type used in EVs. Lithium-ion batteries have many advantages, including a high power-to-weight ratio, high energy efficiency, and robust high-temperature performance. In addition, compared to other technologies, Li-Ion batteries have a low “self-discharge” rate, which means they can maintain a full charge over time.

Several battery technologies have emerged with the development of EVs, including lead-acid, nickel-cadmium (Ni-Cd), lithium-ion (Li-Ion), lithium iron phosphate (Li-phosphate), lithium polymer (Li-Polymer), nickel metal hydride (Ni-MH), zebras, and zinc-air batteries [26]. The Li-Ion battery is the most popular battery type used in EVs. Lithium-ion batteries have many advantages, including a high power-to-weight ratio, high energy efficiency, and robust high-temperature performance. In addition, compared to other technologies, Li-Ion batteries have a low “self-discharge” rate, which means they can maintain a full charge over time. Furthermore, most components of Li-Ion batteries are recyclable, making this technology environmentally friendly. Table 1.4 shows the commonly used battery technologies in electric vehicles [17], [40]. A battery is defined by the three parameters listed below:



FIGURE 1.4: Lithium-Ion battery of the Nissan electric car

- Useful power ($P = V \cdot I$) in kW: Useful power is the product of the battery voltage (V) and the maximum current it can supply (I). The useful power must be at least equal to the peak power of the electric motor so that it is powered over its entire operating range.
- Stored energy in kWh: This energy can be equivalent to the volume of a vehicle's fuel tank. The stored energy will determine the autonomy of an EV and the recovery possibilities for a hybrid car. The energy of an electric battery is represented as a function of its capacity in ampere-hours (Ah) and its voltage.
- C-Rate (charge rate): First, the size of the battery is primarily determined by the capacity (Ah) and charging current (A), which are two characteristics that define the C-rate of the battery: the capacity rate of the battery is charged/discharged [26].

Battery Type	Components	Advantages	Disadvantages
Lead-Acid	<ul style="list-style-type: none"> • Positive electrode: Lead oxide • Negative electrode: Spongy lead • Electrolyte: Diluted sulfuric acid 	<ul style="list-style-type: none"> • Available in production volume • Low price • Mature technology 	<ul style="list-style-type: none"> • Level of discharge cannot reach 20% • Limited life-cycle • Low energy and power density • Bulky • Needs maintenance
Nickel-Metal Hydride (NiMH)	<ul style="list-style-type: none"> • Positive electrode: Alkaline solution • Negative electrode: Nickel Hydroxide • Electrolyte: Alloy of Nickel, Titanium, Vanadium and other metals 	<ul style="list-style-type: none"> • Double energy density compared to lead-acid • Environmentally friendly • Recyclable • safe operation at high voltage • Store volumetric energy and power • Long life-cycle • Long operating range temperature • over-charge and discharge resistant 	<ul style="list-style-type: none"> • Reduced lifetime of 200-300 if discharged rapidly on a high load • Reduced usable power because of memory effect

Battery Type	Components	Advantages	Disadvantages
Lithium-Ion (Li-Ion)	<ul style="list-style-type: none"> Positive electrode: Oxidized Cobalt material Negative electrode: Carbon material Electrolyte: Lithium salt solution in an organic solvent 	<ul style="list-style-type: none"> High energy density twice of NiMH Good performance at high temperature Recyclable low memory effect High specific power High specific energy Long battery life, around 1000 cycles 	<ul style="list-style-type: none"> High price Long charging time, but still better than other batteries
Nickel-Zinc (Ni-Zn)	<ul style="list-style-type: none"> Positive electrode: Nickel oxyhydroxide Negative electrode: Zinc 	<ul style="list-style-type: none"> High energy density High power density Low cost material Capable of deep cycle Friendly to the environment Usable in high temperature range 	<ul style="list-style-type: none"> Fast growth of dendrite, preventing use in vehicles
Nickel-Cadmium (Ni-Cd)	<ul style="list-style-type: none"> Positive electrode: Nickel hydroxide Negative electrode: Cadmium 	<ul style="list-style-type: none"> Long lifetime Can discharge fully without being damaged Recyclable 	<ul style="list-style-type: none"> Cadmium can be polluting Costly for vehicular applications

TABLE 1.4: Commonly used battery types

Battery prices vary widely because economies of scale can be triggered based on the total number of cars manufactured [42]. As a result, battery costs might vary depending on the quantity of units manufactured (Table 1.5). Table 1.6 presents an overview on the existing EVs in the industry with their battery technology [43].

Vehicle	Model Year	Assumed Units Per Year	Pack Costs (€/kWh)
BMW i3	2014	15,000	396
GM Bolt	2016	20,000	224
BMW i3	2017	25,000	254
Renault Zoe	2017	40,000	208
Tesla Model 3	2018	100,000	164
Audi e-tron	2019	100,000	157

TABLE 1.5: Overview of battery costs at pack level for different BEVs

- *Supercapacitor:*

Manufacturer	Model	Autonomy (km)	Battery technology
Citroën	C-Zero	150	Lithium ion
Mia Electric	Mia	130	Lithium iron phosphate
Mitsubishi	I-MiEV	150	Lithium ion
Nissan	Leaf	160	Lithium ion
Peugeot	iOn	130	Lithium ion
Piaggio	Porter	100	Lead acid
Renault	Fluence ZE	185	Lithium ion
Renault	Kangoo	170	Lithium ion
Smart	Fortwo	145	Lithium ion
Tesla	Roadster	390	Lithium ion
Venturi	Fétish	340	Lithium polymer

TABLE 1.6: Overview on the existing EVs in the industry with their battery technology

Supercapacitors (SCs), also referred to as ultracapacitors, have a construction similar to regular capacitors but store energy in the form of an electrolyte solution between two solid conductors. SCs have a substantially larger capacity than traditional capacitors, allowing them to store up to 20 times more energy. SCs are classified into three types: electric double layer capacitors (EDLCs), pseudo-capacitors, and hybrid capacitors. Despite the fact that their energy storage techniques and electrode materials differ, they share properties such as power density, life cycle, and energy efficiency. It is worth noting that EDLCs have a lower specific energy density than the other two (10e15 Wh/kg). The high life cycle (1,105 cycles for about 40 years) distinguishes SCs from other energy storage devices. SCs also have a high power density (1000e2000 kW/kg) and energy efficiency (84e97%). As a result, they can be rapidly charged and discharge a significant quantity of energy with minimal energy loss. The primary drawbacks of SCs are their short life duration and high self-discharge rate, which explains why they cannot be utilized as a standalone power source for automobiles. Another issue is the high capital expenditures (above \$6,000/kWh). As a result, energy storage systems are ideal as a backup energy source for short-term energy storage applications [17], [40], [41].

EVs are frequently subjected to start-stop circumstances, particularly in urban driving. As a result, the rate of battery drain varies greatly. The typical power need of batteries is minimal, but substantial power is required over a short duration amid acceleration or situations such as hill climbing [4, 35]. In a high-performance electric vehicle, peak power may be up to sixteen times that of normal power [4]. UCs are ideal for this circumstance due to their high power for short periods. They can also collect the energy provided by regenerative braking fast [2], [35]. A combined battery/UC system (as seen in Figure 30) compensates for the deficiencies of the other by providing an efficient and dependable energy system. The UCs' low cost, load-leveling capabilities, temperature adjustability, and long life make it an appealing solution [4], [30].

- *Flywheel:*

Flywheels store energy in the angular momentum of a high speed rotating mass (rotor) in a high vacuum environment, allowing them to reduce windage losses and protect the rotor assembly from external disturbances [17], [41]. During the storage phase, an integrated motor/generator (M/G) in motor operating mode accelerates the rotor to a high speed. The rotor decelerates during the discharge phase and converts the kinetic energy of the rotor to electrical energy via the integrated M/G in the generator operation mode [17]. Flywheels have many advantages over other types of EV storage because they are lighter, faster, and more efficient at absorbing power from regenerative braking, faster at supplying a large amount of power in a short period of time when rapid acceleration is required, and can withstand many charge-discharge cycles over their



FIGURE 1.5: Supercapacitor

lifetime. They are notably popular for hybrid racecars, which experience a lot of rapid braking and acceleration while also experiencing significantly more g-force than typical commuter vehicles. In conditions like this, storage technologies like as batteries or UCs are incapable of adequately capturing the energy provided by regenerative braking. Flywheels, on the other hand, offer a higher efficiency in comparable conditions because they employ regenerative braking more efficiently; it also decreases strain on the brake pads. This technology was used in the Porsche 911GT3R hybrid. Flywheels may be built from a variety of materials, each with advantages and disadvantages. [Table 1.7](#) shows the properties of several of these materials; among those given, carbon T1000 has the highest energy density, although it is significantly more expensive than the rest. As a result, there is still a trade-off between cost and performance. The key advantages of flywheels are their cheap maintenance cost, extended life cycle, high efficiency, lack of depth of discharge effect, environmental friendliness, wide operating temperature range, and capacity to withstand severe circumstances [17]. Nonetheless, concerns about safety and gyroscopic force control, as well as flaws like as poor energy density and large self-discharge losses, prevent flywheels from being used in vehicle applications. The particular energy density of high speed flywheels is less than 100 Wh/kg, whereas low speed flywheels can only attain 5 Wh/kg. Because of friction losses, the self-discharge rate can be as high as 20% of the stored energy capacity every hour. As a result, flywheels are unsuitable for long-term storage applications.



FIGURE 1.6: Flywheel

- *Hydraulic accumulator:*

Hydraulic accumulators (HACCs) store and release hydraulic energy using a variable displacement high-pressure pump/motor (P/M). When the P/M is used as a pump, hydraulic fluid is

	Material	Density (Kg/m ³)	Tensile Strength (mpa)	Max Energy Density (mj/Kg)	Cost (USD/Kg)
Monolithic material	4340 steel	7700	1520	0.19	1
Composites	E-glass	2000	100	0.05	11
	S2-glass	1920	1470	0.76	24.6
	Carbon T1000	1520	1950	1.28	101.8
	Carbon AS4C	1510	1650	1.1	31.3

TABLE 1.7: Characteristics of different materials used for flywheels

pumped into the accumulator from a tank, and the gas (often nitrogen) in the accumulator chamber is compressed. Simultaneously, mechanical energy is transferred to hydraulic energy, which is stored in the accumulator. When the external load demands energy, the hydraulic energy from the accumulator is released to drive the P/M acting as a motor [17], [41]. The common accumulators are classified into three types based on the membrane that separates the gas and fluid sides of the accumulator: bladder type, which is commonly found in industrial installations, membrane type, which is commonly found in the automotive industry, and piston type, which is commonly found in the offshore and chemical industries. HACCs have a high power density (about 5 kW/kg), a high energy conversion efficiency, and are inexpensive. Furthermore, they can accept unusually high charging and discharging rates, allowing for effective energy regeneration and reuse for vehicle applications, particularly in metropolitan areas with frequent stop-and-start traffic. However, due to their reduced specific energy density, they cannot be employed as an independent energy source. Although HACCs and SCs have comparable features, SCs have a substantially greater capital cost than HACCs. Furthermore, SC charge leakage might cause environmental problems. As a result, it appears to be a more competitive solution in vehicle applications when compared to HACCs and SCs. When the HACCs release the stored hydraulic energy, high-pressure fluid rushes into the P/M, which acts as a motor to propel the vehicle. When the vehicle slows down, the HACCs store the braking energy via the P/M acting as a pump.



FIGURE 1.7: Hydraulic accumulator

- *Hydrogen storage:*

Taking into account its storability, transportability, and cleanliness, hydrogen energy is one of the most popular forms of energy [17]. Whether the hydrogen gas is consumed in an ICE to convert into mechanical energy or oxidized in a Fuel Cell (FC) to create electricity without pollution, the byproducts are primarily water and heat. The energy conversion efficiency of hydrogen in an FC can exceed 70%, but hydrogen combustion efficiency in an ICE is only approximately 30% [41]. As a result, using hydrogen energy in a fuel cell to generate electricity directly is more promising. Water electrolysis can produce hydrogen, with a conversion efficiency of roughly 60% [17]. The process is incredibly ecologically friendly, but it is very expensive because it requires a lot of power. Renewable energy sources (solar, wind, geothermal, and so on) can also provide clean and sustainable energy for water electrolysis, although the current costs are also quite expensive.

Because of its cheap cost and great efficiency (85%), the majority of worldwide hydrogen is now generated by reforming natural gas with steam and catalyst; nevertheless, this technique contains the extra product of CO₂. Furthermore, direct hydrogen synthesis by photocatalytic water splitting based on nanotechnology appears to be quite promising. Nonetheless, the technology is still in its early stages of development [41]. In terms of hydrogen storage, the most common method is to compress hydrogen under high pressure (about 7000 times atmospheric pressure) in sealed hydrogen tanks. Another technique of storing hydrogen is to use a cryogenic system (at 253 C) to liquefy it, however this uses roughly 30% of the energy in the hydrogen. Furthermore, hydrogen may be kept on surfaces or within some absorbent materials by absorption, but this process has drawbacks such as high temperature or pressure requirements, a lengthy time to release the hydrogen, and difficulties in material recycling.

Energy Generation systems

- *Fuel Cell Systems:*

In 1839, Welsh physicist William Grove invented the first fuel cells. They were originally used commercially in NASA space missions to power probes, satellites, and space capsules. Fuel cells have since been employed in a variety of other applications. Fuel cells provide primary and backup power to commercial, industrial, and residential structures, as well as in distant or inaccessible locations. Fuel cells are also employed in mobile applications such as vehicles, buses, boats, and airplanes, among others. However, the complexity of hydrogen storage and fuel cell dependability place significant limits on the fuel cell's adoption into this sort of application [17], [41], [43].

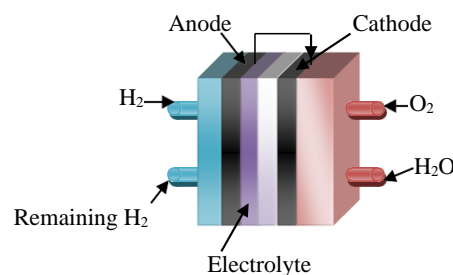


FIGURE 1.8: Hydrogen fuel cell

FC systems use catalysts to convert chemical energy into electricity through chemical reactions between hydrogen (or a hydrocarbon such as methanol or natural gas) and oxygen (from the air). An FC is made up of an anode (A), a cathode (C), and an electrolyte (E), with the fuel delivered to the anode, oxidized there, and the ions produced traveling through the electrolyte to the cathode to mix with the other reactant introduced there. When protons flow through the electrolytes, the electrons created by oxidation at the anode are driven into a circuit to generate an electric current. In general, the process of generating power with FCs is quiet, dependable, pollution-free, and efficient. FCs are classified into six primary classes based on the fuels and electrolytes used: direct methanol fuel cells (DMFC), alkaline electrolyte fuel cells (AFC), molten carbonate fuel cells (MCFC) fuel cells (PEMFC) [43]. DMFCs have high energy density but poor efficiency), phosphoric acid fuel cells (PAFC), solid oxide fuel cells (SOFC), and proton exchange membrane y and release CO₂. The MCFC and SOFC operate at high temperatures (600e1000 C) and are commonly utilized in electric utilities and distributed power production. Taking into account their typical or moderate working temperatures, DMFC, PEMFC, AFC, and PAFC are often employed in transportation. PEMFCs have the highest power density and advantages such as long lifespan, low-temperature operation, and rapid reaction when compared to other FCs. As a result, PEMFCs

are extremely appealing in transportation applications. Although FCs have a high capital cost at the moment, the cost is decreasing because of the rising industry and greater economies of scale.

There are three techniques for storing hydrogen for fuel cell applications: keeping it at room temperature under high pressure, storing it at extremely low temperatures as a liquid or solid, and storing it by trapping it in hydride metal.

For automotive applications, researchers and manufacturers often store hydrogen in high-pressure carbon fiber tanks (up to 300 bar). Nonetheless, hydride metal tank solutions are on the way. This approach has the benefit of keeping the tank at low pressure (about 10 bars), but the tanks are heavy and it also requires a temperature management. Table 1.8 shows the different types of FCs along with their characteristics [17].

TABLE 1.8: Different Types of FCs with their characteristics

	PAFC ¹	AFC ²	MCFC	SOFC ³	SPFC ⁴	DMFC
Working temp (°C)	150-210	60-100	600-700	900-1000	50-100	50-100
Power density (W/cm ²)	0.2 - 0.5	0.2 - 0.3	0.1 - 0.2	0.24 - 0.3	0.35 - 0.6	0.04 - 0.25
Estimates life (kh)	40	10	40	40	40	10
Estimated cost (USD/kW)	1000	200	1000	1500	200	200

¹ PAFC: Phosphoric acid fuel cell

² AFC: Alkaline fuel cell

³ SOFC: Solid oxide fuel cell

⁴ SPFC: Solid polymer fuel cell, also known as proton exchange membrane fuel cell

- *Photovoltaic Cell System:*

Photovoltaic (PV) cells (also called solar cells) can directly convert sunlight into electricity. A single PV cell provides a small amount of energy (only about 1 or 2 W). PV cells are typically connected together (in series and/or parallel) to form modules or panels, and PV modules can be connected to form PV arrays for higher power requirements [44]. In addition to PV modules, a PV system includes a solar inverter to convert direct current (DC) to alternating current (AC), as well as mounting, wiring and other electrical accessories. PV systems do not produce pollution or greenhouse gas emissions when they operate, and they have advantages such as quiet operation, long service life, and low maintenance [41].

The main disadvantages of PV systems are their high initial capital expenditures and unpredictability due to weather conditions [41]. In the market, the primary manufacturing materials for PV cells are crystalline silicon and thin films. In recent years, crystalline silicon PV, specifically first-generation PV cells, has been one of the most widely used, accounting for approximately 90% of global output. Mono-crystalline silicon (mono-si) and multi-crystalline silicon are used in this crystalline silicon PV cell (multi-si). The average efficiency of mono-si PV cells is 14.0%, which is greater than the average efficiency of multi-si PV cells, which is 13.2%, but the multi-si ones have simpler and cheaper manufacturing procedures.

Thin-film PV cells are second-generation PV devices consisting of amorphous silicon or nonsilicon materials such as cadmium telluride (CdTe) and copper indium diselenide (CIS). In general, thin-film PV cells provide advantages such as reduced cost and less weight.

The CdTe type is one of the fastest-growing thin-film PV cell types, with a maximum power conversion efficiency of 21% [45]. Third-generation PV cells are developing new materials such as solar inks employing traditional printing press technology, solar dyes, and conductive polymers to improve energy efficiency and lower PV cell capital costs. PV systems offer a wide range of

practical applications, including powering buildings, spacecraft, water heaters, and street lighting. They can also be placed over parking lots to charge commuter vehicles during the day. However, because to space constraints and poor power generation, it remains difficult to directly apply PV systems in commercial EVs. PV systems, on the other hand, can be utilized to enhance vehicle efficiency (10-20%) or to keep the car pleasant by running the air conditioner.



FIGURE 1.9: Photovoltaic systems

- *Regenerative Braking System:*

Regenerative braking systems can supply energy to automobiles by recovering and storing the kinetic energy of the vehicle's deceleration stage in energy storage devices. There are now four approaches for realizing the functionalities of regenerative braking systems. The first method is to use an electric M/G with batteries or a SC. The M/G acts as a generator during vehicle deceleration, converting kinetic energy into electricity and storing it in the batteries or the SC. When the car accelerates, the M/G acts like an electric motor, releasing energy. Another popular way is to employ a hydraulic P/M with HACCs. The P/M pumps hydraulic fluid from a low-pressure reservoir to the HACCs during braking, converting kinetic energy into hydraulic energy. If the vehicle demands energy, the stored hydraulic energy can be released as auxiliary power by the P/M acting as a hydraulic motor. Third, kinetic energy from a vehicle can be stored as rotating energy in a flywheel. Furthermore, braking energy can be retained as potential energy in the form of springs [41], [46]. Hydraulic and flywheel regenerative systems are more energy efficient than other technologies. Furthermore, hydraulic regeneration systems may charge and discharge faster, have a higher power density, and have a big capacity to recover the maximum amount of regenerative braking energy. In contrast, battery regenerative systems should not be charged and drained regularly to avoid overheating, a reduction in lifetime, or even destruction. The primary disadvantage of SC regenerative systems is their high cost, whereas spring regenerative systems have extremely low energy efficiency [47].

1.4.3 Power Converters

DC-AC converters

Bidirectional DC-AC converters are responsible for increasing the controllability, performance and efficiency of HEVs. The bi-directional converter transports power in both directions, i.e., from the battery to the wheels and from the wheels to the battery through regenerative braking. Traction inverters for hybrid electric vehicles can be categorized as voltage source inverter (VSI), current source inverter (CSI), impedance source inverter (ZSI) and soft-switching inverters. A brief summary of these inverters is given in Table 1.9. From this table, it can be concluded that the ZSI topology, especially the quasi-ZSI, is very advantageous for EVs in terms of high efficiency and fuel economy. Researchers are working on developing new control methods and algorithms for zero voltage switching (ZVS). Research is also underway to develop new ZVS topologies, such as q-ZVS, by modifying the basic topology to make it more efficient [48], [49], [50].

	Specification	Advantages	Disadvantages
VSI Figure 1.10	<ul style="list-style-type: none"> Controlled voltage source. Feedback diodes are necessary It can be classified into series, parallel and bridge. Used in UPS and AC drives 	<ul style="list-style-type: none"> Low power consumption & high energy efficiency up to 90%. Capable to handle high power rating. High tolerance against temperature Variation and no degradation in linearity. Smooth implement and controlling. Compatible with most of the recent controller as well. 	<ul style="list-style-type: none"> Distortion of the fundamental waveform. Sudden enhancement in switching frequencies. Harmonic issues High stress on switches
CSI Figure 1.11	<ul style="list-style-type: none"> Controlled current source. Current is controlled by a series Inductance. Not suitable for light load. Application in AC motor drives. 	<ul style="list-style-type: none"> Simple circuit Reverse blocking capability Withstand high voltage spikes. Converter-inverter combined. Thyristor used for commutation are simple 	<ul style="list-style-type: none"> Limited operating frequency Cannot provide uninterruptible power supply systems. Sluggish performance and stability problems. Extra converter stage is required Distortion of the fundamental waveform. Sudden enhancement in switching frequencies. Harmonic issues High stress on switches

	Specification	Advantages	Disadvantages
<p>ZSI Figure 1.12</p>	<ul style="list-style-type: none"> • Buck & boost in a single-stage conversion. • A special Z-network composed of 2 capacitors & inductors connected to a 3-Φ inverter bridge allows working in buck boost mode using the shoot through state. 	<ul style="list-style-type: none"> • Provides desired AC voltage output regardless of the input voltage. • Yields high voltage utility factor. • Overcomes voltage sags without any additional circuits. • Decreases the motor ratings to deliver the required power [118]. • Improves the power factor. • Reduces harmonic current & common-mode voltage of the line 	<ul style="list-style-type: none"> • The lower average-switching device • Power in low boost ratio. range (1/2). • In case of low voltage boost ratio much higher than 2. • Right-hand plane zero in ZSI cannot be eliminated by adjusting the Z-source parameters.

TABLE 1.9: Types of inverters with their advantages and disadvantages

The voltage source inverter (VSI), Figure 1.10, is one of the traditional inverter configurations used in electric vehicles. The advantages of this inverter are low cost, robustness, and loss reduction. To mitigate harmonics in this type of inverter, the switching frequency must be increased, which further increases the switching losses. The other disadvantage of this inverter is the requirement for a high DC link voltage. However, it is still attractive due to its robust, simple and well-established topology [51]. If a current source inverter (CSI), Figure 1.11, is used instead of a VSI, there is no need for an additional converter for current injection into the grid [52]. However, these inverters have major drawbacks such as high voltage stresses on the switches, voltage boosting and reducing operations cannot take place at the same time.

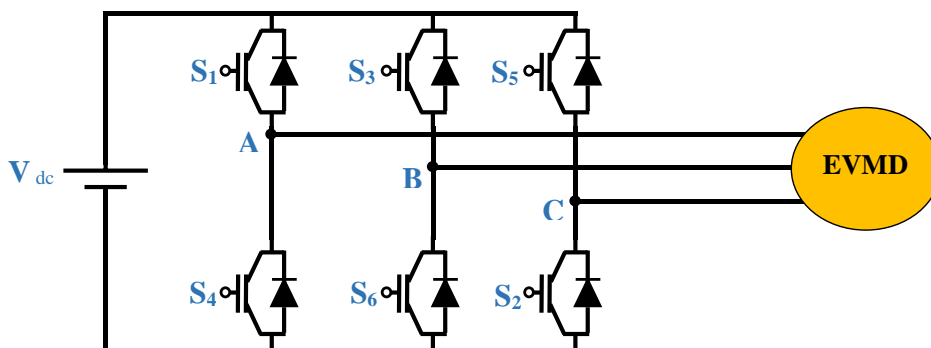


FIGURE 1.10: Voltage source inverter

Multilevel inverters (MLIs) have been introduced to alleviate the shortcomings of VSI and CSI, since they have lower switching losses and rates of change of voltage (dv/dt). As a result, MLIs can be used

in high-voltage applications [53]. MLIs have disadvantages such as more switches, complex control strategies, high cost, etc. Z-source inverters which are a combination of inductors and capacitors, have been shown to be more advantageous than VSIs, CSIs, and PWMs. ZSIs can use either a voltage source or a current source as an input, and thus function as a buck-boost converter. To overcome all the drawbacks of the basic Z-source topology, many topologies have been introduced in Figure 1.13.

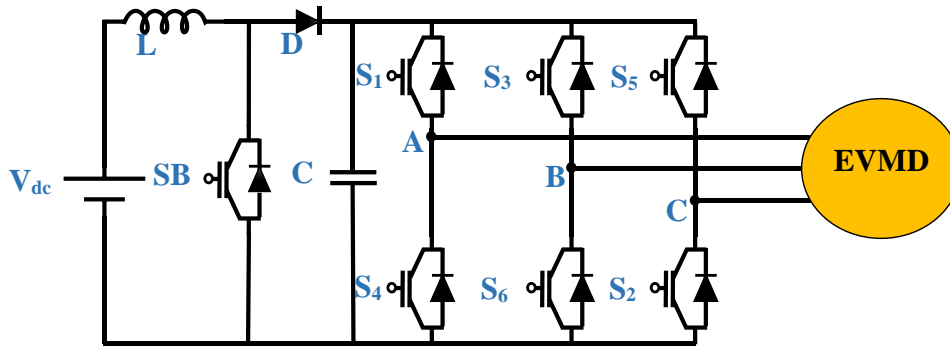


FIGURE 1.11: Current source inverter

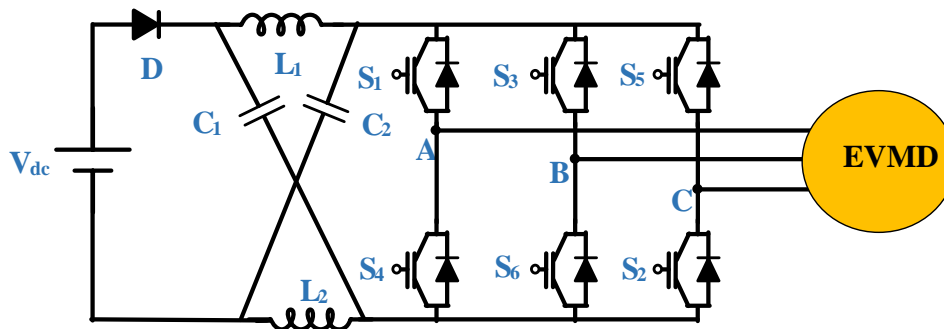


FIGURE 1.12: Impedance source inverter

DC-DC converters

The chopper is a static DC-DC converter that allows us to obtain from a fixed DC voltage source, a DC voltage source of adjustable average value with higher or lower value (voltage step-up or step-down). It is essentially made up of power switches (transistors, diodes . . .) and passive components (inductors, capacitors . . .). The latter acts by chopping the current of the load circuit, by the periodic opening-closing switching of a unidirectional switch. In EV systems, DC-DC converters can be isolated or non-isolated. These are classed as unidirectional or bidirectional based on the direction of power flow. In this section, various non-isolated/isolated topologies with unidirectional/bidirectional power flow are presented [54].

1. Buck converter

A Buck converter, also referred to as a series chopper, is a switching power supply that converts one DC voltage to a lower DC voltage. A well-designed Buck converter has great efficiency (up to 95%) and can control the output voltage. The operational cycle has two stages, with a chopping period T ($T = 1/f$).

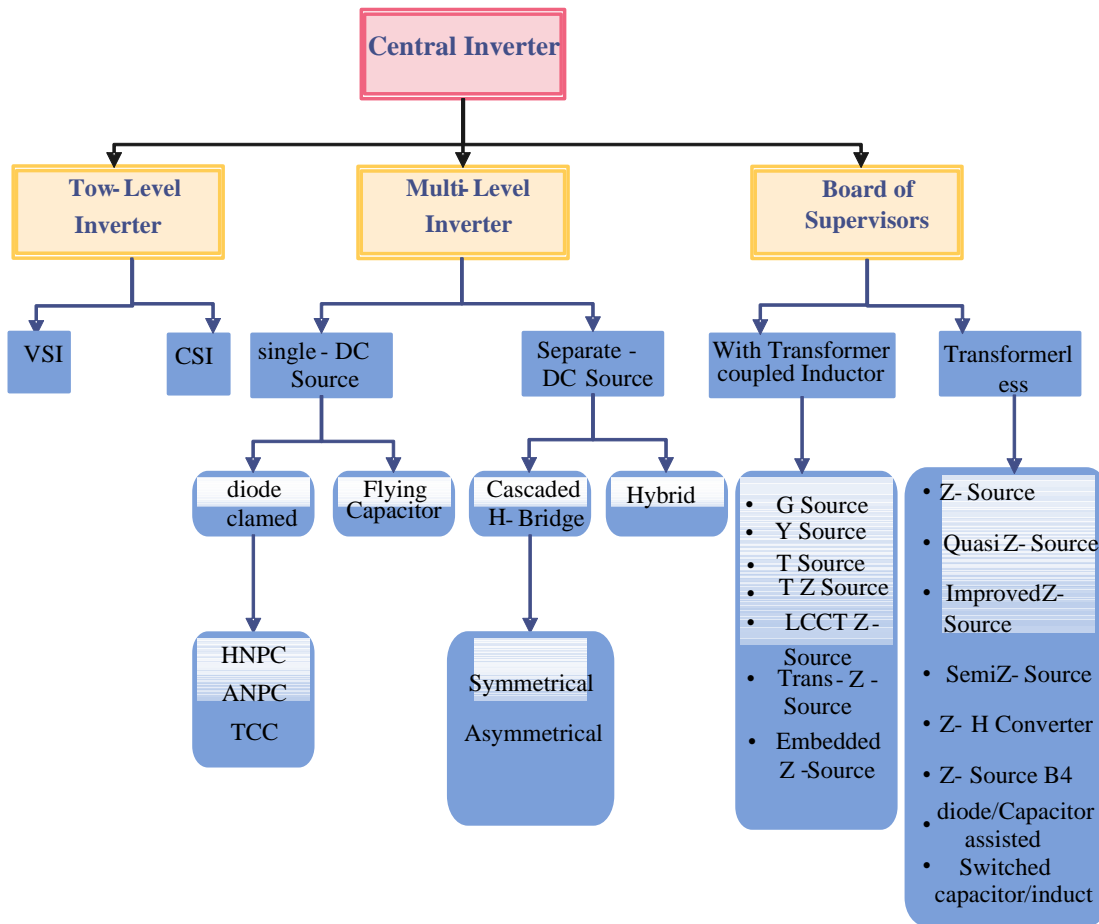


FIGURE 1.13: Inverters types

The transistor is turned on in the first stage, and the diode, which is polarized in reverse, is blocked. The initial zero current supplied by the generator increases linearly and passes through the inductance. This increase in current is opposed by the inductance, which produces an opposing voltage and retains the energy absorbed in a magnetic form. Due to the negative voltage across the diode, no current passes through it. The generator is shut off during the second, and no electricity flows through it. To maintain the continuation of the current in the inductor, the diode becomes conducting. The current flowing through the inductor is reduced. The inductor resists this current reduction by producing a voltage that converts it into a source for the downstream circuit by utilizing the magnetic energy stored [54].

2. Boost converter

The Boost converter (Figure 2.14(b)) is a step-up chopper. The operation of a boost converter can be divided into two distinct phases depending on the state of the switch. An energy accumulation phase: when the switch is closed (on state), this leads to an increase in the current in the inductance, thus storing a quantity of energy in the form of magnetic energy. The diode 'D' is then blocked and the load is then disconnected from the power supply. When the switch is open, the inductor is then in series with the generator and its e.m.f. is added to that of the generator

(booster effect). The current flowing through the inductor then crosses the diode, the capacitor and the load. The result is a transfer of the energy accumulated in the inductor to the capacitor [54].

3. Buck-boost converter

A Buck-Boost converter (Figure 2.14(c)) is a switching power supply that transforms a direct current voltage to a greater or lower direct current voltage. If the duty cycle is larger than 0.5, the converter runs in boost mode; otherwise, the converter functions in buck mode. One downside of this converter is that its switch lacks a terminal connected to zero, making control more difficult [54]. Depending on the state of the switch, the operation of a Buck-Boost converter can be separated into two modes:

- The switch is closed in the on state, increasing the energy stored in the inductor.
- The switch is open in the blocked state, the inductance is linked to the capacitor and the load. This causes the energy stored in the inductance to be transferred to the capacitance and the load.

4. Cuk converter

The Cuk converter is a variant of the standard buck-boost converter. It combines all of the benefits of fundamental DC-DC converter topologies, such as continuous input and output current and the flexibility to operate in both buck and boost mode. As shown in Fig. 5d, a Cuk converter consists of a switch (S1), two inductors (L1 and L2), two capacitors (C1 and Co), and a diode (D1). The main energy transfer element is the capacitor (C1), which is coupled to the input and output via D1 and S1, respectively. During the off-state of S1, the input source charges the capacitor C1 through L1 and D1. When S1 is turned on, the capacitor (C1) discharges its stored energy to the load via L2. The voltage sources are converted to equivalent current sources via the inductors (L1 and L2). This conversion is required to prevent excessive current from flowing via capacitor C1. The fundamental disadvantage of the Cuk converter is that the output voltage polarity is reversed in relation to the input voltage polarity [54].

5. SEPIC converter

The fundamental buck-boost topology is used to create a SEPIC converter, as shown in Fig. 5e. This converter is effectively a buck-boost converter and a boost converter combined. This converter can work in both buck and boost modes without reversing the output voltage polarity. The load terminal voltage can be controlled by adjusting the duty ratio of S1. When S1 is activated, L1 stores energy from the input, C1 delivers energy to L2, and Co supplies the load. As soon as S1 is opened, L1 transfers the stored energy to C1 and the load via D1. Furthermore, L2 transmits its stored energy to the load via D2. The disadvantages of the SEPIC converter include high output current ripple and the need for a large capacitor (C1) to transfer energy between the source and the load [54].

6. Zeta converter

A popular DC-DC converter architecture is created by rearranging the circuit parts of a SEPIC converter. This converter can transfer power in both buck and boost modes and generates continuous output current. This converter also generates output voltage with the same polarity as the input voltage. In comparison to the SEPIC converter, the zeta converter has a minimal output voltage ripple. However, its input current ripple is considerable, necessitating a big input capacitor. When switch S1 is turned on, the input supply energizes both L1 and L2. The energy from the capacitor (C1) is now transferred to L2 and the load. Two current loops form as S1 is turned off. L1's stored energy charges the capacitor (C1) in one loop, while L2 discharges to the load through D1 in another [54].

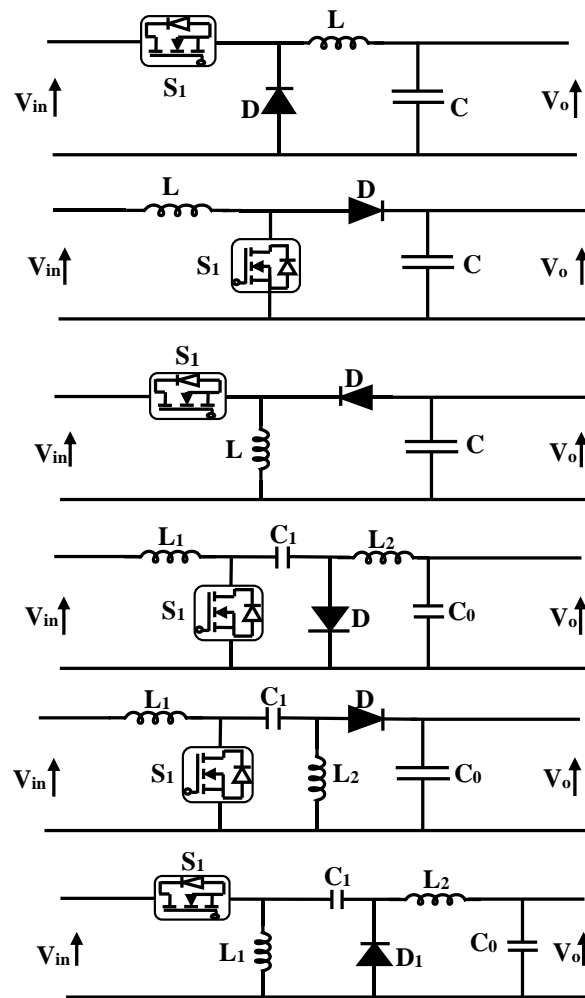


FIGURE 1.14: (a) Buck converter. (b) Boost converter. (c) Buck-boost converter. (d) Cuk converter. (e) SEPIC converter. (f) Zeta converter

7. Bi-directional DC-DC converters

The dc-dc converter in an electric powertrain of an electric and hybrid electric vehicle (EV/HEV) between the energy storage device and the inverter is used to condition the voltage levels and provide steady dc bus voltage [1]. Furthermore, the dc-dc converter must be capable of bidirectional power flow in order for regenerative energy to be captured and stored in the energy storage. Furthermore, some applications may necessitate overlapping input-output voltage ranges.

In recent years, there has been a surge in interest in vehicle-to-grid (V2G) mode operating to feed-back stored battery energy to the grid to meet peak energy demand. Various non-isolated bidirectional DC-DC converter topologies are depicted in Fig. 6(a-d). The topology in Fig. 15a runs in buck mode during G2V operation and in boost mode during V2G operation. Switch S_1 controls the buck operation, whereas switch S_2 controls the boost operation. Figure 15b depicts a bidirectional buck-boost converter that can operate in both G2V and V2G modes. The switches S_1 and S_2 in G2V and V2G mode operations respectively regulate the output voltage. Likewise, the bi-directional Cuk-Cuk and Zeta-SEPIC converters are shown in Figures 15c-d. The non-isolated converters described above have the advantage of fewer components, higher power density, and better efficiency, but they have the disadvantage of not being electrically isolated from the grid.

To ensure user safety, the load (battery) must be electrically isolated from the grid. Several isolated DC-DC converters, such as flyback converter, forward converter, half-bridge converter and full-bridge converter, are widely used in battery charging systems [54].

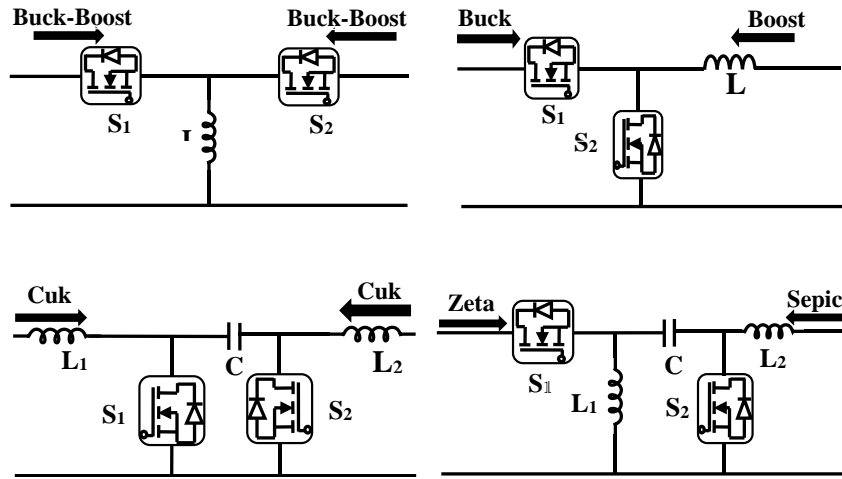


FIGURE 1.15: Non-isolated bidirectional DC-DC converter topologies

8. Flyback converter

The flyback architecture, depicted in Fig. 16, is a simple and low-cost isolated DC-DC converter with few components. This converter is based on the normal buck-boost converter, but the inductor has been replaced by a linked inductor (transformer). It employs a single controlled switch S1, as well as a high-frequency transformer (HFT) and a diode (Do). To reduce the size and weight of the flyback transformer, the switch is operated at a high switching frequency. The transformer acts as an electrical barrier between the grid and the load. When S1 is turned on, the transformer’s magnetizing inductance stores energy while the output diode (Do) is reverse-biased. When S1 is deactivated, the energy stored in the magnetizing inductance is supplied to the load via Do. A regulated output voltage is accomplished by adjusting the duty ratio of S1. The voltage gain of this converter is determined by the duty ratio and turns ratio of the HFT. Flyback converters, on the other hand, produce large voltage spikes across the switch (S1) due to the HFT’s leakage inductance. To reduce this voltage surge, snubber circuits are required. Flyback converters are common in low-power applications [54].

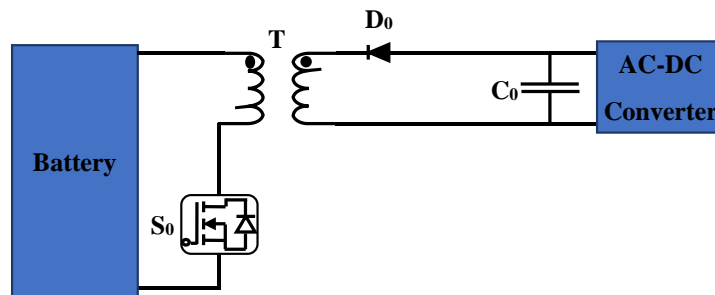


FIGURE 1.16: Flyback converter

9. Forward converter

The topology of the forward converter, as shown in Fig. 17, is nearly identical to that of a flyback converter with one extra diode linked in antiparallel with the LC filter. Another variation in circuit layout is the forward converter's output diode (D_o), which is connected in reverse polarity to the flyback converter's. When the switch S_1 is activated, current passes through the HFT's primary winding and power is transmitted to the load via D_o . When the switch is turned off, the forward-biased freewheeling diode D_1 begins conduction [54].

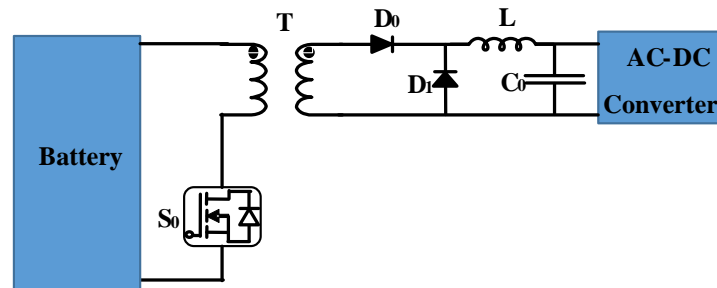


FIGURE 1.17: Forward converter

10. Half bridge converter

Although half-bridge and full-bridge converters can handle high amounts of power, they require a greater number of active and passive components. Power can be transferred in either direction using half-bridge and full-bridge converters. At the primary side of the HFT, a half-bridge bidirectional converter (shown in Fig. 18) employs two semiconductor switches (S_1 , S_2) with body diodes and two capacitors (C_{11} and C_{12}). The secondary side is made up of comparable components. When S_1 is turned on, half of the input voltage is impressed across the HFT's primary. The capacitor (C_{21}) is now charged via the body diode of S_3 . When S_2 is turned on, a reverse polarity voltage is impressed across the primary of the HFT, charging the capacitor (C_{22}) via the body diode of S_4 . As a result, the battery connected across the series combination of C_{21} and C_{22} receives power. In this mode, the switches on the primary side function as inverters, while the diodes on the secondary side function as rectifiers. If the battery energy is to be supplied back to the input side, the primary and secondary circuits' roles are reversed. Now, the secondary side switches (S_3 and S_4) operate in inverter mode, and the body diodes of S_1 and S_2 operate as rectifiers [54].

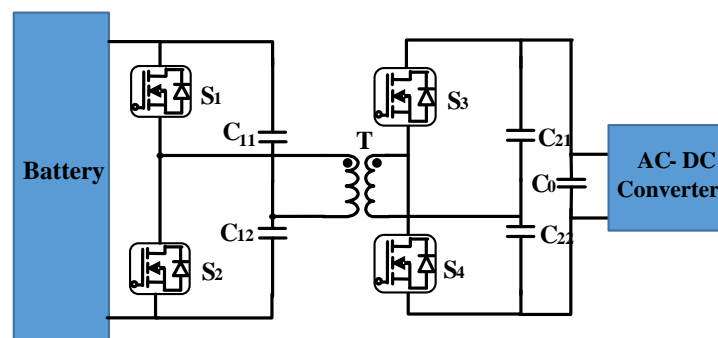


FIGURE 1.18: Half bridge bidirectional DC-DC converter

11. Full bridge converter

The operation of a full-bridge converter is similar to that of a half-bridge converter, with the exception that two diagonal switches (S_1, S_2 or S_3, S_4) are kept in the on state to impress supply voltage across the primary of the HFT. Through two diodes, the secondary induced voltage charges the output capacitor (C_0) (D_1, D_2 or D_3, D_4). In this case, the primary switches are inverters, while the secondary diodes are rectifiers. By running the secondary switches in inverter mode and the primary diodes as rectifiers, the bidirectional full-bridge converter depicted in Fig. 11 allows power to flow from the load (battery) to the input [54].

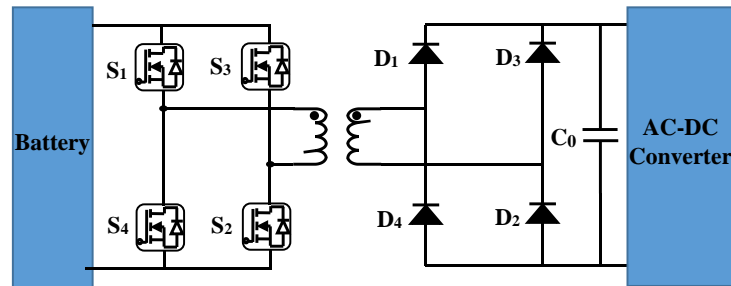


FIGURE 1.19: Full bridge converter

12. Four-Quadrant Converter

The four-quadrant converter is commonly used in DC-DC applications due to its ability to adjust the direction of the voltage source based on semiconductor control devices. Therefore, it is possible to be set apart in various ways to control. The simplified structure of the four quadrant (4-Q) DC-DC converter is illustrated in the figure.20 [55]. The four-quadrant DC-DC converter topology consists of four semiconductor switches each of which disposes a reversed biased diode, The DC motor is located in between the four pairs along with its armature resistance and armature inductance . The switching action of the control pairs leads to the generation of a DC voltage, while the generated current contributes in charging the inductance ; the latter will eventually act as a power source for the circuit [56].

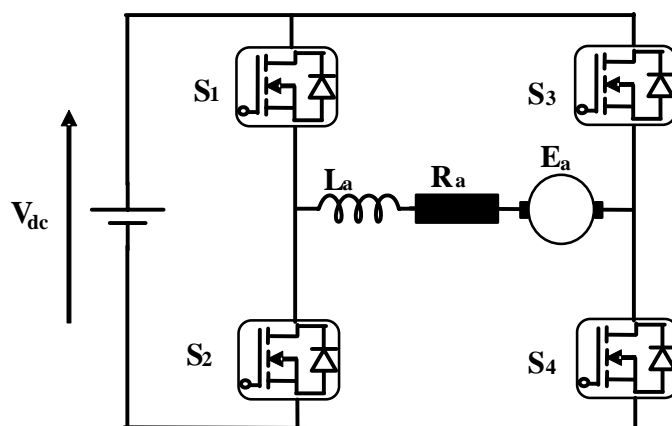


FIGURE 1.20: Four-quadrant DC-DC converter

1.4.4 Gear Box

The gearbox is coupled to the electric machine and transmits the torque from the machine to the wheels. This requires a transmission ratio between the torque and the machine. In the case of BEVs, the electric

machine is usually equipped with a gearbox with a fixed ratio. There are currently only a few exceptions of BEVs with more than one gear (but they cannot be considered here), such as the Rimac Concept Two and the Porsche Taycan. The literature review shows that the gearbox ratio of fixed-ratio BEVs varies in a range of 6 and 14. It is not possible to define an exact value because the required ratio depends on both the electric machine (maximum torque and speed) and the desired maximum speed of the vehicle.

The presence of a gearbox causes additional losses and therefore increases the vehicle's consumption. These losses can be attributed to the main components of the gearbox. A further distinction must be made between losses that are dependent on the operating point (load dependent) and those that are independent of the operating point (load independent) [20]: Gear losses include friction losses (which vary with load) and splash losses in the event of splash lubrication (load independent)

- Bearing losses: friction and lubrication losses (load dependent) (load independent).
- Losses as a result of sealing components
- Gearbox auxiliaries, such as oil pumps, cause losses.

Because of the vast range of gearbox losses, correct modeling of gearbox performance is extremely difficult, and it is dependent on the size and kind of component placed, as well as the operating points (speed and torque at the gearbox input shaft). As a result, most authors studied generally employ a constant figure that accounts for all gearbox losses. According to the literature, BEV gearboxes can reach great efficiency due to their small size and low number of moving parts. The identified gearbox efficiency range between 92% and 97% [20].



FIGURE 1.21: Gear box

1.4.5 Glider

A glider is a vehicle that does not include a powertrain (especially without an engine). The body, chassis, low-voltage electrical components, exterior, and interior are all part of it. A glider price can be computed from the bottom up or from the top down.

According to [20], using the top-down technique, the production costs of an existing car can be deduced from the selling price by assuming a surcharge factor. The production costs (material + labor + depreciation) are estimated to be roughly 60% of the selling price excluding taxes. After determining the total vehicle production costs, the powertrain costs are subtracted to yield the glider manufacturing costs.

The single component prices are determined and totaled to estimate glider costs using the bottom-up method. [20] presented typical costs for a variety of glider components which are listed in (Table 1.10). [20] also disclosed the costs of the materials used for the white body as well as the interior. Costs vary depending on optional features (for example, LED headlights) and vehicle size.

Component	Costs (€)
Windows	75
Window lifer	12
Exterior lights	140
Low-voltage electronics (excluding wiring harness)	520
Wiring harness	210
ESP	160
Airbag	20
HVDC	80
Seat warmer	10
Windshield wiper	30
Front seat	100
Body in white and exterior (ICEV)	1700
Body in white and exterior (BEV)	2100
Material	Specific Costs (€/kg)
Aluminium	2.5-4
High-strength steel	0.6-1
Plastic PP	1.6-2
Plastic ABS	2.5-3

TABLE 1.10: Cost of standard components of a glider based on reference [20]

1.4.6 Charging of the Electric Vehicle

AC Charging

Depending on the charging pace required, EV batteries can be charged from an AC or DC power supply at varying voltage or current levels. To charge the batteries, AC charging methods require AC-DC converters. AC charging systems are classified into three power levels according to Society of Automotive Engineers (SAE) specifications [17], [57].

- Level 1: The voltage is 120/240 V, and the current ranges from 12 to 16 amps depending on the charger rating. This method does not require any extra setup and may thus be utilized in household outlets. With this configuration, charging the batteries of small EVs can take anywhere from 0.5 to 12.5 hours. This feature qualifies the system for overnight charging.
- Level 2: in this level charging uses a direct connection to the grid through an electric vehicle service equipment (EVSE). An on-board charger is used for this system. The maximum power rating of the system is 240 V, 60 A and 14.4 kW. This system is used as a primary charging method for EVs.
- Level 3: This system uses a permanent hardwired power supply dedicated to EV charging, with power ratings above 14.4 kW. "Fast chargers," which recharge an average EV battery in 30 minutes or less, can be considered Level 3 chargers.

DC Charging

DC charging systems include dedicated wiring and installations that include a permanently wired charger, which is typically located in a parking lot or at a public charging station. DC charges are more efficient than AC chargers. In current DC charging stations, the output voltage level is automatically altered to meet the need of the battery packs. DC charging systems are further classified into three power levels.

- Level 1: Such systems have rated voltages, currents, and power ratings of 450 V, 80 A, and 36 kW, respectively.
- Level 2: It has the same voltage rating as Level 1, but its current and power ratings are 200 A and 90 kW, respectively.
- Level 3: This category's voltage, current, and power levels are 600 V, 400 A, and 240 kW, respectively.

Wireless charging

Wireless charging, also called as wireless power transfer (WPT), is gaining popularity due to the benefits it provides. This technology does not require the plugs and cables that are necessary in wired charging systems, there is no need to connect the cable to the car, there is a reduced risk of sparks and shocks in unclean or damp environments, and there is less chance of vandalism. Because of the health and safety problems connected with existing technology, this technology is not currently available for commercial EVs.

Pioneers in WPT research include R&D centers and government organizations such as Phillips Research Europe, the Energy Dynamic Laboratory (EDL), the US Department of Transportation (DOT), and the Department of Energy (DOE); universities such as the University of Tennessee, the University of British Columbia, and the Korea Advance Institute of Science and Technology (KAIST); and automobile manufacturers such as Daimler, Toyota, BMW, GM, and Chrysler. Witricity, LG, Evatran, HaloIPT (acquired by Qualcomm), Momentum Dynamics, and Conductix-Wampfler are among the companies that provide such technology [17]. There are various technologies being studied to supply WPT facilities. They differ in terms of operating frequency, efficiency, electromagnetic interference (EMI), and other aspects. Table 1.11 represents a comparison of wireless charging systems [17].

Wireless Charging System	Performance			Cost	Volume/Size	Complexity	Power level
	Efficiency	EMI	Frequency				
Inductive power transfer (IPT)	Medium	Medium	10-50 kHz	Medium	Medium	Medium	Medium/High
Capacitive power transfer (CPT)	Low	Medium	100-500 kHz	Low	Low	Medium	Low
Permanent magnet coupling power transfer (PMPT)	Low	High	100-500 kHz	High	High	High	Medium/Low
Resonant magnet coupling power transfer (RIPT)	Medium	Low	1 - 20 kHz	Medium	Medium	Medium	Medium/Low

Wireless Charging System	Performance			Cost	Volume/Size	Complexity	Power level
	Efficiency	EMI	Frequency				
On-line inductive power transfer (OLPT)	Medium	Medium	10 - 50 kHz	High	High	Medium	High
Resonant antennae power transfer (RAPT)	Medium	Medium	100-500 kHz	Medium	Medium	Medium	Medium/Low

TABLE 1.11: Comparison of wireless charging systems

On-board AC systems are used for the lowest power levels in contemporary EV systems, whereas DC systems are used for higher power levels. There are presently three existing standards for DC systems [16]:

- System of Combined Charging (CCS)
- CHAdeMO (CHArge de MOve, which translates as move by charge)
- Turbocharger (for Tesla vehicles)

1.5 Barriers of EV adoption

The adoption activity of EVs has been increasing since 2015. Yet, several barriers are still facing its widespread purchasing activity. Various articles investigated the modest electric mobility market and pointed to many barriers to the successful diffusion of EVs throughout the world. The identified barriers are classified into five categories: technical, social, economic, infrastructure, and policy.

1.5.1 Technical barriers

Range anxiety

Regarded as one of the major impediments to buying EVs, it is defined as the fear of blackout in the middle of the road, effecting the driver's daily trips or long trips. This is due to the limited amount of stored energy and can only travel as far as that energy allows. Range is further affected by vehicle speed, driving style, load carried, terrain, and energy-consuming equipment such as air conditioning. Users therefore experience "range anxiety" [17], [26], [39], as they worry about finding a charging station before the battery runs out.

Long charging period

Another significant drawback of EVs is the long time it takes them to charge. Depending on the type of charger and battery, charging can take anywhere from a few minutes to several hours, making EVs incompetent against internal combustion engine vehicles that take only a few minutes to charge. Hidrue et al. found that to reduce charging time by an hour, people are willing to pay between \$425 and \$3,250 [17]. One way to speed up charging time is to increase the voltage level and use better chargers. Some fast-charging facilities are currently available, and more are being considered. There are also fuel cell vehicles that do not require charging like other EVs. These vehicles only need to fill the hydrogen tank,

which is as convenient as filling a fuel tank, but fuel cell vehicles need a sufficient number of hydrogen refueling stations and a viable way to produce hydrogen to develop.

Safety concerns

The concerns about safety are rising mainly about the FCVs nowadays. There are speculations that, if hydrogen escapes the tanks it is kept into, can cause serious harm, as it is highly flammable. It has no color either, making a leak hard to notice. There is also the chance of the tanks to explode in case of a collision. To counter these problems, the automakers have taken measures to ensure the integrity of the tanks; they are wrapped with carbon fibers in case of the Toyota Mirai. In this car, the hydrogen handling parts are placed outside the cabin, allowing the gas to disperse easily in case of any leak, there are also arrangements to seal the tank outlet in case of high-speed collision [53].

1.5.2 Social barriers

Social acceptance

The adoption of a new and immature technology together with its consequences takes some time in society because it involves the change of certain habits [26]. The use of an EV in place of a conventional vehicle involves a change in driving habits, refueling habits, preparation for the use of alternative transportation in case of low battery, and these changes are not easy to embrace.

1.5.3 Economic barriers

ICVs have an economic advantage because they are sold at lower purchase prices than EVs. This relative advantage of ICVs hinders EV adoption, which is a significant barrier [17], [26], [39], [53]. Even though the total cost of ownership of electric vehicles is lower than that of ICEVs, due to fuel savings and lower maintenance costs, many potential EV users are not aware of these benefits and only compare the price of the two types of vehicles. In addition, battery replacement is one of the barriers due to the high cost of battery packs and their limited lifespan. In addition, because EVs use electricity as their primary energy source, high electricity prices do not motivate potential customers to purchase an EV, resulting in high charging costs compared to refueling an ICEV. Finally, the lack of monetary incentives, such as subsidies and tax exemptions, decreases customer interest in these types of vehicles.

1.5.4 Infrastructure barriers

Charging stations

The electrification of road traffic is highly dependent on the available charging infrastructure. Due to the shorter range and longer refueling times of BEVs, businesses and individuals must install charging infrastructure on their premises. This adds additional costs to the purchase and installation. Considering that not all public charging stations are compatible with all vehicles, finding a suitable charging station when the battery needs to be recharged becomes problematic. There is also the risk of having a charging station that is completely filled, with no capacity for another car. However, automakers are working to address this issue. Tesla and Nissan have developed their own charging networks in order to sell more electric vehicles. Hydrogen fueling stations are also in short supply. They are also required to expand the use of fuel cell electric vehicles. [17], [20], [26], [57] discusses a concept for locating hydrogen filling stations in California. It appears that a total of 68 such stations will be required to give service to FCVs in the region.

1.5.5 Policy barriers

Although some nations, particularly in Europe and Algeria, have already formed a clear strategy for climate neutrality and EV dissemination, others are currently experiencing difficulties. The government's lack of long-term planning and goals has been noted as an impediment to EV adoption. Similarly, the lack of a strategy for annual tax exemption encourages customers to convert to electric mobility [26], [57].

Chapter 2

Mathematical Modeling of the Traction System Components

The objective of this part of our work is the modeling of the drive train of our electric vehicle, which is powered by an electricity generation system. This generation uses two sources, such as fuel cells and batteries. The electricity coming from the sources via power converters ensures a continuous availability of energy for the electric motor to guarantee the traction of the vehicle. A power management strategy is used in order to improve the power flow in the EV.

2.1 DESCRIPTION OF THE TRACTION SYSTEM OF THE ELECTRIC VEHICLE

An EV powertrain arrangement is composed of three primary subsystems namely electric motor propulsion, power supply, and auxiliary systems. The vehicle controller, electronic power converter, electric motor, mechanical transmission, and drive wheels comprise the electric propulsion subsystem. The power source, power management unit, and power supply unit are all part of the power source subsystem. The power steering unit, the hotel air conditioning unit, and the auxiliary power supply unit are the main part of the auxiliary subsystem. The vehicle controller sends appropriate control signals to the electronic power converter, which regulates the power flow between the electric motor and the energy source based on control inputs from the gas and brake pedals. The EV's regenerative braking causes the energy to flow backward, and this regenerated energy can be returned to the energy source if the source is receptive. The majority of EV batteries, as well as UCs and flywheels, can receive regenerative energy. The latter is controlled by energy management units and energy recovery in conjunction with the vehicle controller. It also collaborates with the refueling unit in order to control it and monitor the energy source's usage. The auxiliary power supply delivers power at various voltage levels to all of the electric vehicle's auxiliaries, particularly the air conditioning and power steering components.

The schema illustrated in [Figure 2.1](#) demonstrates the components of the electric traction system based electric vehicle. The constituents are made up of: a battery supplied DC voltage source, a fuel cell, a

MOSFET based power converters, a control applied on two electric motors located in the rear of the electric vehicle connected to the two wheels [58] ,[59], [60].

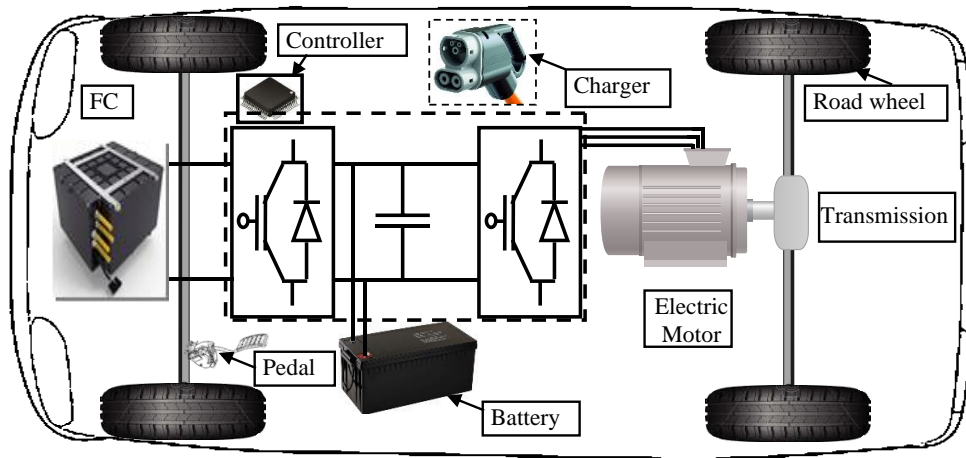


FIGURE 2.1: EV components

2.2 DYNAMIC MODELING OF THE EV

The propulsion system generates mechanical energy, which can either be stored in the vehicle as kinetic energy when the latter accelerates or as potential energy when the vehicle reaches higher altitudes.

The quantity of mechanical energy supplied by a vehicle when driving is primarily determined by three factors:

- losses due to aerodynamic friction.
- Losses due to rolling friction.
- Energy lost in the brakes.

The mechanical model presented in this section deduces the torque and driving force necessary for the operation of the vehicle [Figure 2.2](#). The propulsion system must provide a tractive effort at the wheel equal to the sum of the forces to overcome aerodynamic drag, rolling resistance, and road inclination. It must also provide the force required to accelerate the vehicle. The force required to pull the vehicle at the wheels is defined from the following equation [60], [61], [62], [63]:

$$F_T = F_{r_0} + F_{ad} + F_{cr} + F_{sf} \quad (2.1)$$

Where:

- F_{ad} : Aerodynamic drag
- F_{sf} : Stokes or viscous friction force
- F_{r_0} : Rolling resistance force
- F_{cr} : Slope resistance force

2.2.1 Rolling Resistance Force

$$F_{r_0} = C_d \cdot m \cdot g \cdot \cos(\alpha) \quad (2.2)$$

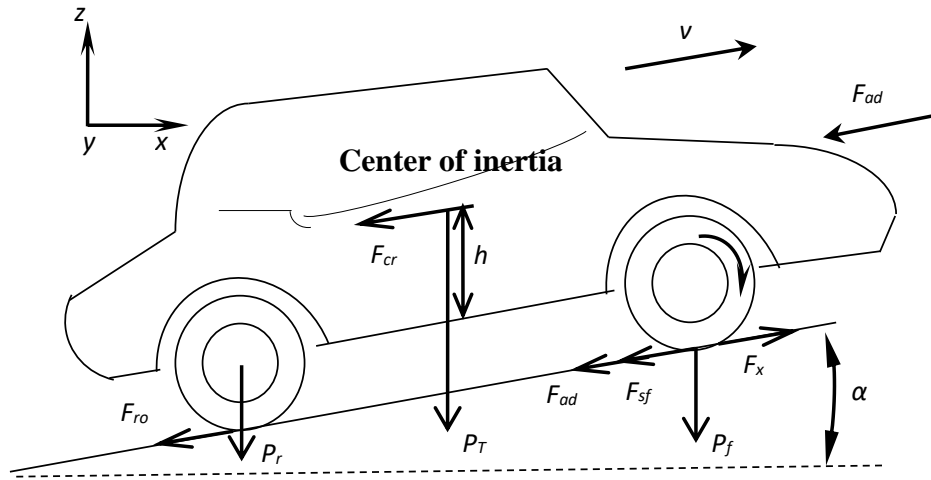


FIGURE 2.2: Elementary forces applied on an electric vehicle

- m : Vehicle weight (Kg).
 g : Gravitational acceleration (m/s^2)
 C_d : Rolling resistance coefficient of tires, it combines all the properties and physical phenomena that exist

2.2.2 Aerodynamic Drag

$$F_{ad} = \frac{1}{2} \cdot \rho \cdot C_f \cdot A_f (V_r)^2 = \frac{1}{2} \cdot \rho \cdot C_f \cdot A_f (V + V_W)^2 \quad (2.3)$$

- ρ : Air density ($\rho = 1.29 \text{ kg}/\text{m}^3$).
 C_f : Aerodynamic coefficient of friction of penetration in the air.
 A_f : Frontal surface of the vehicle (m^2).
 V_r : Relative speed of the vehicle (m/s)
 V : Vehicle speed (m/s)
 V_W : Wind speed (m/s).

2.2.3 Slope resistance force

$$F_{cr} = \pm m \cdot g \cdot \sin(\alpha) \quad (2.4)$$

2.2.4 Stokes or viscous friction force

$$F_{sf} = k_a V_r \quad (2.5)$$

- k_a : Stokes coefficient.

In the literature, researchers sometimes use the acceleration force F_a of the vehicle instead of the viscous friction force F_{sf} with [45]:

$$F_a = m \lambda \frac{dV_r}{dt} = m + \sum J \left(\frac{i^2}{r} \right) \frac{dV_r}{dt} \quad (2.6)$$

Where mass factor λ with $\lambda \in [1.06; 1.34]$, which depends on the engaged speed. J is the moment of inertia at the circumference of the driving wheel, i is the gearbox ratio and r is the wheel radius.

The electric motor provides the traction force of an electric vehicle that must overcome the load of the road. The equation of motion is then given by:

$$k_m m \frac{dv}{dt} F_{tr} - F_T \Leftrightarrow m_i a = F_{tr} - F_T \quad (2.7)$$

F_{tr} : Tire traction force.
 k_m : Rotational coefficient of inertia (mass factor).
 $m_i = k_m m$: Inertia mass of the vehicle.
 a : Acceleration of the vehicle.

The net force ($F_{tr} - F_T$) accelerates the vehicle, or decelerates it if F_T exceeds F_{tr} . The work is defined by the following expression:

$$\vec{w} = \sum_{i=1}^4 \vec{F}_i d\vec{x} \quad (2.8)$$

When the work is derived with respect to time, we will have the following expression:

$$p = \frac{d\vec{w}}{dt} = \vec{F} \left(\frac{d\vec{x}}{dt} \right) \Leftrightarrow p = \vec{F} \cdot v \quad (2.9)$$

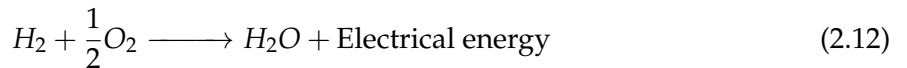
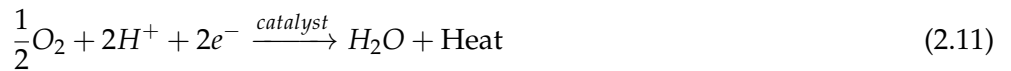
Where

p : is mechanical power.

2.3 ENERGY SOURCES AND ENERGY STORAGE SYSTEMS MODEL

2.3.1 Fuel Cell Modeling

FCs produce electricity through an electrochemical reaction, with the chemical energy being converted to electrical energy through the process of electrolysis. A fuel cell has an anode (A), a cathode (C) and an electrolyte (E) in between. The fuel is introduced into the anode, where it is oxidized, the ions created pass through the electrolyte to the cathode and combine with the other reactant. The electrons produced by the oxidation at the anode generate electricity based on the following equations [64], [65].



The change in the Gibbs free energy (ΔG) in a hydrogen fuel cell reaction is expressed as:

$$\Delta G_{FC} = G_{H_2O} - G_{H_2} - G_{O_2} \quad (2.13)$$

The change in the Gibbs varies with temperature, so the previous equation can be written as:

$$\Delta G_{FC} = \Delta G_0 - (T_{FC} - T_0)\Delta S_0 - RT_{FC} \ln \left(\frac{p_{H_2} p_{O_2}}{p_{H_2O}} \right) \quad (2.14)$$

For each mole of hydrogen, two moles of electrons pass around the external circuit and the resulted electrical work is:

$$\text{Electric l work} = -nFE \quad (2.15)$$

The open circuit voltage can be expressed as follows

$$E_{FC} = 0.229 - 0.85 \times 10^{-3}(T_{FC} - 298.15) + 4.3085 \times 10^{-5}T_{FC} \ln(p_{H_2}p_{O_2}^{0.5}) \quad (2.16)$$

The previous equation can be divided into two parts:

$$E_{FC} = E_0 - \Delta E_{FC} \quad (2.17)$$

Where

$$E_0 = \frac{\Delta G_0}{-2F} = 1.229 \quad (2.18)$$

And

$$\Delta E_{FC} = 0.85 \times 10^{-3}(T_{FC} - 298.15) - 4.3085 \times 10^{-5}T_{FC} \ln(p_{H_2}p_{O_2}^{0.5}) \quad (2.19)$$

When the fuel cell starts working the actual fuel cell voltage becomes:

$$V_{cell} = E_{FC} - \Delta V_{FC} \quad (2.20)$$

Where

$$\Delta V_{FC} = A_{FC} \ln\left(\frac{j_{FC}}{j_0}\right) + rj_{FC} + B \ln\left(1 - \frac{j_{FC}}{j_{lim}}\right) \quad (2.21)$$

j_{FC} is the fuel cell current density and it can be expressed as follows:

$$j_{FC} = \frac{i_{FC}}{S_{FC}} \quad (2.22)$$

For the FC stack of n_{FC} cells in series the gas flow of the consumed hydrogen and oxygen are described in the following equations:

$$q_{H_2} = \frac{n_{FC}}{2F} i_{FC} \quad (2.23)$$

$$q_{O_2} = \frac{n_{FC}}{4F} i_{FC} \quad (2.24)$$

The output voltage of the stack can be written as:

$$u_{FC} = n_{FC}V_{cell} \quad (2.25)$$

Finally, in an effort to represent the losses; which are due to the irreversibility of the fuel cell; the variable 'entropy flow is introduced, and the total power losses caused by the thermal flow are:

$$\Delta S_{total} = \Delta S_{E_{FC}} + \Delta S_{V_{cell}} \quad (2.26)$$

Where

$$\Delta S_{E_{FC}} = n_{FC} \frac{\Delta E_{FC} i_{FC}}{T_{FC}} \quad (2.27)$$

And

$$\Delta S_{V_{cell}} = n_{FC} \frac{\Delta V_{cell} i_{FC}}{T_{FC}} \quad (2.28)$$

Where

- ΔG_{FC} : Change in Gibbs free energy of the hydrogen fuel cell reaction
- G_{H_2O} : Gibbs free energy of H_2O
- G_{H_2} : Gibbs free energy of H_2
- G_{O_2} : Gibbs free energy of O_2
- ΔG_0 : Change in Gibbs free energy
- ΔS_0 : Entropy change in standard temperature
- T_0 : Standard temperature
- T_{FC} : Fuel cell temperature
- p_{H_2} : Hydrogen pressure
- p_{O_2} : Oxygen pressure
- p_{H_2O} : Water vapor pressure
- R : Universal gas constant $8.31451 (J/Kg.K)$
- n : Number of moles of electrons
- F : Faraday constant
- E : Fuel cell voltage
- E_{FC} : Theoretical thermodynamic voltage
- ΔE_{FC} : Voltage drop
- j_{FC} : Fuel cell current density
- i_{FC} : Fuel cell current
- S_{FC} : Active surface area

The overall output voltage of the fuel cell can be obtained as follows [66], [67]:

$$V_{PAC} = E_{nerst} - V_{oct} - V_{ohm} - V_{conc} \quad (2.29)$$

- E_{nerst} : The Nerst tension, which is the thermodynamic tension of the cells and depends on the temperatures and partial pressures of the reactants and products inside the stack.

$$\begin{cases} E_{nerst} = N_0 \left[E_0 + \frac{RT}{2F} \log \left(\frac{p_{H_2} p_{O_2}^{0.5}}{p_{H_2O}} \right) \right] \\ V_{ohm} = R_m I \end{cases} \quad (2.30)$$

- E_0 : Is the standard reversible cell potential (V)
- N_0 : Is the number of cells in the stack
- R : is the universal gas constant ($8.3145j \cdot mol^{-1}$)
- T : Is the temperature of the chimney (K)
- F : Is the Faraday constant ($96485A \cdot C \cdot mol^{-1}$)

Where: p_{H_2} , p_{O_2} , p_{H_2O} : are the partial pressures of hydrogen, oxygen and water respectively.

Figure 2.3 shows the fuel cell stack current-voltage characteristics curves for different temperatures, in order to evaluate the influence of the temperature on the stack voltage.

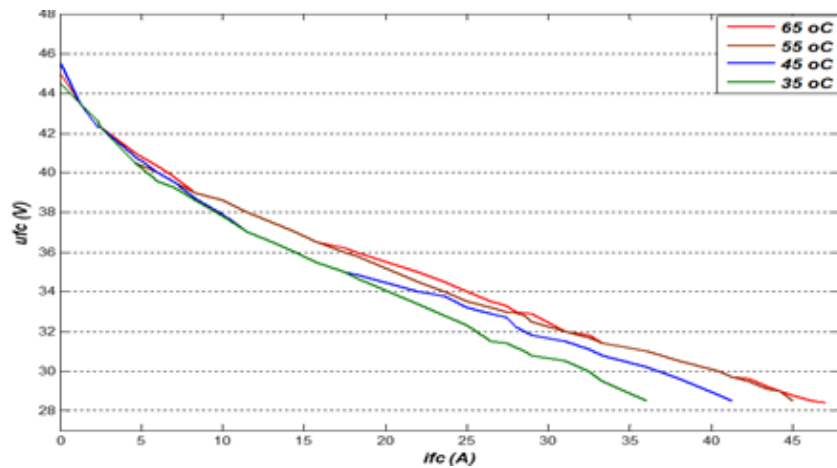


FIGURE 2.3: Fuel cell characteristics

2.3.2 Battery Modelling and Control

Batteries are energy storage devices consisting of one or more electrochemical cells that convert the chemical energy they contain into electrical energy. A distinction is made between primary and secondary batteries. Secondary batteries, which are preferred for automotive applications, are rechargeable, whereas primary batteries are not. The capacity of the battery is measured in ampere-hours (Ah) and its energy in watt-hours (Wh). It should be noted that the energy stored in the battery (capacity \times average voltage during discharge) must be correctly estimated in Wh. The usable SOC of the battery, expressed as a percentage, is particularly crucial as it reveals the state of charge available in the battery.

The electrical model of the battery is illustrated in the [Figure 2.4](#). [60], [68]

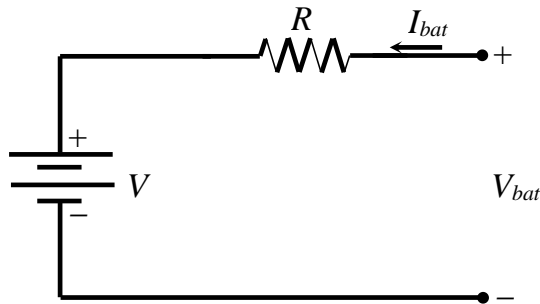


FIGURE 2.4: Battery model

Where:

$$v_{bat} = E_{bat} + R_{bat} I_{bat} \quad (2.31)$$

The battery capacity C_{bat} can be calculated as follows:

$$C_{bat} = C_0 \frac{1.67(1 + 0.005\Delta T)}{1 + 0.67 \left(\frac{I_{bat}}{I_0} \right)} \quad (2.32)$$

The state of charge of the battery is given as:

$$SOC = 1 - \frac{Q}{C_{bat}} \tag{2.33}$$

Where:

$$Q = I_{bat} \cdot t \tag{2.34}$$

V_{bat} and I_{bat} depend on the battery state of charge (soc), temperature variations and internal resistance R . This simple model study based on the “CIEMAT model” for the battery is considered sufficiently accurate to evaluate energy management objectives and compare the performance of several strategies. During the charging and discharging process, the state of charge (soc) in terms of time (t) can be expressed as [47]:

$$SOC(t) = \begin{cases} soc(t - \Delta t) + p_{bat} \cdot \frac{\eta_{ch}}{C_n \cdot V_{dc}} \cdot \Delta t \\ soc(t - \Delta t) + p_{bat} \cdot \frac{1}{\eta_{dis} \cdot C_n \cdot V_{dc}} \cdot \Delta t \end{cases} \tag{2.35}$$

With:

- Δt : is time variation.
- p_{bat} : represents the power of the battery.
- C_n : is the nominal capacity of the battery.
- η_{ch} : the efficiency of the battery during the charge.
- η_{dis} : the discharge phase.
- v_{dk} : is the nominal voltage of the DC bus. At any time step Δt , the SOC must respect the following constraints: $SOC_{min} \leq SOC_t \leq SOC_{max}$
- SOC_{min} and SOC_{max} are the minimum and maximum storage capacities allowed.

For the battery control (Figure 2.5), the purpose of the control system is to regulate the battery current in order to achieve the desired power, which is shown in references [60].

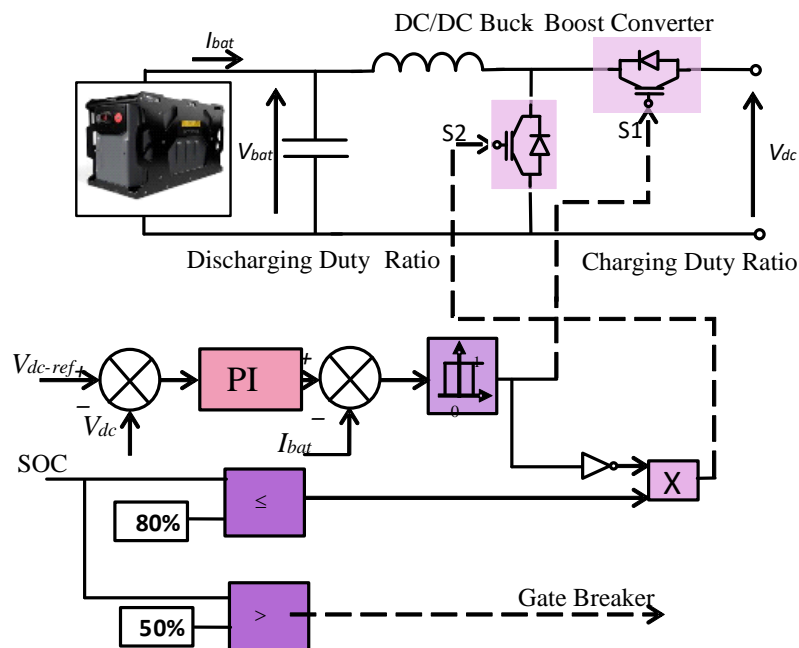


FIGURE 2.5: Battery control

2.3.3 Supercapacitor Modeling and Control

The supercapacitor; also referred to as an ultra-capacitor; is characterized by low series resistance, significant equivalent capacitance and a large number of charge/discharge cycles permitting a prolonged service duration. A capacitor stores energy via a static charge, as contrasted with an electrochemical reaction [69]. Figure 2.6 shows the equivalent average electrical model, a DC-DC buck-boost converter and a choke filter are associated with the supercapacitor tank as a means to adapt the voltage levels between the DC-DC converter and supercapacitor [70].

The super-capacitor tank can be modelled as follows [70]:

$$C_{sc} \frac{du_{sc}}{dt} = -i_{sc} \quad (2.36)$$

The choke filter model is written as follows:

$$L_{sc} \frac{di_{sc}}{dt} = u_{sc} - u_m \quad (2.37)$$

The average model can be described as follows:

$$\langle u_m \rangle = \langle m_{sc} \rangle u_{dc} \quad (2.38)$$

$$\langle i_m \rangle = \langle m_{sc} \rangle i_{sc} \quad (2.39)$$

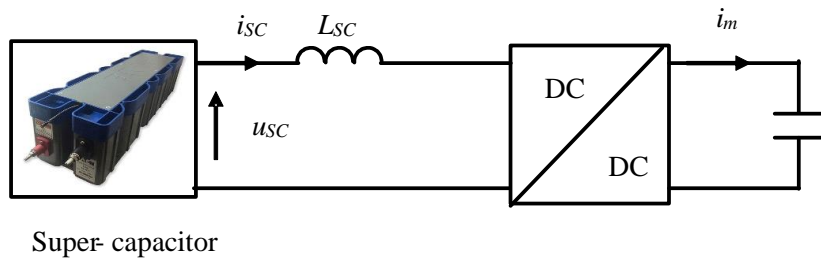


FIGURE 2.6: Supercapacitor electrical model

2.4 ELECTRIC ENGINES MODELING

2.4.1 Permanent Magnet DC Motor (PMDC) Modeling

The system structure of a DC motor is depicted in Figure 2.7. The bloc diagram of the PMDC motor is shown in Figure 2.8, it is used in industrial motion control systems like the electric vehicle, electric wheelchair, etc:

The dynamic equations of a PMDC motor are modelled using equations (5) - (8) [71].

$$V_a(t) = R_a i_a(t) + L_a \frac{di_a(t)}{dt} + E_a(t) \quad (2.40)$$

$$T(t) = J \frac{d\omega_r(t)}{dt} + f\omega_r(t) + T_L(t) \quad (2.41)$$

$$T(t) = K_t i_a(t) \quad (2.42)$$

$$E_a(t) = K_m \omega_r(t) \quad (2.43)$$

where R_a is the armature resistance, L_a is the winding leakage inductance, i_a is the armature current, E_a is the back electromotive force voltage, $K_m [Wb \cdot N \cdot m \cdot A^{-1}]$ is the velocity constant determined by the flux density of the permanent magnet, $\omega_r [rpm]$ is the rotational velocity of the armature and $v_a [V]$ is the voltage source.

Equations (2.40) and (2.41) can be rearranged using equation (2.42) and (2.43), we obtain:

$$\frac{di_a(t)}{dt} = -\frac{R_a}{L_a} i_a(t) - \frac{K_m}{L_a} \omega_r(t) + \frac{1}{L_a} v_a(t) \quad (2.44)$$

$$\frac{d\omega_r(t)}{dt} = \frac{K_m}{J} i_a(t) - \frac{f}{J} \omega_r(t) - \frac{T_L(t)}{J} \quad (2.45)$$

where J is the inertia of the rotor and the equivalent mechanical load, $f [N \cdot m \cdot rad/s]$ is the viscous friction coefficient, $T [N \cdot m]$ is the electromagnetic torque and $T_L [N \cdot m]$ is the load torque.

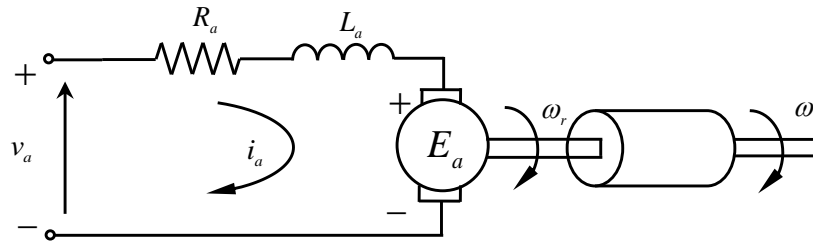


FIGURE 2.7: Schematic of PMDC motor

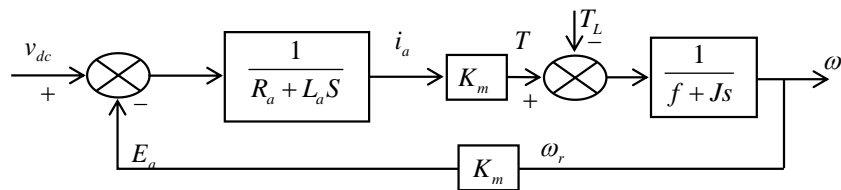


FIGURE 2.8: Bloc diagram of the PMDC motor

2.4.2 Permanent Magnet Synchronous Motor Modeling (PMSM)

Simplifying hypotheses

For the PMSM control application, the modeling of the permanent magnet synchronous machine is based on the electrical and mechanical parameters (the moment of inertia, viscous friction, resistances

and inductances, magnet excitation flux ...), which describe the electromagnetic and electromechanical phenomena, and the following simplifying assumptions [1], [72] :

- The hysteresis effect, the skin effect as well as the temperature effect and the losses in the steel are negligible.
- The machine operates in an unsaturated regime.
- The leakage resistances are independent of the rotor position.
- The distribution of the magnetomotive force is sinusoidal which allows us to consider only the first space harmonic of the M.M.F. distribution created by each armature phase.

PMSM equations in the reference frame (a, b, c)

The graphical representation of the (MSAP) is given in Figure 2.9 [73], [74].

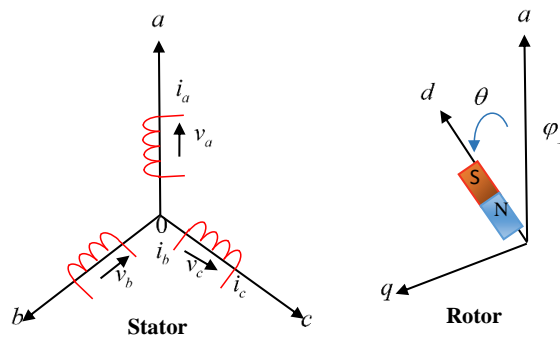


FIGURE 2.9: PMSM Graphical representation

In order to establish simple relationships between motor supply voltages and currents, we consider the MSAP model which includes three types of equations:

1. Electric equations:

The three-phase voltage equations can be written as follows:

$$[V_s] = [R_S] \cdot [i_s] + \frac{d[\phi_s]}{dt} \quad (2.46)$$

Where:

$$\begin{aligned}
 [V_s] &= [V_{sa} \quad V_{sb} \quad V_{sc}]^T && : \text{Stator voltage vector.} \\
 [i_s] &= [i_{sa} \quad i_{sb} \quad i_{sc}]^T && : \text{Stator current vector.} \\
 [\phi_s] &= [\phi_{sa} \quad \phi_{sb} \quad \phi_{sc}]^T && : \text{Stator flux vector.} \\
 [R_S] &= \begin{bmatrix} R_S & 0 & 0 \\ 0 & R_S & 0 \\ 0 & 0 & R_S \end{bmatrix} && : \text{Stator resistance matrix.}
 \end{aligned}$$

For all stator phases, the following equations can be deduced [75]:

$$\begin{bmatrix} V_{sa} \\ V_{sb} \\ V_{sc} \end{bmatrix} = \begin{bmatrix} R_S & 0 & 0 \\ 0 & R_S & 0 \\ 0 & 0 & R_S \end{bmatrix} \begin{bmatrix} i_{sa} \\ i_{sb} \\ i_{sc} \end{bmatrix} + \frac{d}{dt} \begin{bmatrix} \phi_{sa} \\ \phi_{sb} \\ \phi_{sc} \end{bmatrix} \quad (2.47)$$

The three-phase stator flux equations:

$$[\phi_s] = [L_s] \cdot [i_s] + [\phi_{sf}] \quad (2.48)$$

Where:

$$[L_S] = \begin{bmatrix} L_a & M_{ab} & M_{ac} \\ M_{ab} & L_b & M_{bc} \\ M_{ac} & M_{bc} & L_c \end{bmatrix} \quad (2.49)$$

With:

$[L_S]$: Stator inductance matrix.
L_a, L_b, L_c	: The proper inductances of the three phases a, b and c .
M_{ab}, M_{bc}, M_{ac}	: Mutual inductances between phases.
$[\phi_f]$: Flux vector generated by the magnet defined by the following equation:

$$[\phi_{sf}] = \begin{bmatrix} \phi_{af} \\ \phi_{bf} \\ \phi_{cf} \end{bmatrix} = \begin{bmatrix} \phi_f \cos p\theta \\ \phi_f \cos(p\theta - \frac{2\pi}{3}) \\ \phi_f \cos(p\theta + \frac{2\pi}{3}) \end{bmatrix} \quad (2.50)$$

ϕ_f	: The constant peak value of the flux created by the smooth magnet through the stator windings.
θ	: Load angle designating the position of the rotor with respect to the stator defined by:

$$\theta(t) = \int_0^t \omega_r dt \quad (2.51)$$

Taking into account the following equation :

$$\omega_r = \frac{\omega}{p} \quad (2.52)$$

With:

ω_r	: Rotor speed (rad/s).
ω	: Pulsation of alternating currents (rad/s).
p	: Number of pole pairs.

2. Mechanical equations

The application of Newton's 2nd law gives the fundamental equation of mechanics describing the dynamics of the rotor of the machine [76]:

$$J_m \dot{\omega}_r + f_m \omega_r = C_{em} - C_r \quad (2.53)$$

With:

- J_m : Moment of inertia.
- f_m : Friction coefficient.
- C_{em} : Electromagnetic couple.
- C_r : Resistant couple

3. Transformation of Park

The Park transformation [Figure 2.10](#) is a mathematical technique which consists in transforming the three-phase system (a, b, c) into a two-phase system (d, q) . This mathematical passage, transforms the three fixed stator coils out of phase by $2\pi/3$ into two equivalent fictitious coils out of phase by $\pi/2$ and located on the rotor magnet, is located on the d axis. This transformation makes the dynamic equations of AC motors simpler which facilitates their studies and analyses.

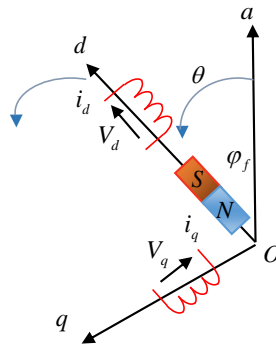


FIGURE 2.10: Graphical representation of Park transformation

The transition from the real three-phase system to the rotor-related (d, q) system is done using the following relations [1]:

$$\begin{cases} [V_{dpo}] = p(\theta) \cdot [V_{Sabc}] \\ [i_{dpo}] = p(\theta) \cdot [i_{Sabc}] \\ [\phi_{dpo}] = p(\theta) \cdot [\phi_{Sabc}] \end{cases} \quad (2.54)$$

$P(\theta)$: The transformation matrix defined by :

$$P(\theta) = \frac{2}{3} \begin{bmatrix} \cos(\theta) & \cos(\theta - \frac{2\pi}{3}) & \cos(\theta - \frac{4\pi}{3}) \\ -\sin(\theta) & -\sin(\theta - \frac{2\pi}{3}) & -\sin(\theta - \frac{4\pi}{3}) \\ \frac{1}{2} & \frac{1}{2} & \frac{1}{2} \end{bmatrix} \quad (2.55)$$

The inverse Park transformation is necessary to return to three-phase quantities, it is defined by [61] :

$$p(\theta)^T = \frac{2}{3} \begin{bmatrix} \cos(\theta) & -\sin(\theta) & 1 \\ \cos(\theta - \frac{2\pi}{3}) & -\sin(\theta - \frac{2\pi}{3}) & 1 \\ \cos(\theta - \frac{4\pi}{3}) & -\sin(\theta - \frac{4\pi}{3}) & 1 \end{bmatrix} \quad (2.56)$$

4. State space equations of the PMSM

The final form of the MSAP model can be deduced in the d - q frame of reference in normal operation, i.e., the only unknown disturbance is the load torque applied to the machine and we consider the voltages (V_d, V_q) and the excitation flux (ϕ_m) as control quantities, the stator currents (I_d, I_q) as state variables [1].

This will allow writing the Equation 2.57

$$\begin{cases} V_d = R_S I_d + \frac{d\phi_d}{dt} - \omega_r \phi_q \\ V_q = R_S I_q + \frac{d\phi_q}{dt} + \omega_r \phi_d \end{cases} \quad (2.57)$$

in the following form :

$$\frac{d}{dt} [X] = [A] [X] + [B] [U] \quad (2.58)$$

With:

X : State space vector.

U : Control vector.

A : Fundamental matrix that characterizes the system.

B : Control application matrix.

$$\begin{cases} V_d = R_S I_d + L_d \frac{dI_d}{dt} - L_q \omega I_q \\ V_q = R_S I_q + L_q \frac{dI_q}{dt} - L_d \omega I_d + \omega \phi_f \end{cases} \Rightarrow \begin{cases} \frac{dI_d}{dt} = \frac{-R_S}{L_d} I_d + \frac{L_q}{L_d} \omega I_q + \frac{1}{L_d} V_d \\ \frac{dI_q}{dt} = \frac{-R_S}{L_q} I_q + \frac{L_d}{L_q} \omega I_d + \frac{1}{L_q} V_q - \frac{1}{L_q} \omega \phi_f \end{cases} \quad (2.59)$$

In matrix format :

$$\begin{bmatrix} \frac{dI_d}{dt} \\ \frac{dI_q}{dt} \end{bmatrix} = \begin{bmatrix} \frac{-R_S}{L_d} & \frac{L_q}{L_d} \omega \\ -\frac{L_d}{L_q} \omega & \frac{-R_S}{L_q} \end{bmatrix} \begin{bmatrix} I_d \\ I_q \end{bmatrix} + \begin{bmatrix} \frac{1}{L_d} & 0 & 0 \\ 0 & \frac{1}{L_q} & -\frac{1}{L_q} \omega \end{bmatrix} \begin{bmatrix} V_d \\ V_q \\ \phi_f \end{bmatrix} \quad (2.60)$$

Assuming that :

$$X = \begin{bmatrix} I_d \\ I_q \end{bmatrix}; \quad U = \begin{bmatrix} V_d \\ V_q \\ \phi_f \end{bmatrix}; \quad Y = \begin{bmatrix} I_d \\ I_q \end{bmatrix}$$

$$A = \begin{bmatrix} \frac{-R_S}{L_d} & \frac{L_q}{L_d} \omega \\ -\frac{L_d}{L_q} \omega & \frac{-R_S}{L_q} \end{bmatrix}; \quad B = \begin{bmatrix} \frac{1}{L_d} & 0 & 0 \\ 0 & \frac{1}{L_q} & \frac{1}{L_q} \end{bmatrix}; \quad C = \begin{bmatrix} 1 & 0 \\ 0 & 1 \end{bmatrix}$$

The mechanical equation is given by:

$$f \Omega + J \frac{d\Omega}{dt} = C_{em} - C_r$$

$$C_e = \frac{3}{2} p [(L_d - L_q) I_d I_q + \phi_f I_q] \quad (2.61)$$

$$\Omega = \frac{\omega}{p}$$

5. Equations of the machine in d-q axes

Electric equations :

$$\begin{cases} V_d = R_S \cdot I_d - \omega_r \cdot \phi_q + \frac{d}{dt}(\phi_d) \\ V_q = R_S \cdot I_q + \omega_r \cdot \phi_d + \frac{d}{dt}(\phi_q) \end{cases} \quad (2.62)$$

Magnetic equations :

$$\begin{cases} (\phi_d) = L_d \cdot I_q + \phi_f \\ (\phi_q) = L_q \cdot I_d \end{cases} \quad (2.63)$$

Replacing ϕ_d and ϕ_q by their expression (2.62) in (2.63) we will have:

$$\begin{cases} V_d = R_S \cdot I_d - \omega_r \cdot L_q \cdot L_q + L_d \cdot \frac{d}{dt}(I_d) \\ V_q = R_S \cdot I_q + \omega_r \cdot L_d \cdot I_d + L_q \cdot \frac{d}{dt}(I_q) + \omega_r \cdot \phi_f \end{cases} \quad (2.64)$$

By applying the LAPLACE transformation to the previous equation we find:

$$\begin{cases} V_d(S) = (R_S + SL_d) \cdot I_d(S) - \omega_r(S) \cdot L_q \cdot I_q(S) \\ V_q(S) = (R_S + SL_q) \cdot I_q(S) - \omega_r(S) \cdot L_d \cdot I_d(S) + \omega_r(S) \cdot \phi_f \end{cases} \quad (2.65)$$

Where S is LAPLACE operator

In matrix form we can write :

$$\begin{bmatrix} V_d \\ V_q \end{bmatrix} = \begin{bmatrix} (R_S + SL_d) - \omega_r \cdot L_q \\ \omega_r \cdot L_d (R_S + SL_q) \end{bmatrix} \cdot \begin{bmatrix} I_d \\ I_q \end{bmatrix} + \begin{bmatrix} 0 \\ \omega_r \cdot \phi_f \end{bmatrix} \quad (2.66)$$

The electromagnetic torque in the PARK referential is written as follows:

$$C_{em} = \frac{3}{2} \cdot p \cdot (\phi_d \cdot I_q - \phi_q \cdot I_d) \quad (2.67)$$

By replacing equation (2.63) in (2.67) the expression of the electromagnetic torque becomes :

$$C_{em} = \frac{3}{2} \cdot p \cdot [(L_d - L_q) \cdot L_d \cdot I_q + \phi_q \cdot I_q] \quad (2.68)$$

Note that:

- $\phi_q \cdot I_q$: The electromagnetic torque of a smooth pole machine.
- $(L_d - L_q) \cdot I_d \cdot I_q$: Additional torque due to rotor salience.

Mechanical equation :

$$J \cdot \frac{d\Omega}{dx} = C_{em} - C_r - f_r \cdot \Omega \quad (2.69)$$

2.5 POWER CONVERTERS MODELING

2.5.1 DC-DC Boost Converter Modeling

A parallel chopper gives a voltage at the output that is greater than that at the input [77], [78]. Figure 2.11 represents the structure of a Boost chopper used to increase the available voltage of a DC source

- **First case:** S is passing D is blocked (Figure 2.12)

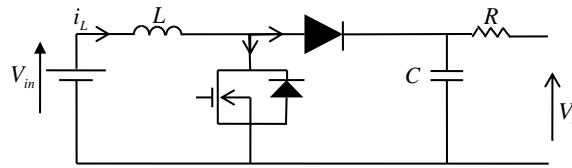


FIGURE 2.11: Boost converter scheme

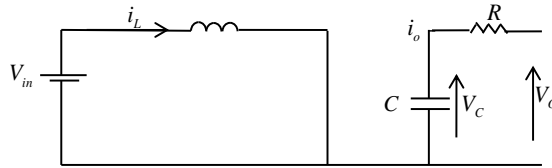


FIGURE 2.12: Boost circuit when the MOSFET is closed

$$\begin{cases} V_{in} = L \frac{dI_L}{dt} \\ \frac{dI_L}{dt} = \frac{1}{L} V_{in} \\ \frac{1}{R}(V_C - V_0) - C \frac{dV}{dt} = 0 \\ \frac{dV_C}{dt} = \frac{1}{RC}(V_C - V_0) \end{cases} \quad (2.70)$$

State space model can be written as:

$$X = A_1 X + B_1 U \quad (2.71)$$

With:

$$\begin{cases} U = \begin{bmatrix} V_{in} \\ V_0 \end{bmatrix} \\ X = \begin{bmatrix} I_L \\ V_C \end{bmatrix} \end{cases} \quad (2.72)$$

Therefore:

$$\begin{bmatrix} \frac{dI_L}{dt} \\ \frac{dV_C}{dt} \end{bmatrix} = \begin{bmatrix} 0 & 0 \\ 0 & \frac{1}{RC} \end{bmatrix} \begin{bmatrix} I_L \\ V_C \end{bmatrix} + \begin{bmatrix} \frac{1}{L} & 0 \\ 0 & -\frac{1}{RC} \end{bmatrix} \begin{bmatrix} V_{in} \\ V_0 \end{bmatrix} \quad (2.73)$$

- **Second case:** *S* is blocked *D* is passing (Figure 2.13)

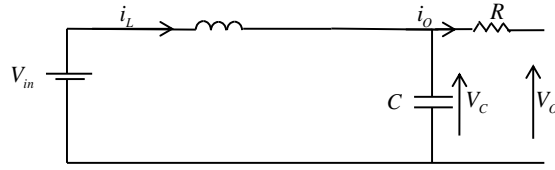


FIGURE 2.13: Boost circuit when the MOSFET is open

$$\begin{cases} V_{in} = L \frac{dI_L}{dt} + V_C \\ \frac{dI_L}{dt} = -\frac{1}{L} V_C + \frac{1}{L} V_{in} \\ I_L = C \frac{dV_C}{dt} + \frac{1}{R} (V_C - V_0) \\ \frac{dV_C}{dt} = \frac{1}{C} I_L + \frac{1}{RC} (-V_C + V_0) \end{cases} \quad (2.74)$$

The state space model can be written as follows :

$$X = A_2 X + B_2 U \quad (2.75)$$

Hence, it can be written as follows :

$$\begin{bmatrix} \frac{dI_L}{dt} \\ \frac{dV_C}{dt} \end{bmatrix} = \begin{bmatrix} 0 & -\frac{1}{L} \\ \frac{1}{C} & \frac{1}{RC} \end{bmatrix} \begin{bmatrix} I_L \\ V_C \end{bmatrix} + \begin{bmatrix} \frac{1}{L} & 0 \\ 0 & \frac{1}{RC} \end{bmatrix} \begin{bmatrix} V_{in} \\ V_0 \end{bmatrix} \quad (2.76)$$

The state space average model can then be obtained by the following :

$$\begin{cases} X = AX + BU \\ A = A_1 \cdot d + A_2(1 - d) \\ B = B_1 \cdot d + B_2(1 - d) \end{cases} \quad (2.77)$$

Thus, the matrices A and B can be calculated as follows:

$$A = \begin{bmatrix} 0 & \frac{-(1-d)}{L} \\ \frac{1-d}{C} & -\frac{1}{RC} \end{bmatrix} \quad \text{and} \quad B = \begin{bmatrix} \frac{1}{L} & 0 \\ 0 & \frac{1}{RC} \end{bmatrix} \quad (2.78)$$

Which leads us to the following :

$$\begin{cases} L \frac{dI_L}{dt} = -(1-d)V_C + V_{in} \\ \frac{dV_C}{dt} = \frac{1-d}{L} I_L - \frac{1}{RC} V_C + \frac{1}{RC} V_0 \end{cases} \quad (2.79)$$

The control law is giving by the following:

$$\begin{cases} L \frac{di_L}{dt} = U \\ d = 1 + \frac{U - V_{in}}{V_C} \end{cases} \quad (2.80)$$

2.5.2 Bidirectional DC-DC Buck Boost Converter Modeling

A buck-boost is a DC-DC converter that provides a controlled output voltage higher or lower than the input voltage level. The converter topology shown in Figure 2.14 consists of a DC input voltage source v_{bat} , two controlled switches, a filter inductor (L), a filter capacitor (C), and output voltage v_{dc} .

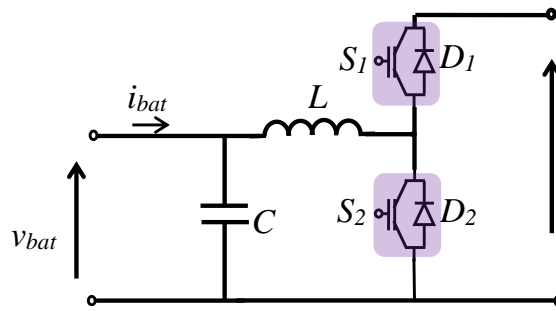


FIGURE 2.14: DC-DC Buck-Boost model

When the switch (S_1) is on for a time D_T , where D is the duty ratio and T is the period, the switch conducts the inductor current and the diode becomes reverse biased. A voltage occurs across the inductor. This voltage leads to an increase in the inductor current i_L .

When the switch is turned off, the inductor current i_L continues to circle because of the energy stored in the inductor. This current flows through the diode and the voltage across the inductor becomes $v_L = -v_{dc}$ for the time $(1 - D)T$ until the switch is turned on again.

The mathematical model of the DC-DC Buck-Boost converter can be done using the equations obtained from the figures shown in Figure 2.15, (a) is for the forward mode where the energy flows from the battery to the DC output, and (b) is dedicated to the reverse mode where the energy flows from the DC output back to battery [79], [80].

Introducing u the control output, representing the switch position function, its values vary from 1 when the switch is ON and 0 when the switch is OFF.

The state-space model of the buck-boost converter can be written as follows [81]:

$$\frac{di_L}{dt} = (1 - u) \frac{v_C}{L} + \frac{v_{bat}}{L} u \quad (2.81)$$

$$\frac{dv_C}{dt} = (1 - u) \frac{i_L}{C} - \frac{v_C}{RC} \quad (2.82)$$

2.5.3 Modeling of the Two-Level Voltage Inverter

The inverter is a static converter ensuring the DC-AC conversion, it allows to impose at the terminals of the machine voltages of amplitude and frequency adjustable by the control [81], [82]. There are several

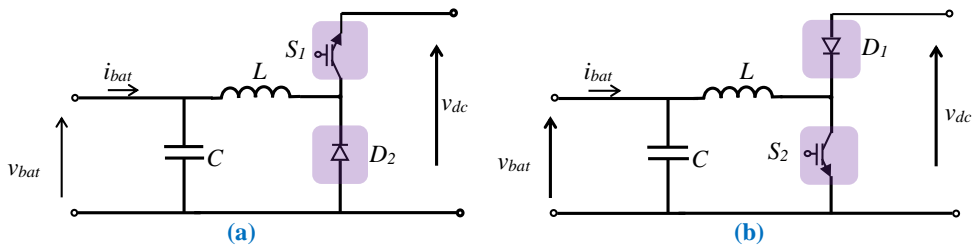


FIGURE 2.15: Buck-Boost model in two transfer directions (a) From v_{bat} to v_{dc} (forward mode), (b) From v_{dc} to v_{bat} (reverse mode)

types of inverters:

- According to the source:
- Voltage inverters.
- Current inverters.
- According to the number of phases (single-phase, three-phase).
- According to the number of levels (2,3, etc.).

Figure 2.16 shows a diagram of the PMSM permanent magnet synchronous motor supply by a two-level voltage inverter.

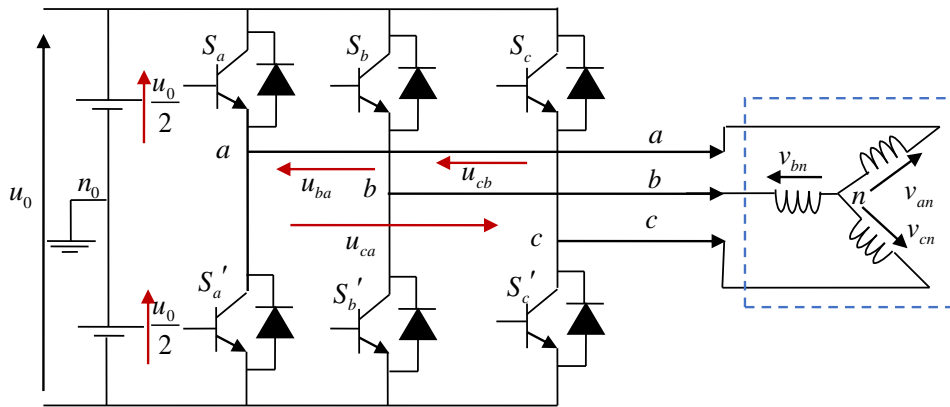


FIGURE 2.16: Schematic of the two-level voltage inverter

To obtain an AC voltage, the input DC voltage must be split and applied to the load in one direction and in the other. The inverter supplied by a perfect voltage source imposes at its output, thanks to the opening and closing of the switches, an alternating voltage formed by a succession of two-level rectangular slots. The operating frequency is fixed by the control of the switches.

In order to avoid the short-circuit of the DC voltage source, the controls of the switches of the same arm are complementary.

Considering an ideal converter, hence the following hypotheses:

- The switching of the components is instantaneous.
- The voltage drops at their terminals are negligible.

- The load is three-phase balanced and star-connected with isolated neutral point.

The simple voltages as a function of the voltages measured between the points a, b, c and the fictitious middle point are then given by:

$$\begin{cases} V_{an} = \frac{1}{3}(2V_{an0} - V_{bn0} - V_{cn0}) \\ V_{bn} = \frac{1}{3}(2V_{bn0} - V_{an0} - V_{cn0}) \\ V_{cn} = \frac{1}{3}(2V_{cn0} - V_{an0} - V_{bn0}) \end{cases} \quad (2.83)$$

Finally, we obtain in matrix form :

$$\begin{bmatrix} V_{an} \\ V_{bn} \\ V_{cn} \end{bmatrix} = \frac{1}{3} \begin{bmatrix} 2 & -1 & -1 \\ -1 & 2 & -1 \\ -1 & -1 & 2 \end{bmatrix} \begin{bmatrix} V_{an0} \\ V_{bn0} \\ V_{cn0} \end{bmatrix} \quad (2.84)$$

For a three-phase inverter, the switch commands of one arm are complementary. For each arm there are two independent states. These two states can be considered as a Boolean quantity such as :

- $S_{a,b,c} = 1$: Switches of the upper arm are closed and switches of the lower arm are open.
- $S_{a,b,c} = 0$: Switches of the upper half arm are open and switches of the lower half arm are closed.

This allows us to write :

$$\begin{bmatrix} V_{an0} \\ V_{bn0} \\ V_{cn0} \end{bmatrix} = U_0 \begin{bmatrix} S_a \\ S_b \\ S_c \end{bmatrix} \quad (2.85)$$

The converter is modeled by the following connection matrix:

$$\begin{bmatrix} V_{an} \\ V_{bn} \\ V_{cn} \end{bmatrix} = \frac{1}{3} \begin{bmatrix} 2 & -1 & -1 \\ -1 & 2 & -1 \\ -1 & -1 & 2 \end{bmatrix} U_0 \begin{bmatrix} S_a \\ S_b \\ S_c \end{bmatrix} \quad (2.86)$$

Pulse Width Modulation (PWM) control

The PWM. is realized by comparing a low frequency modulating wave (reference voltage) to a high frequency carrier wave of triangular shape. The switching times of the switches are determined by the intersection points between the carrier and the modulating wave. The schematic diagram of this technique is given in [Figure 2.17](#).

[Figure 2.18](#) shows the commutation instants of the switches

This technique is characterized by the following two parameters:

$$m = \frac{f_p}{f_r} \quad (2.87)$$

With:

- m : The modulation index which defines the ratio between the carrier frequency and the reference frequency.

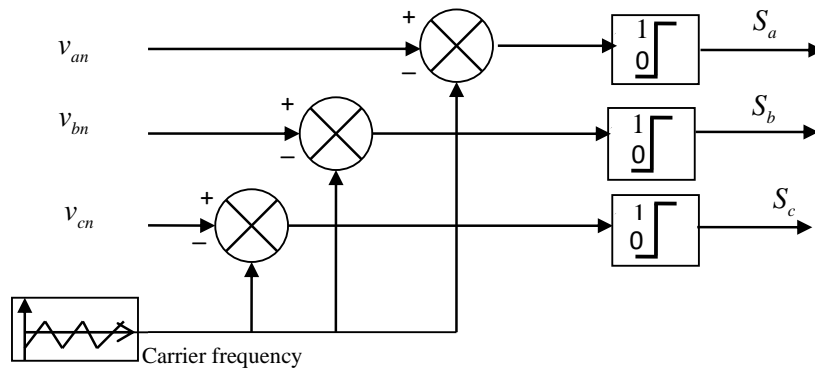


FIGURE 2.17: Principle diagram of the PWM

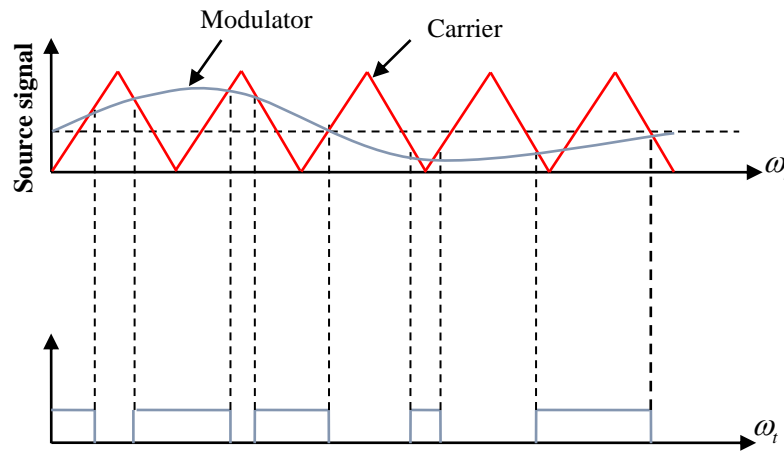


FIGURE 2.18: PWM technique

$$r = \frac{V_r}{V_p} \tag{2.88}$$

Where:

r : The modulation rate (or adjustment coefficient) which gives the ratio of the amplitude of the modulator to the peak value of the carrier.

2.5.4 Description and Modeling of the Z-Source Inverter

Figure 2.19 shows basic topology of the ZSI, which looks like a lattice network containing two inductors (L1 and L2) and two capacitors (c1 and c2) connected in X shape to couple the inverter to DC voltage source, the latter can be a battery, fuel cell, photovoltaic array, diode rectifier, thyristor converter, inductor, capacitor or combination of inductor and capacitor. The full bridge consists of two legs, each of which contains two mutually complementary switches. Thus, the load will be continuously supplied by the output current and the voltage is exclusively imposed by the state of the switch [83].

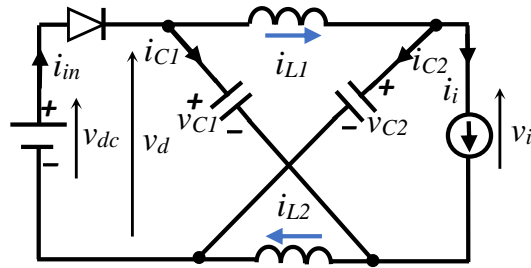


FIGURE 2.19: Equivalent circuit of the impedance network

In steady state, the modelling of the Z-source inverter can be expressed as follow [84], [85]:

During the time interval T_0 :

$$v_{L1} = v_{L2} = v_L = v_{C1} = v_{C2} = v_C \quad (2.89)$$

$$v_d = v_L + v_C = 2v_C \quad (2.90)$$

$$v_i = 0 \quad (2.91)$$

During time interval T_1 :

$$v_L = v_{dc} - v_C \quad (2.92)$$

$$v_d = v_{dc} \quad (2.93)$$

$$v_i = v_C - v_L = 2v_C - v_{dc} \quad (2.94)$$

The average voltage of the inductors over one switching period (T) should be zero in steady state and $T = T_0 + T_1$ giving:

$$v_c = \frac{T_1}{T_1 - T_0} v_{dc} \quad (2.95)$$

Using the above mentioned equations, the peak DC voltage \hat{v}_i and the peak AC output voltage \hat{v}_x can be written as:

$$\hat{v}_i = 2v_c - v_{dc} = \frac{1}{1 - \frac{2T_0}{T}} v_{dc} = Bv_{dc} \quad (2.96)$$

$$\hat{v}_x = M \frac{\hat{v}_i}{2} = B \frac{M v_{dc}}{2} \quad (2.97)$$

It's obvious in Equation 2.97 that the AC output voltage is boosted by the factor B, thus the use of a boost (DC-DC) converter is no longer needed. In a view of its special structure, the ZSI has an extra switching state, when the load terminals are shorted through both the upper and lower switching devices of any phase leg, which is called the shoot-through (ST) state besides the eight traditional non-shoot through (NST) states. This switching state provides the unique buck-boost feature to the inverter. The Table 2.1 shows how the shoot-through state of a three-phase leg Z-source can be controlled [85].

The control strategy applied to the Z-source inverter is a pulse width modulation (PWM), its principle consists of inserting the Shoot-through states at each transition by overlapping the upper and lower conductor signals, which can be derived by a suitable level by shifting the modulation signals of the VSI (Voltage Source Inverter) [85]. The offset values are adjusted correctly to ensure that the occupancy time of the two zero states is identical. The characteristic of this modulation strategy, shown in Figure 2.20;

Switching states	S1	S2	S3	S4	S5	S6	(V)
Active states	1	0	0	0	1	1	Finite
	1	1	0	0	0	1	
	0	1	0	1	0	1	
	0	1	1	1	0	0	
	0	0	1	1	1	0	
	1	0	1	0	1	0	
Zero states	0	0	0	1	1	1	Zero
	1	1	1	0	0	0	
ST states	1	S2	S3	1	!S2	!S3	Zero
	S1	1	S3	!S1	1	!S3	
	S1	S2	1	!S1	!S2	1	
	1	1	S3	1	1	!S3	
	1	S2	1	1	!S2	1	
	S1	1	1	!S1	1	1	
	1	1	1	1	1	1	

TABLE 2.1: Switching states of three phase ZSI. (!S1, !S2 and !S3 are the complements of S1, S2 and S3 respectively)

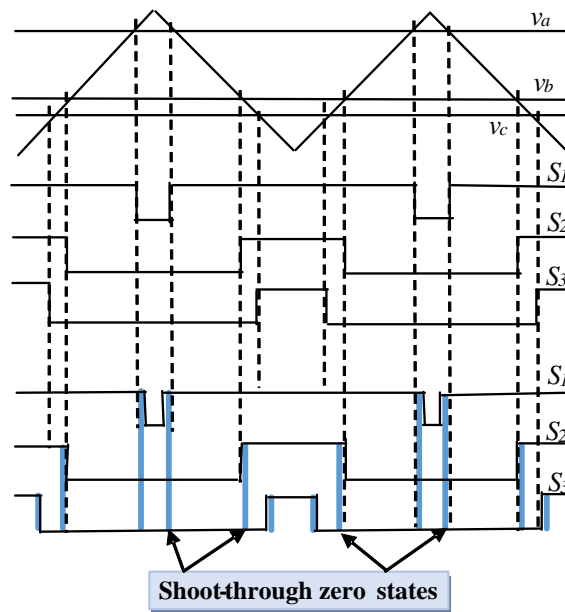


FIGURE 2.20: The difference between a traditional carrier-based PWM and a ST PWM

is that the transition time in a switching cycle is the similar to that of the Voltage Source Inverter (VSI), the “Shoot-Through ST” state is divided into six parts and the equivalent switching frequency of the impedance network is six times the switching frequency. Therefore, the volume of the inductors could be considerably reduced [86], [87].

Operating modes

The general operation of a ZSI can be illustrated by simplifying the AC side circuit and the D input diode with two switches.

As already discussed, the Z-source inverter uses the shoot-through zero states to increase the voltage in addition to the traditional 6 active states and 2 zero states [88]. Assuming that the inductor current is almost constant; when the inductance is low, the inductor current can become very rippled or even discontinuous. Instead of having the two operating modes [89], the Z-source inverter can have five different operating modes.

- Mode 1: shown in Figure 2.21 (a), the inverter bridge is operating in a shoot-through zero state. During this mode the bridge can be viewed as an open-circuit, the DC voltage appears across the ‘inductor and the capacitor’, except that no current flows to the load, from the DC source.

The voltages across the capacitors are:

$$v_{L1} = v_{C1}, v_{L2} = v_{C2} \tag{2.98}$$

Assuming that the inductors L1 and L2 and capacitors C1 and C2 have the same value respectively. The voltage equations of the ZSI can be written as:

$$\begin{cases} v_{L1} = v_{L2} = v_L \\ v_{C1} = v_{C2} = v_C \end{cases} \tag{2.99}$$

The inductor current increases linearly with the assumption that the capacitor voltage is constant during this period.

$$i_{L1} = i_{L2} = i_L \tag{2.100}$$

- Mode 2: The inverter is in a non-shoot through state (one of the eight conventional states), in this mode according to Figure 2.21 (b), the DC source voltage is linked to the inductor and the capacitor allowing the energy flow to the load via the inductor. The inductor discharges in this mode; its voltage is given by the following equation.

$$v_L = v_0 - v_C \tag{2.101}$$

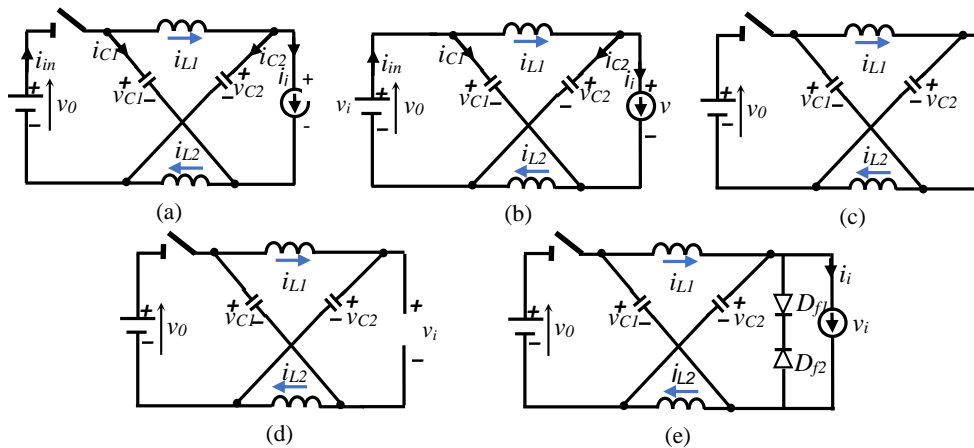


FIGURE 2.21: Operating modes of the Z-source inverter

The capacitor voltage is higher than that of the output which makes the inductor voltage negative, that leads to a linear decrease in the inductor current. This latter has to approve the following condition:

$$i_L \geq \frac{1}{2}i_i \quad (2.102)$$

The input current from the DC source becomes:

$$i_{in} = i_{L1} + i_{C1} = i_{L1} + (i_{L2} - i_i) = 2i_L - i_i \geq 0 \quad (2.103)$$

- Mode 3: Illustrated in Figure 2.21 (c), the inverter is in one of the 6 active states, and at the end of Mode 2, the inductor current decreases to half of the inverter DC side current. As a result, the input current becomes zero and the diode becomes reverse-biased. Supposing that the inductances L_1 and L_2 are negligible, the inverter voltage and current are given as:

$$\begin{cases} v_i = v_c \\ i_i = 2i_L \end{cases} \quad (2.104)$$

- Mode 4: In this mode, the ZSI is isolated from the load because the inverter current is equal to zero. Hence, the diode is blocked and the inverter is in an open-circuit, as shown in Figure 2.21 (d).
- Mode 5: The Figure 2.21 (e) shows that the inverter is in an active state during this mode and enters a free-wheeling state owing to the fact that the inductor current is smaller than half of the inverter DC current. The free-wheeling diodes, shown in Figure 4, ensure that the inverter enters in a shoot-through state and all the equations of mode.1 hold true.

2.6 POWER MANAGEMENT

An efficient energy management aims to make powertrain components operate in high efficacy while maintaining a satisfactory amount of energy in the storage devices. Moreover, the consumption of the fuel has to be minimized without effecting the vehicle performances, that can only be obtained by adapting an appropriate control strategy [90].

Figure 2.22 displays the different driving modes along with the energy flow.

- Mode 1: Is the high power generation mode, in case of acceleration or uphill driving the energy demand is high, both of the fuel cell (FC) and the battery are providing energy to the motor.

$$P_{load} = P_{FC} + P_{bat} \quad (2.105)$$

- Mode 2: Known as medium power mode, the fuel cell (FC) is the only energy source in this mode, it can also provide energy to the battery if its state of charge (SOC) is less than 30%.

$$P_{load} = P_{FC} \quad (2.106)$$

- Mode 3: The low power mode, in this case the vehicle is run by the energy generated by the battery alone, the fuel cell is stopped because its system efficiency, including the energy consumption of the auxiliary parts, such as the air compressor, decreases in the low power consumption.

$$P_{load} = P_{bat} \quad (2.107)$$

- Mode 4: The regenerative braking mode, the Fuel cell is not generating any power; on the other hand, the battery absorbs the energy provided by the motor, which acts as a generator in this case.

$$P_{load} = -P_{bat} \quad (2.108)$$

Note that there is another mode called the stop mode, where there is no energy flow between the components.

$$P_{load} = P_{FC} = P_{bat} = 0 \quad (2.109)$$

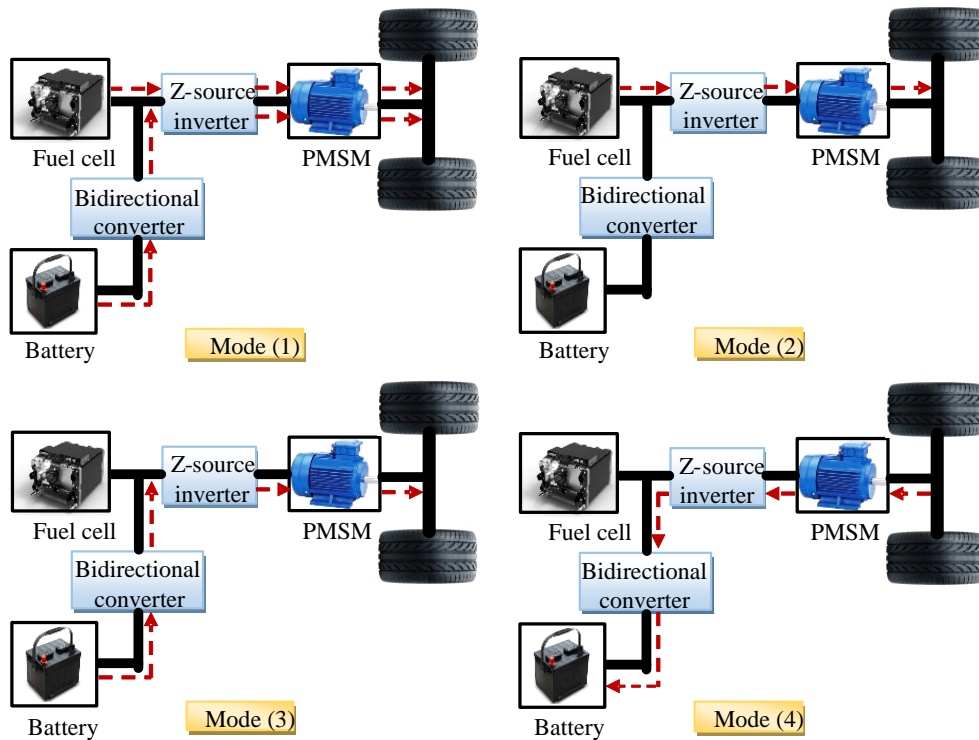


FIGURE 2.22: The different modes of energy flow

The proposed chart of the power management system is described in Figure 2.23. It defines in the first place the different powers involved in our hybrid system; if the power supplied is greater than the requested power in this case the excess power will be stored in the battery. If the requested power is greater than that of the generated that leads us to the following two cases. If the state of charge is greater than 30% the storage devices are switched on. In the opposite case, the battery stops working, which forces the fuel cell to charge it.

In an effort to validate the efficiency and dynamic performance of the proposed strategy, numerical simulations were performed using MATLAB/Simulink software under varying load conditions on an electric vehicle powered by a permanent magnet synchronous motor (PMSM), whose engine parameters are listed in Table 2 of the appendix. The battery and fuel cell parameters are also listed in Table 3 of the same appendix.

Starting with the acceleration pedal positions illustrated in Figure 2.24, which is considered as the input of the controlled system, in other words; it is the reference that all of the components are compelled to follow. Figures (2.25), (2.26) and (2.27) show the DC voltage, Fuel cell (FC) voltage and the fuel cell current respectively.

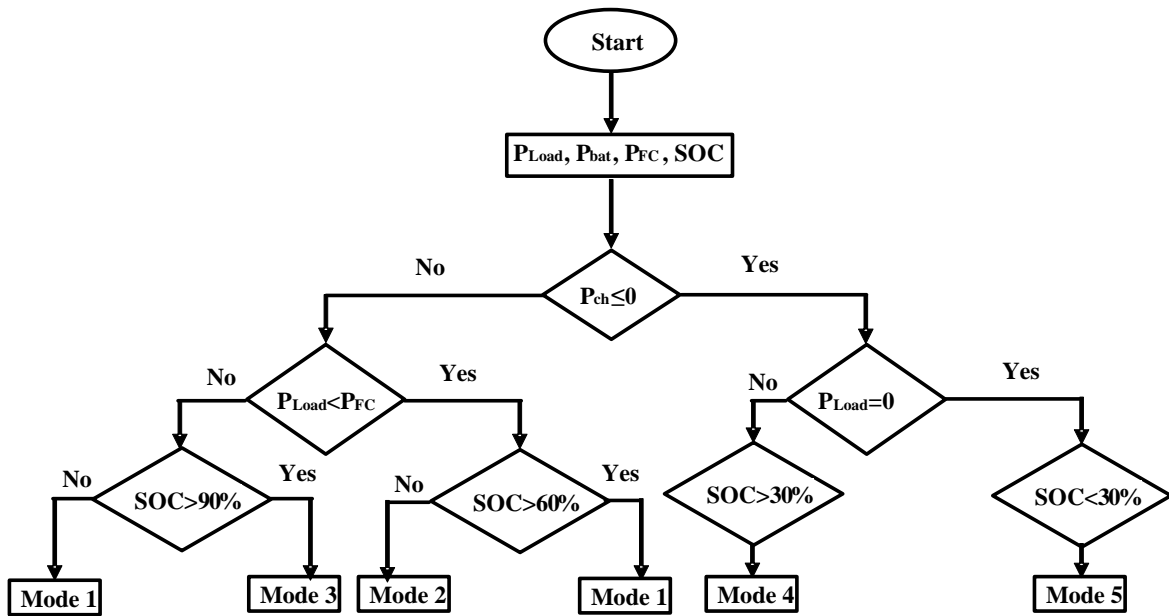


FIGURE 2.23: The flowchart of the energy management controller

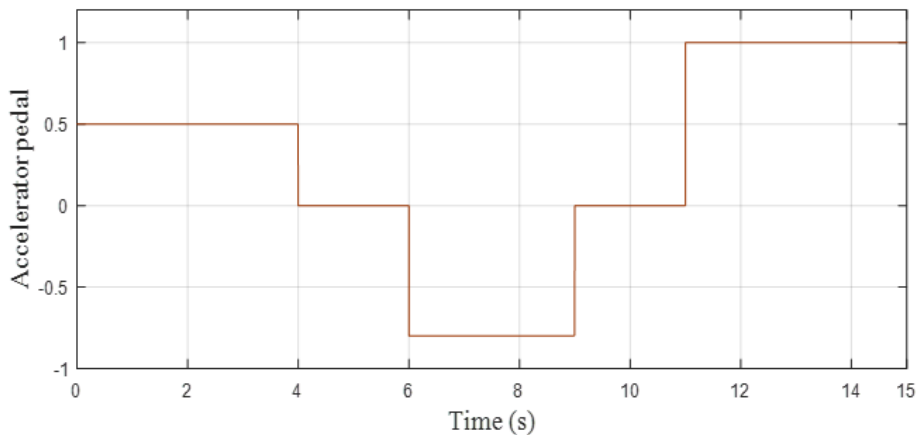


FIGURE 2.24: The acceleration pedal positions

Figures (2.28), (2.29) and (2.30) show the voltage, the current and the state of charge of the secondary source of energy.

Figure 2.31 represents the dynamic of the electromagnetic torque, which is one of the key performance advantages of any type of vehicle, it can be considered as the ‘strength’ of the car; that is to say; the greater the torque, the faster the acceleration that propels the vehicle. The measured torque follows perfectly its reference even with the sudden changes and that shows the effectiveness of the control technique applied to the system.

The current in d-q components is illustrated in Figure 2.32, Figure 2.33 is dedicated to the stator current responses to the load variations. The direct current is equal to zero and the quadrature current is similar to that of the electromagnetic torque, which means that the decoupling is established. We can see that the stator current is perfectly sinusoidal and the variation in its dynamic matches the changes in the acceleration.

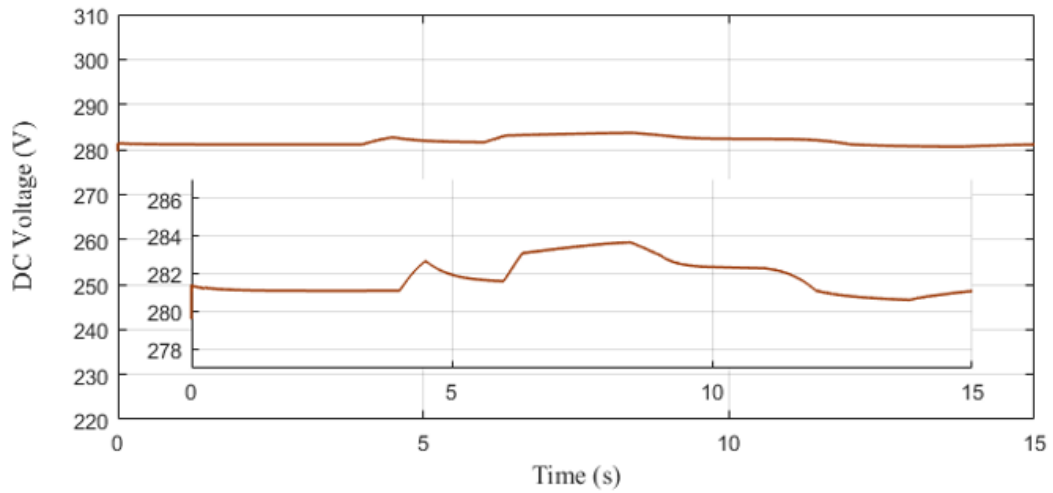


FIGURE 2.25: The DC bus voltage

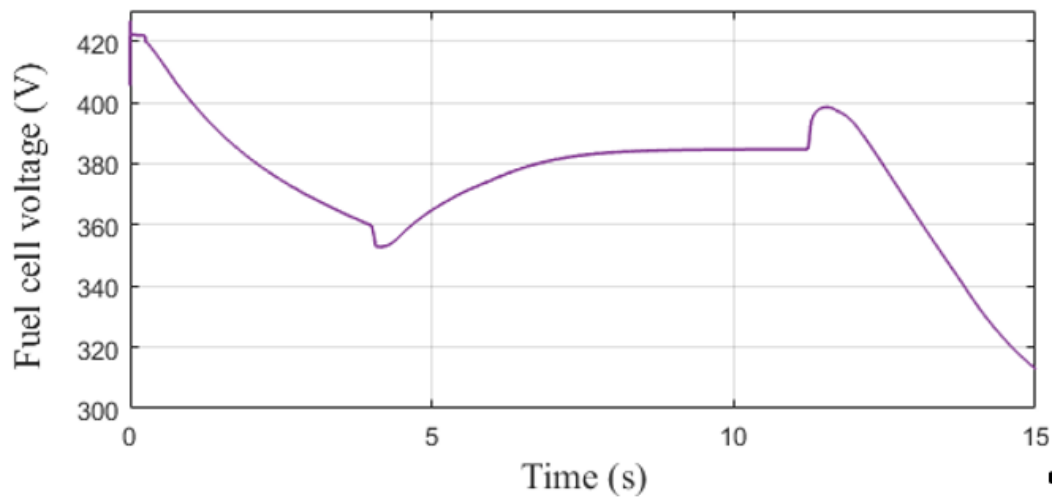


FIGURE 2.26: The fuel cell voltage

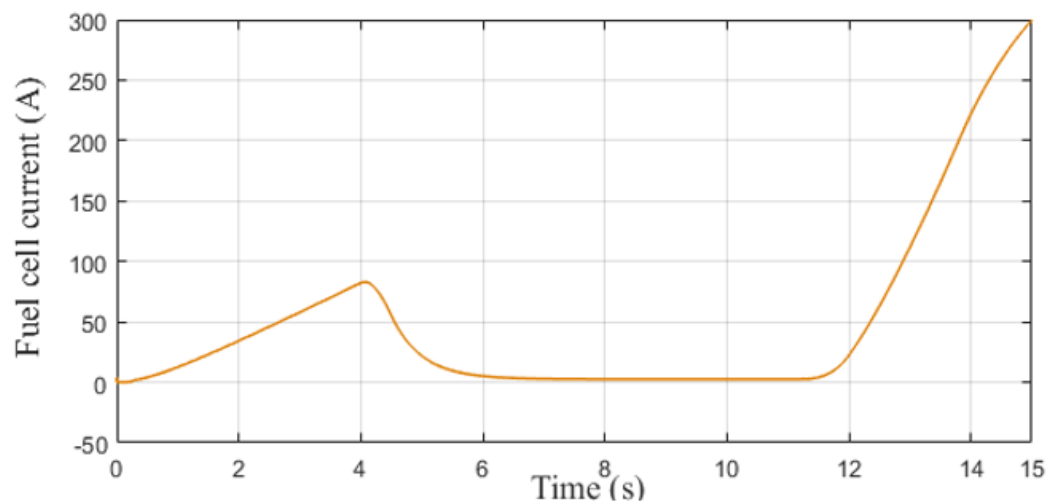


FIGURE 2.27: The Fuel cell current

The [Figure 2.34](#) is for the motor's speed responses; it is clear that it is a smoother version of the pedal

acceleration that comes to the fact that they are proportional. Thus, the sudden changes in the pedal are translated into a gentle continuous slope. The motor's power is represented in the [Figure 2.35](#), the measured power follows its reference with a good performance.

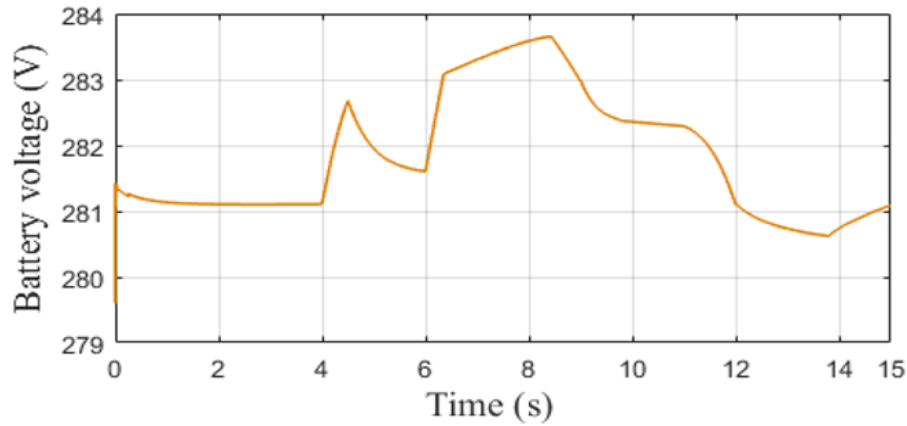


FIGURE 2.28: The battery voltage

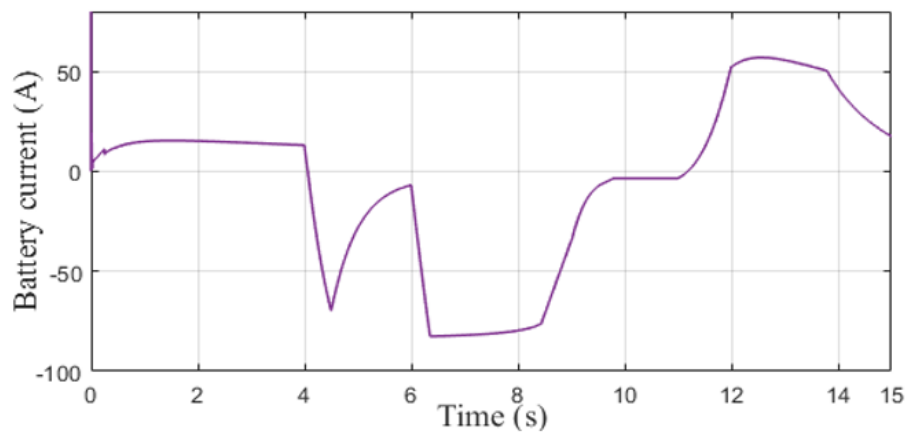


FIGURE 2.29: The battery current

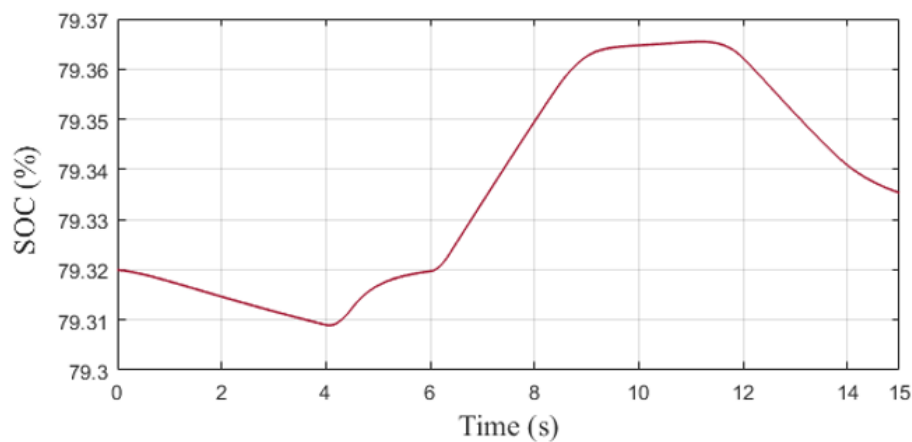


FIGURE 2.30: The State of charge of the battery

[Figure 2.36](#) shows the power management applied to the electric vehicle; it is a way to validate the theory of the previous section. It is undeniable that the simulation results correspond to the before mentioned theoretical characteristics and the different driving modes can be seen clearly. For example,

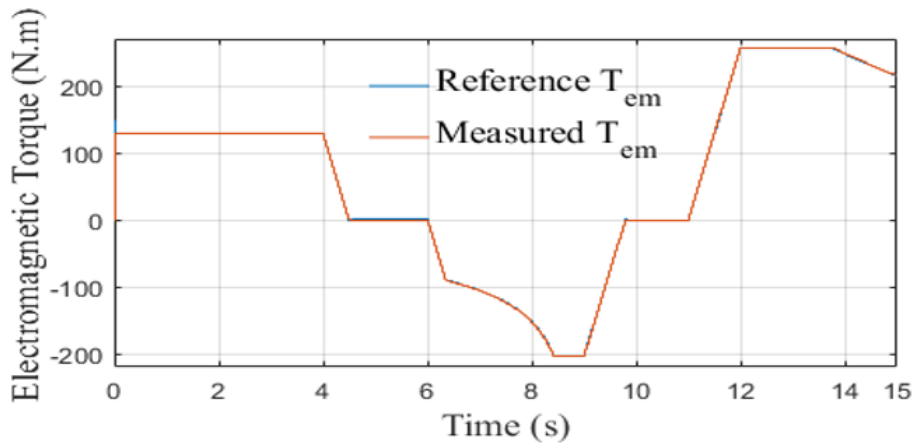


FIGURE 2.31: The Electromagnetic torque response

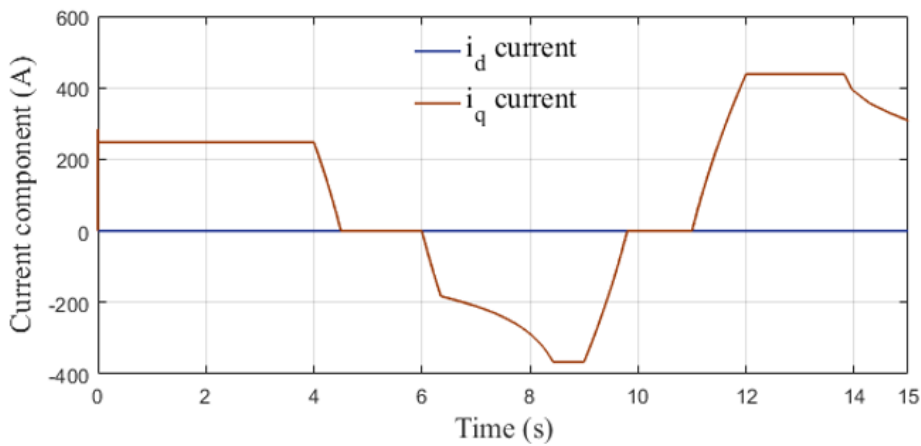


FIGURE 2.32: The stator current in d-q coordinates

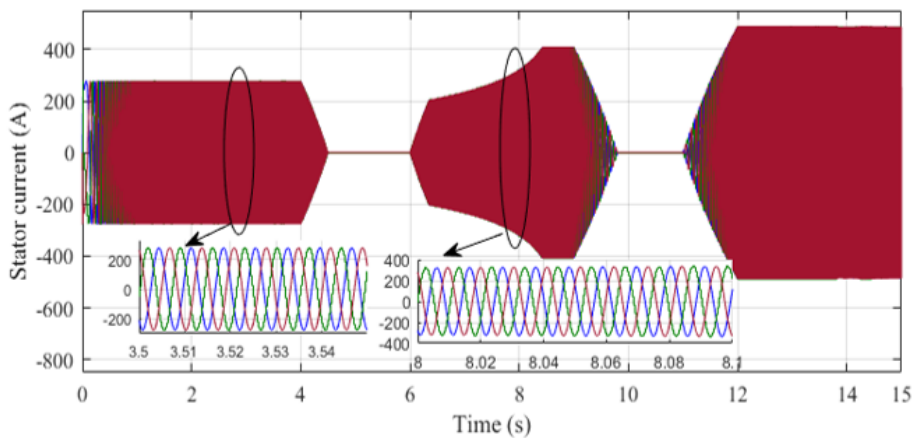


FIGURE 2.33: The stator current of the PMSM

at $t = 0s$ is the low power generation mode; the battery feeds the motor alone till $t = 0.4s$ when the fuel cell starts to work properly. From $t = 4s$ to $t = 6s$ is the medium power generation mode, the fuel cell supplies the motor, while charging the battery. At $t = 6s$ the regenerative braking mode starts, and here the motor acts as generator and starts to charge the battery. At $t = 9.5s$ the motor finally stops, the power is non-existent in all of the components. It's at $t = 11s$ when the high power generation modes is ON and here the fuel cell and the battery work hand in hand to feed the motor. Not that at any time t

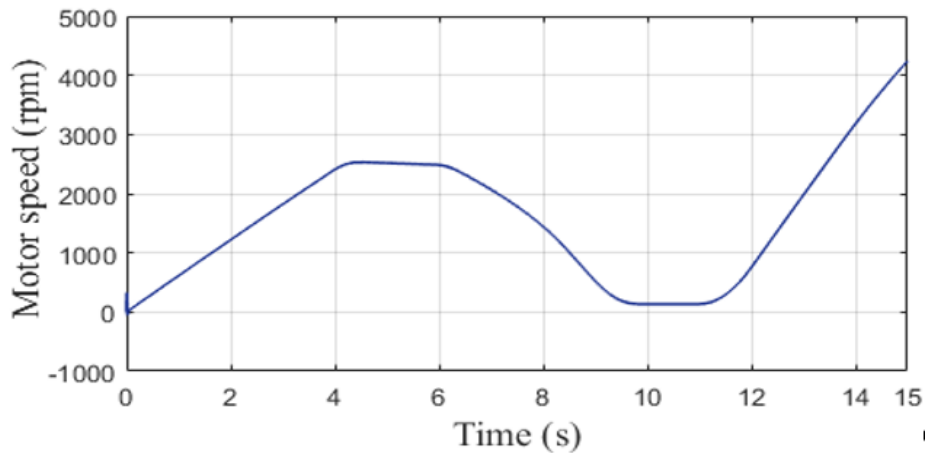


FIGURE 2.34: The motor speed responses

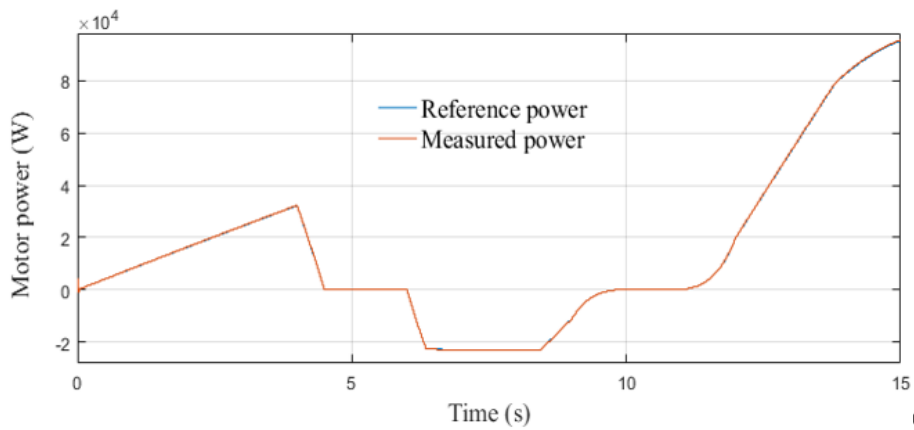


FIGURE 2.35: The motor power response

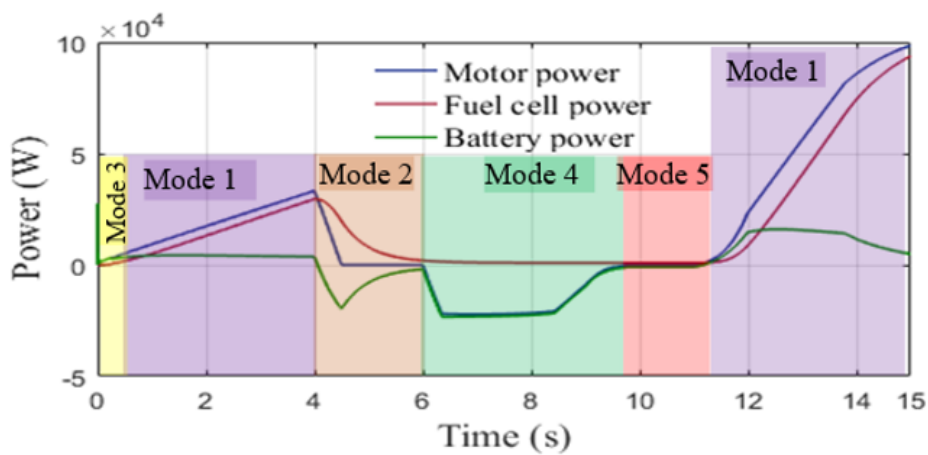


FIGURE 2.36: The power management under different driving modes

the load power is insured by summing both of the fuel cell power and the battery power.

Chapter 3

Control of the Four-quadrant DC-DC converter

This chapter presents a comparison between the conventional PI controller and the Genetic algorithms based PI controller in order to improve the system's performances. These control methods are applied on the 4-Q DC-DC chopper based Traction system.

3.1 FOUR-QUADRANT DC-DC CONVERTER

3.1.1 General description

The four-quadrant converter is commonly used in DC-DC applications due to its ability to adjust the direction of the voltage source based on semiconductor control devices. Therefore, it is possible to be set apart in various ways to control. The simplified structure of the four-quadrant (4-Q) DC-DC converter is illustrated in [Figure 3.1](#) [91].

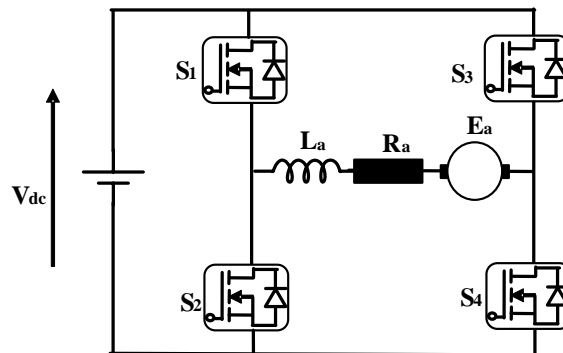


FIGURE 3.1: Four-quadrant DC-DC chopper model

The four-quadrant DC-DC converter topology consists of four semiconductor switches each of which disposes of a reversed biased diode, The DC motor is located in between the four pairs along with its armature resistance R_a and armature inductance L_a . The switching action of the control pairs leads to the generation of a DC voltage, while the generated current contributes to charging the inductance L_a ; the latter will eventually act as a power source for the circuit [92].

3.1.2 Operation and modeling of the 4-Q DC-DC converter

The four-quadrant DC-DC converter attempts to get a variable DC voltage out of a fixed DC voltage by controlling the voltage and current flow in the four-quadrant functions as shown in Figure 3.2 [93].

1. First quadrant: The motor rotates in the forward direction, the switches T_1 and T_4 are turned ON, thus the positive voltage from the DC source flows into the DC motor, which leads to a positive torque and a positive speed.

In this case, the output voltage is positive, allowing the permanent control of the closing of T_4 .

The current is positive (motor operation) and is chopped by T_1 : For $0 \leq t \leq \alpha T$, T_1 and T_4 closed (supply phase) : We obtain the following equations:

$$U_{out} = U_{in}, \quad i_{out} = i_{in} \quad (3.1)$$

With:

$$\begin{cases} U_{out} = Ri_{out} + V_L + E \\ V_L = L \frac{di_{out}}{dt} \end{cases} \quad (3.2)$$

Ignoring the resistor R :

$$\begin{aligned} U_{in} = L \frac{di_{out}}{dt} + E &\Rightarrow i_{out}(t) = \frac{U_{in} - E}{L}t - I_{out \min} \\ - I_{out \min} = I_{out}(t = 0) \end{aligned} \quad (3.3)$$

Thus, the current i_{out} increases linearly for $\alpha T \leq t \leq T$, D_1 and D_4 passing (freewheeling phase) the following equations are obtained:

$$U_{out} = 0, \quad i_{in} = 0 \quad (3.4)$$

With:

$$\begin{cases} U_{out} = R \cdot i_{out} + V_L + E \\ V_L = L \frac{di_{out}}{dt} \end{cases} \quad (3.5)$$

Ignoring the resistor R :

$$\begin{aligned} L \frac{di_{out}}{dt} + E = 0 &\Rightarrow i_{out}(t) = \frac{-E}{L}(t - \alpha T) + I_{out \max} \\ I_{out \max} = i_{out}(t = \alpha T) \end{aligned} \quad (3.6)$$

Thus, the current I_{out} increases linearly

2. Second quadrant: It is referred to as the forward breaking mode. At the beginning of this mode, only the switch T_2 is turned ON, the inductance L_a takes charge of supplying the circuit with the current. After that T_2 is switched OFF and DC voltage turns out to be smaller than that of the

generated voltage, which calls for a freewheeling assured by the Diodes D_1 and D_4 . Consequently, the torque is negative while the speed remains positive.

Consequently, the torque is negative while the speed remains positive.

For a positive output voltage, and a negative current (generator operation), we chopped by T_2 : for $0 \leq t \leq \alpha T$, T_2 closed and D_4 passed The following equations are obtained:

$$U_{out} = 0, \quad i_{in} = 0 \quad (3.7)$$

With:

$$\begin{cases} U_{out} = Ri_{out} + V_L + E \\ V_L = L \frac{di_{out}}{dt} \end{cases} \quad (3.8)$$

Ignoring the resistor R :

$$\begin{aligned} 0 = L \frac{di_{out}}{dt} + E &\Rightarrow i_{out}(t) = \frac{-E}{L}t - I_{out \min} \\ -I_{out \min} = I_s(t = 0) \end{aligned} \quad (3.9)$$

for $\alpha T \leq t \leq T$, D_1 and D_4 passing (freewheeling phase)

$$U_{out} = U_{in}, \quad i_{in} = -i_{out} \quad (3.10)$$

With:

$$\begin{cases} U_{in} = R.i_{out} + V_L + E \\ V_L = L \frac{di_{out}}{dt} \end{cases} \quad (3.11)$$

Ignoring the resistor R :

$$\begin{aligned} L \frac{di_{out}}{dt} + E = U_{in} &\Rightarrow i_{out}(t) = \frac{U_{in} - E}{L}(t - \alpha T) - I_{out \max} \\ -I_{out \max} = i_s(t = \alpha T) \end{aligned} \quad (3.12)$$

3. Third quadrant: Known as the reverse direction mode, at this point, the switches T_2 and T_3 are turned ON, hence, the voltage and current flowing to the load are negative; thereby, the torque and the speed become negative, as a result, the motor's polarity is reversed.

The output voltage is negative, so T_3 is permanently controlled to close. The current is negative (motor operation), chopping via T_2 : for $0 \leq t \leq \alpha T$, T_2 and T_3 are closed (supply phase):

The following equations are obtained:

$$U_{out} = -U_{in}, \quad i_{in} = -i_{out} \quad (3.13)$$

With:

$$\begin{cases} U_{out} = R.i_{out} + V_L + E \\ V_L = L \frac{di_{out}}{dt} \end{cases} \quad (3.14)$$

Ignoring the resistor R :

$$\begin{aligned} -U_{in} &= L \frac{di_{out}}{dt} + E \Rightarrow i_{out}(t) = \frac{-(U_{in} + E)}{L}t - I_{out \min} \\ -I_{out \min} &= I_{out}(t = 0) \end{aligned} \quad (3.15)$$

for $\alpha T \leq t \leq T$, T_3 closed and D_1 on (freewheeling phase):

$$U_{out} = 0, \quad i_{in} = 0 \quad (3.16)$$

With:

$$\begin{cases} U_{out} = Ri_{out} + V_L + E \\ V_L = L \frac{di_{out}}{dt} \end{cases} \quad (3.17)$$

Ignoring the resistor R :

$$\begin{aligned} L \frac{di_{out}}{dt} + E &= 0 \Rightarrow i_{out}(t) = \frac{-E}{L}(t - \alpha T) - I_{out \max} \\ -I_{out \max} &= i_{out}(t = \alpha T) \end{aligned} \quad (3.18)$$

4. Fourth quadrant: It is called the reverse braking mode; similarly to the second quadrant; the switch T_4 is the only switch that gets operated in the first half period, the inductance L_a works as a current source. In the second half period, T_4 is turned off, The DC source voltage is now smaller than the generated voltage leading to induced voltage feedback to the source through diodes D_2 and D_3 . Therefore, the input voltage flows in negative form, meanwhile, the current is positive. That gives at the end a positive torque and negative speed.

For a negative output voltage and a positive current (generator operation), we chopped by T_1 :

for $0 \leq t \leq \alpha T$: T_1 closed and D_3 open, We obtain:

$$U_{out} = 0, \quad i_{in} = 0 \quad (3.19)$$

With:

$$\begin{cases} U_{out} = R \cdot i_{out} + V_L + E \\ V_L = L \frac{di_{out}}{dt} \end{cases} \quad (3.20)$$

Ignoring the resistor R :

$$\begin{aligned} 0 &= L \frac{di_{out}}{dt} + E \Rightarrow i_{out}(t) = \frac{-E}{L}t + I_{out \min} \\ I_{out \min} &= I_{out}(t = 0) \end{aligned} \quad (3.21)$$

For $\alpha T \leq t \leq T$: D_3 and D_2 passing (recovery phase):

$$U_{out} = -U_{in}, \quad i_{in} = -i_{out} \quad (3.22)$$

With:

$$\begin{cases} U_{out} = R \cdot i_{out} + V_L + E \\ V_L = L \frac{di_{out}}{dt} \end{cases} \quad (3.23)$$

Ignoring the resistor R :

$$L \frac{di_{out}}{dt} + E = -U_{out} \Rightarrow i_{out}(t) = \frac{-(U_{int} + E)}{L}(t - \alpha T) + I_{out \max}$$

$$I_{out \max} = i_{out}(t = \alpha T)$$
(3.24)

The average value of the voltage across the load can be written as follows:

$$\hat{V}_{out} = \frac{1}{T} \int_0^T V_{out}(t).dt = \frac{1}{T} \int_0^{\alpha T} V_{in}(t).dt + \frac{1}{T} \int_{\alpha T}^T -V_{in}(t).dt$$
(3.25)

$$\hat{V}_{out} = V_{int}(2\alpha - 1)$$
(3.26)

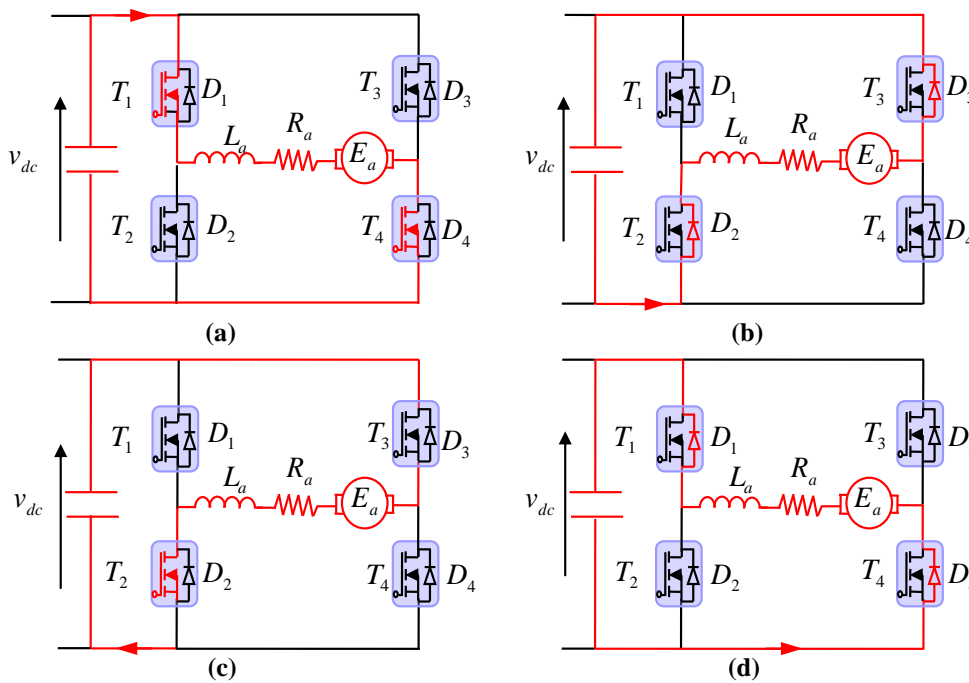


FIGURE 3.2: Schematic diagram show the switching type of triggering in all quadrants. (a) First quadrant (b) Second quadrant (c) Third quadrant (d) Fourth quadrant.

3.2 PWM CONTROL OF THE FOUR-QUADRANT DC-DC CHOPPER

The quality of the output voltage of a chopper depends largely on the control technique used to operate the chopper’s switches. There are several control techniques available, and the choice of which one to use depends primarily on the type of application for which the device is intended. The most commonly used technique in PMDC drives is PWM control. There are many different pulse width modulation techniques. However, four categories of PWM have been developed.

- Sine-triangle modulations that compare a reference signal to a carrier, usually triangular.
- Pre-calculated modulations for which the switching angles are calculated off-line to to cancel certain components of the spectrum.

State of cells switching	Direction of current flow
T_1, T_4 ON T_2, T_3 OFF D_1, D_2, D_3, D_4 OFF	$v_a > 0, i_a > 0$
T_4 ON T_1, T_2, T_3 OFF D_1, D_4 OFF D_2, D_3 ON	$v_a < 0, i_a > 0$
T_2, T_3 ON T_1, T_4 OFF D_1, D_2, D_3, D_4 OFF	$v_a > 0, i_a < 0$
T_1, T_2, T_3, T_4 OFF D_1, D_4 ON D_2, D_3 OFF	$v_a < 0, i_a < 0$

TABLE 3.1: 4Q DC-DC converter operating modes

- Post-calculated modulations also called regular symmetrical PWM or vector PWM in which the switching angles are calculated online.
- The stochastic modulations for which the objective is the whitening of the spectrum (constant and minimal noise on the whole spectrum). The pulse widths are distributed according to a probability density representing the control law. The considerable development of the pulse width modulation technique opens up a wide range of applications in control systems and many other functions. It allows flexible and cost-effective implementation of chopper control circuits [94]. Figure 3.3 illustrates the PWM control applied to the four-quadrant chopper.

3.3 PI CONTROL of the 4-Q DRIVING a DC-DC CONVERTER

The control system must be analyzed and an appropriate controller must be selected and designed [95], [96]. Some important properties of widely used P, PI and PID controllers are as follows:

1. Mode of action
2. Process delay.
3. Speed of error correction.
4. Error acceptability in steady state. According to the above information, controllers and systems can be assigned to each other as:
 - For easily controlled systems where steady-state errors are acceptable, P controllers are used.
 - In systems with a large offset where offset is tolerable, PD controllers are used.
 - For applications with a low dynamic control requirement and where the system does not exhibit large offsets, I controllers are used.
 - For dynamic control response without exhibiting steady state error, PI controllers are used.

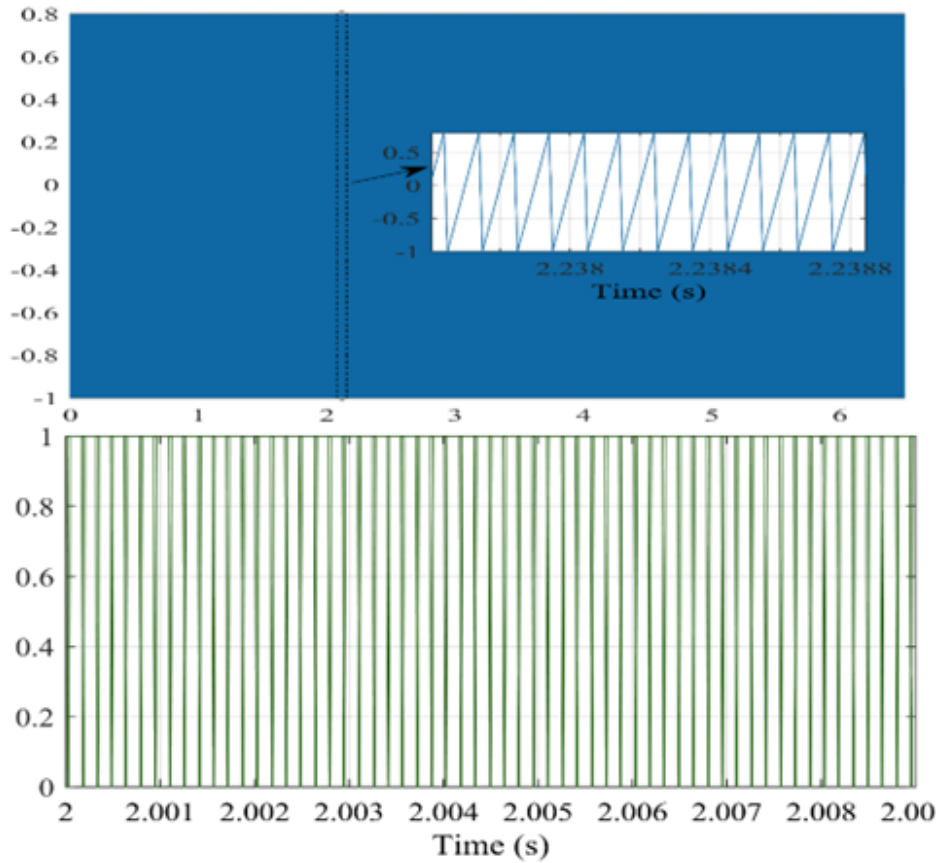


FIGURE 3.3: PWM control applied on the 4-Q chopper.

- If there is a need for the speed of response to be as high as possible, regardless of the large lag, PID controllers are used.

The classical PID controller directly links the control signal $u(t)$ to the deviation signal $e(t)$. Its temporal description is as follows:

$$u(t) = K_p e(t) + K_i \int e(t) dt + K_d \frac{de(t)}{dt} \tag{3.27}$$

Where $e(t)$ is the control error; the controller parameters K_p , K_i and K_d are proportional, integral and derivative gains, respectively; and $C(s)$ is the controller transfer function in Laplace form.

Consider the following:

$$C(s) = \frac{U(s)}{E(s)} = K_p + \frac{K_i}{s} + K_d s \tag{3.28}$$

$$C(s) = K_p \left(1 + \frac{1}{T_i s} + T_d s \right) \tag{3.29}$$

The K_i and K_p parameters of the controllers of the variables mentioned below are calculated in the same way as follows:

Where K_p is the proportional coefficient and K_i the integral coefficient of the corrector. Thus, the coefficients of the correctors will be designed so that the dynamics of the system is predetermined. a and b are parameters of the model. The transfer function of the closed loop system in figure is of the second order with a natural pulse ω and a damping coefficient ζ .

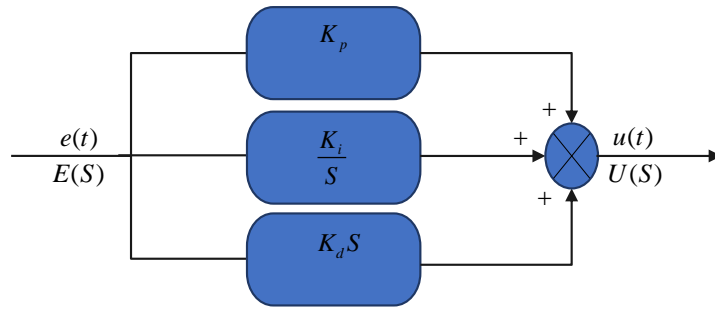


FIGURE 3.4: PID controller scheme

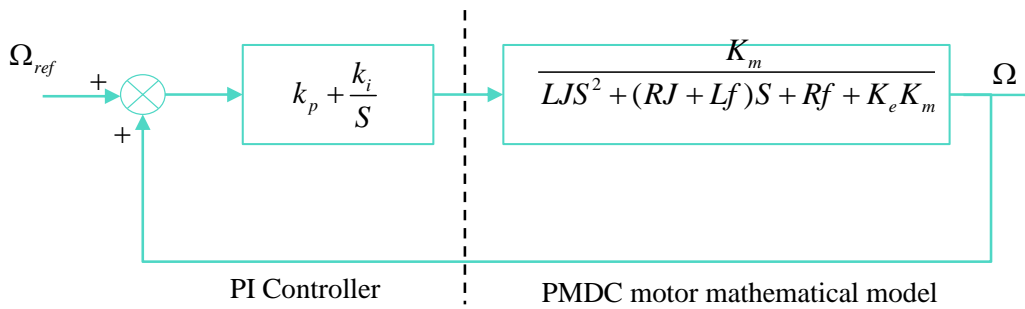


FIGURE 3.5: PI Controller with the PMDC motor

The transfer function defining the PMDC motor can be written as follows:

$$G(s) = \frac{K_m}{LJs^2 + (RJ + Lf)s + Rf + K_e + K_m} \tag{3.30}$$

$$C(s) = K_p + \frac{K_i}{s} \tag{3.31}$$

$$TF_1 = G(s) \cdot C(s) = \frac{K_m}{LJs^2 + (RJ + Lf)s + Rf + K_e + K_m} \cdot \left(K_p + \frac{K_i}{s} \right) \tag{3.32}$$

$$FT_2 = \frac{TF_1}{1 + TF_1} \tag{3.33}$$

$$B(s) = \frac{\omega_n^2}{s^2 + 2\zeta\omega_n s + \omega_n^2} \tag{3.34}$$

By assuming $k_i \succ k_p$, the expressions of the parameters of the controllers obtained by identification are given by :

$$\begin{cases} K_i = b\omega_n^2 \\ K_p = 2\zeta b\omega_n - a \end{cases} \tag{3.35}$$

Considering that:
$$\begin{cases} \omega_n > 0 \\ \xi > 0 \end{cases}$$

For the motor speed controller, $a = f, b = J$.

3.4 GENETIC ALGORITHMS based OPTIMIZED PI CONTROL of the 4-Q CHOPPER DRIVING a PMDC MOTOR

The topic of optimization is widely used and has been the subject of much research for several decades. Optimization is the task of minimizing or maximizing a given function. The most popular techniques are for example, stochastic algorithms, such as those based on genetic algorithms or the simulated annealing algorithm, deterministic algorithms such as the Levenberg-Marquardt algorithm, the conjugate gradient algorithm, and intermediate techniques.

In this chapter, we are interested in the optimization of the gains of a PID controller by the genetic algorithm method.

3.4.1 Optimization problem (generality)

When solving an optimization problem, it is important to identify to which category this problem belongs. Indeed, the algorithms developed are designed to solve a given type of problem and are not very efficient for a different type. The classification of optimization problems changes from one author to another. For example, we distinguish [97]:

Continuous versus discrete optimization problems

In some cases, the decision variables are discrete, most often in the form of integers or binaries. The optimization problem is said to be discrete. On the contrary, in continuous optimization problems, the variables can take any value, they are real. Continuous optimization problems are generally simpler to solve. An optimization problem mixing continuous and discrete variables is called mixed.

Constrained and unconstrained optimization problems

It is important to distinguish between problems where constraints exist on the decision variables. These constraints can be simply bounds and go up to a set of equations of type equality and inequality. It is sometimes possible to eliminate an equality constraint by substitution in the objective function. Naturally, problems with constraints are more complicated to solve and use dedicated algorithms.

Single-objective or multi-objective optimization problems

Single-objective problems are defined by a single objective function. Multi-objective problems exist when a compromise is to be sought between several contradictory objectives. It is possibly possible (but not necessarily efficient) to reformulate a multi-objective problem with a single objective function as a combination of different objectives or by transforming objectives into constraints.

Deterministic and stochastic optimization problems

Deterministic optimization problems consider that the data are perfectly known, while in stochastic optimization problems this is not the case; for example, a stochastic approach can be relevant in the case where the variables of a problem are the future sales of a product. In this case, uncertainty can be introduced into the model.

3.4.2 Heuristic methods

Simple rules of thumb that are not based on analysis. They are based on experience and results already obtained and on analogy, generally, one does not obtain the optimal solution but an approximate solution.

The use of a heuristic is efficient to compute an approximate solution of a problem and thus speed up the exact solution process. A heuristic is designed for a particular problem [98]. It relies on its own structure without offering any guarantee as to the quality of the computed solution. Heuristics can be classified into two categories:

- Constructive methods: (e.g. gluttonous methods) which generate solutions from an initial solution by trying to add elements little by little until a complete solution is obtained,
- Local excavation methods: which start with an initial complete solution (probably less interesting), and repeatedly try to improve this solution by exploring its proximity.

A heuristic is a common sense strategy to move intelligently in the solution space, in order to obtain an approximate solution, the best possible one, within a reasonable time.

3.4.3 Metaheuristic methods

Faced with the difficulties encountered by heuristics to get a good quality feasible solution for difficult optimization problems, meta-heuristics have appeared. These algorithms are more complete and complex than a simple heuristic, and generally allow to obtain a solution of very good quality for problems coming from the fields of operational research or engineering for which no efficient methods are known to treat them or when the solution of the problem requires a high time or a large storage memory.

The ratio between the execution time and the quality of the solution found by a meta-heuristic remains in most cases very interesting compared to the different types of solution approaches.

Most metaheuristics use random and iterative processes as a means to gather information, explore the search space, and deal with problems such as combinatorial explosion. A meta-heuristic can be adapted for different types of problems, while a heuristic is used for a given problem.

Several of them are often inspired by natural systems in many domains such as: biology (evolutionary and genetic algorithms), physics (simulated annealing) and also ethology (ant colony algorithms).

One of the challenges of designing metaheuristics is therefore to facilitate the choice of a method and the adjustment of parameters to adapt them to a given problem.

Metaheuristics can be classified in many ways. We can distinguish between those that work with a population of solutions and those that handle only one solution at a time. Methods that iteratively attempt to improve a solution are called local search methods or trajectory methods. These methods construct a trajectory in the solution space by attempting to move toward optimal solutions. The best known examples of these methods are: Taboo search and Simulated Annealing. Genetic algorithms, particle swarm optimization and ant colony algorithms are the best known examples of methods that work with a population. However, these methods use a high level of abstraction, allowing them to be adapted to a wide range of different problems. Metaheuristics (M) are often algorithms using probabilistic sampling.

They try to find the global optimum (G) of a difficult optimization problem (with D discontinuities, for example), without being trapped by the local optima (L) (Figure 3.6) [98].

The main characteristics of Metaheuristics are the following:

- Metaheuristics are strategies that guide the search for a solution

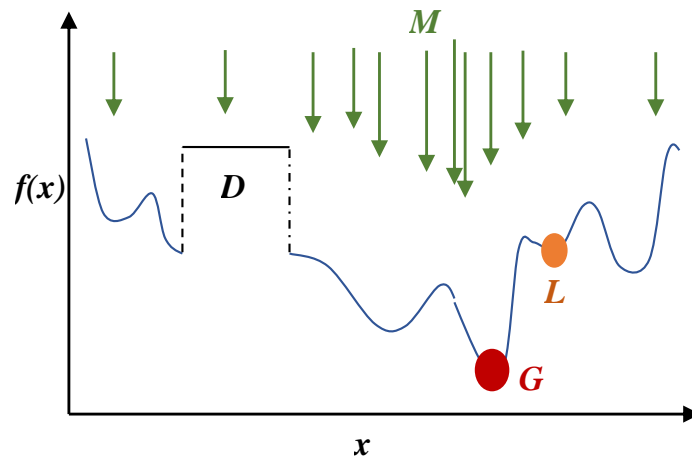


FIGURE 3.6: General principle of Metaheuristics

- The goal of metaheuristics is to explore the search space efficiently in order to determine (almost) optimal points
- The techniques that constitute meta-heuristic algorithms range from simple local search procedures to complex learning processes
- Metaheuristics are in general non-deterministic and do not provide any guarantee of optimality
- Metaheuristics can contain mechanisms to avoid being blocked in regions of the search space
- The basic concepts of metaheuristics can be written in an abstract way, without calling upon a specific problem
- Metaheuristics can make use of heuristics that take into account the specificity of the problem being treated, but these heuristics are controlled by a higher level strategy
- Metaheuristics can make use of the experience accumulated during the search for the optimum, to better guide the rest of the search process.

3.4.4 Classification of Metaheuristics

One way of classifying metaheuristics is to distinguish those that work with a population of solutions from those that handle only one solution at a time. Methods that iteratively attempt to improve a solution are called local search methods or path methods.

The Taboo method, Simulated Annealing, and Variable Neighborhood Search are typical examples of trajectory methods. These methods construct a trajectory in the solution space by attempting to move towards optimal solutions. The best known example of a method that works with a population of solutions is the genetic algorithm. [Figure 3.7](#) below gives an overview of the most used methods [99].

3.4.5 Genetic Algorithm

Evolutionary algorithms (EAs) are stochastic global optimization methods based on the Darwinian theory of the evolution of biological species, they use both the principles of survival of the best adapted individuals and those of the propagation of the genetic heritage which are inspired by the mechanisms

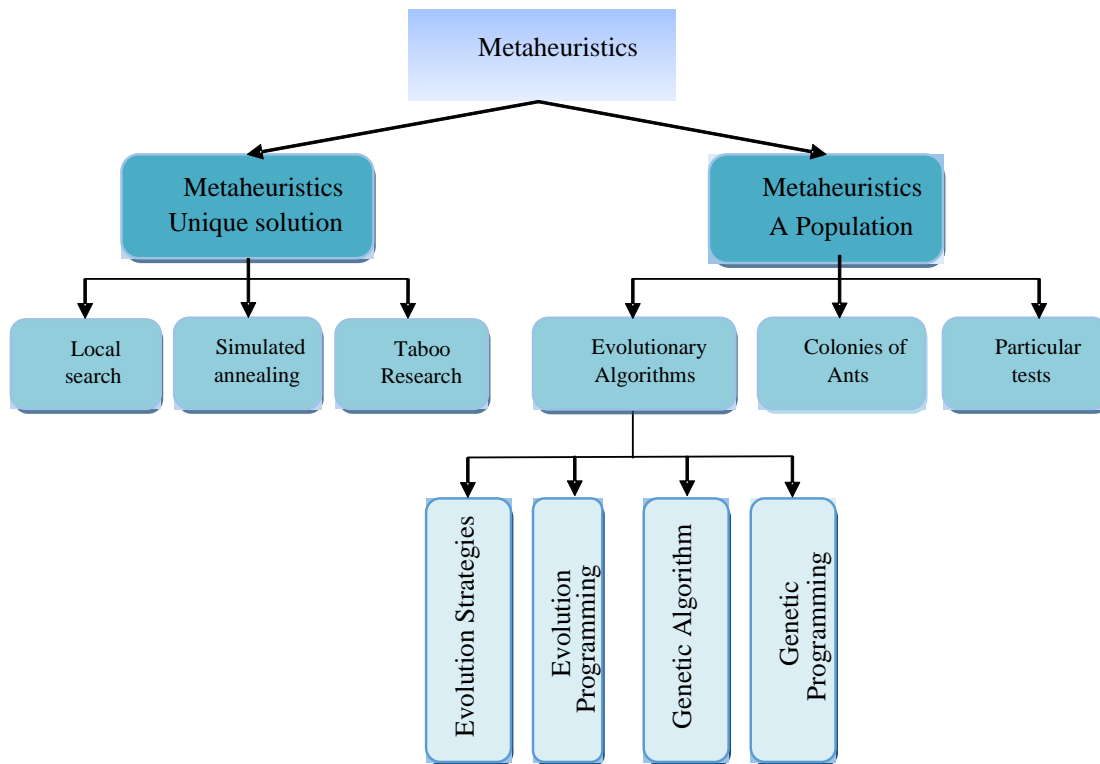


FIGURE 3.7: Classification of metaheuristics

of natural selection and genetic phenomena such as the mechanisms of evolution in nature: crossovers, mutations, selections, etc.

The best known evolutionary method is inspired by the theory of evolution and the biological processes that allow organisms to adapt to their environment. It is the genetic algorithm which was initially developed by John Holland (1975) [100] in the book “Adaptation of Natural and Artificial System” which formalizes genetic algorithms in the framework of mathematical optimization. Their fields of application are very vast: economics, function optimization (cost or losses), planning, and many other fields. The reason for this large number of applications is clear, simplicity and efficiency [101].

Genetic algorithms attempt to simulate the process of natural selection in an unfavorable environment by drawing inspiration from the theory of evolution proposed by Darwin in 1859 “Journal of Research in to the Geology and Natural History”. According to these concepts, when a population is subjected to the constraints of a natural environment, only the best adapted individuals survive and generate offspring. Over the generations, natural selection allows the appearance of individuals better and better adapted to the natural environment.

Operating principle of genetic algorithms

Genetic algorithms provide solutions to problems that do not have solutions that can be computed in a reasonable time in an analytical or algorithmic way. According to this method, thousands of more or less good solutions (genotypes) are created at random and are then subjected to a process of evaluation of the relevance of the solution simulating the evolution of the species: the most “adapted”, i.e. the solutions to the problem which are the most optimal survive more than those which are less so and the population evolves by successive generations by crossing the best solutions between them and by

making them mutate, then by rerunning this process a certain number of times in order to try to tend towards the optimal solution (Figure 3.8).

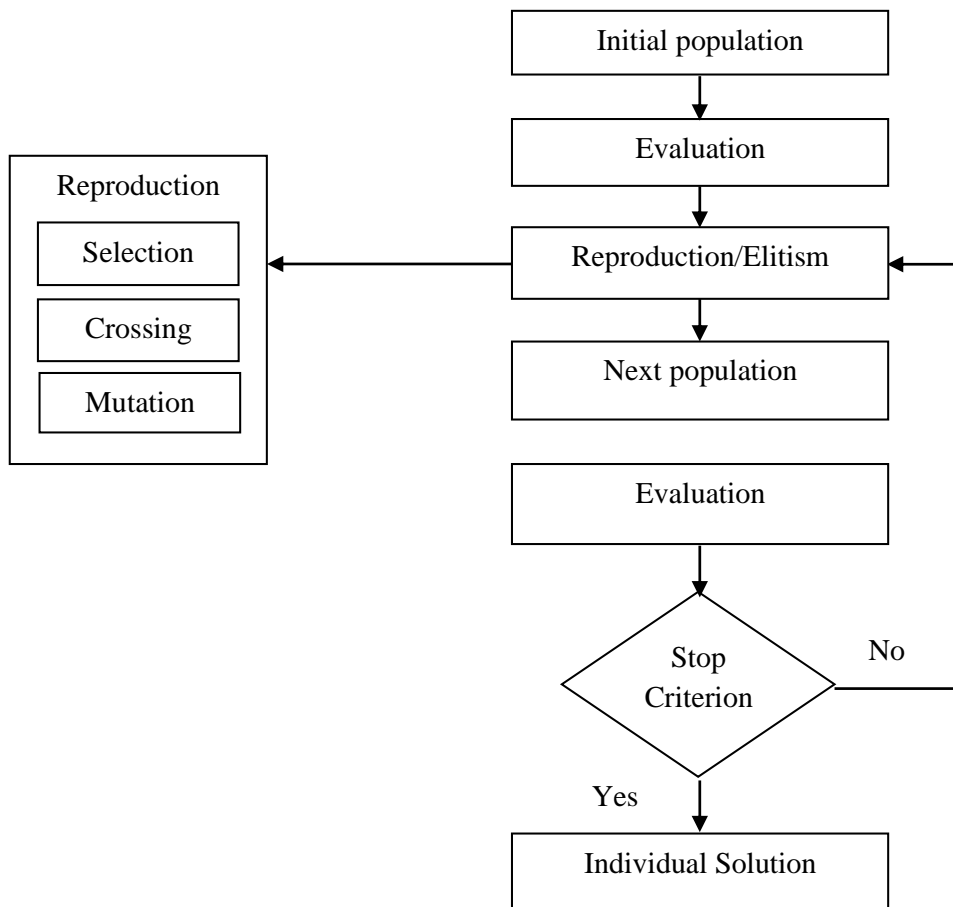


FIGURE 3.8: Schematic of the Genetic Algorithm principle.

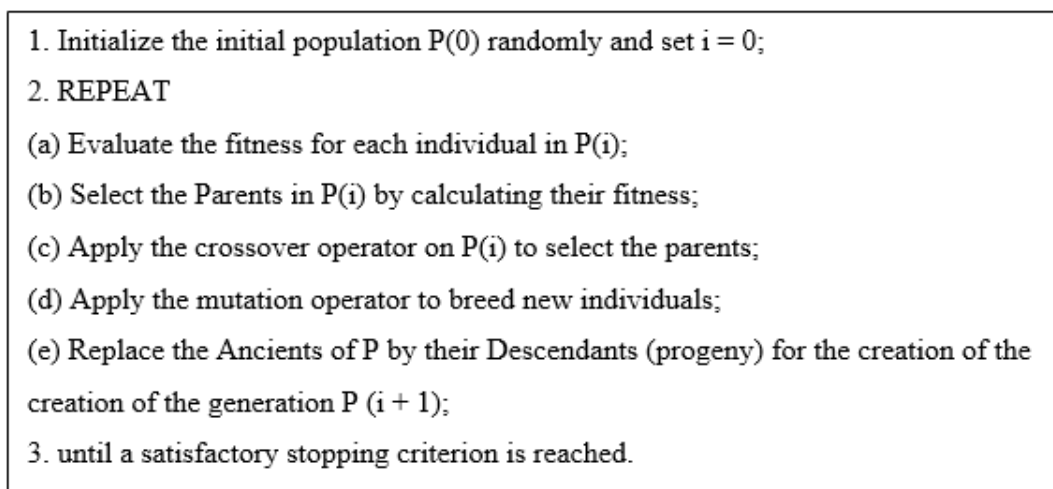


FIGURE 3.9: Structure of a canonical genetic algorithm [102].

The stopping criterion can be of various kinds, for example:

- A minimum rate that one wishes to achieve of population adaptation to the problem

- A certain calculation time not to be exceeded
- A certain number of generations not to be exceeded
- A combination of these three points

In fact, the use of genetic algorithms does not require knowledge of the nature of the problem, it is only necessary to provide a function allowing to code a solution in the form of genes (and thus to do the reverse work) as well as to provide a function allowing to evaluate the relevance of a solution to the given problem. To summarize, GA is based on [102]:

- A chromosomal representation of the problem solutions
- A method to generate an initial population of solutions;
- A fitness function to rank the solutions according to their dispositions;
- Genetic operators that define how the genetic characteristics of the parents are transmitted to the children;
- The values of the parameters used by the GA.

Detailed description of genetic algorithms

In this section we will present in more detail the different operators and parameters of a GA, namely, the population, the coding of the chromosomes, the evaluation, the selection, crossover and mutation operators.

1. Initial population

The first step in the implementation of genetic algorithms is to create a population composed of N individuals, each representing a possible solution of the given problem. The choice of individuals strongly conditions the speed of the algorithm. If the position of the optimum in the search space is totally unknown, it is interesting that the population is distributed over the whole search space. Moreover, this step presents a main problem which is the choice of the size of the population. Indeed, a population size that is too large increases the computation time and requires a considerable memory space, whereas a population size that is too small leads to obtaining a local optimum. On the other hand, if a priori information on the problem is available, it seems obvious to generate the individuals in a particular space in order to accelerate the convergence [103].

2. Coding

The key step in a genetic algorithm is to define and code appropriately the variables of a given problem. There are different coding techniques. Each individual of the population is coded by a chromosome or genotype. A population is thus a set of chromosomes, each chromosome codes a point of the search space.

There are mainly two types of coding: binary coding and real coding.

(a) Binary coding

In Goldberg's genetic algorithm, the user must choose the smallest alphabet that allows a natural expression of the problem parameters [104]. This is why the binary alphabet $\{0, 1\}$ is particularly well suited to the representation of the parameters (principle of minimal alphabets).

Let f be a function to be optimized with parameters x . The variable x represents an individual of the population, it is coded as a string of n bits. Let $x \in [x_{min}, x_{max}]$ with $x \in \mathbb{R}$ and x has a number of decimal places denoted d .

In a binary representation, the size of the individual n checks the following equation:

$$|x_{\max} - x_{\min}| \cdot 10^d \leq 2^n \quad (3.36)$$

(b) The real coding

The representation of solutions in the framework of GAs is not necessarily reduced to an alphabet of low cardinality (0,1), there is a whole school for which the most efficient representation is that based on real numbers. This representation is the basis of the evolutionary approach "Evolution strategy". This type of coding has certain advantages over binary coding:

- Real coding is robust for problems considered difficult for binary coding.
- This coding requires an adaptation of the crossover and mutation operators.

3. Evaluation function (Management of constraints) or performance

The adaptation function, or fitness, associates a value for each individual. The purpose of this value is to evaluate whether an individual is better adapted than another to its environment. This means that it quantifies the response provided to the problem for a given potential solution. Thus, individuals can be compared with each other [105].

4. Selection

The selection is in charge of defining which individuals of P will be duplicated in the new population $P + 1$ and will serve as parents (application of the crossover operator). This operator is perhaps the most important since it allows the individuals of a population to survive, reproduce or die.

In general, the number of copies of an individual is directly related to the relative fitness of the individual within the population. The higher an individual's performance relative to others, the more likely it is to be reproduced in the population. Individuals with high relative fitness are therefore more likely to be selected [106].

The selection is carried out on a set of individuals called reproducer which is composed :

- Either the whole population.
- A subset built by selection: Only the best adapted individuals (whose evaluations are the strongest) will "survive", the others are eliminated. We generally fix at 1/2 the part of the population which survives, in this case the sorting of the population according to the objective function is compulsory.
- A subset constructed by thresholding: All individuals who have an evaluation above a pre-defined threshold survive. If there are none, a new random population is created, which does not require the sorting of the population according to the objective function.

5. Crossover

After selecting the most suitable chains, these will undergo the operation of crossover (or recombination in Anglo-Saxon terminology) which consists of exchanging genetic material between two reproductive chains (parents) to produce two new chains (children). It is a process according to which the bits of two selected chains are interchanged: in the genetic language, we will say that these chains are crossed. It allows the exchange of information between chromosomes (individuals). This exchange of information gives genetic algorithms a part of their power: sometimes, good genes from one parent replace bad genes from another and create sons better adapted than the parents.

There are several crossover operators which depend essentially on the type of coding and the nature of the problem to be treated. Figures (3.10) and (3.11) below, illustrate some of the techniques in the following [107]:

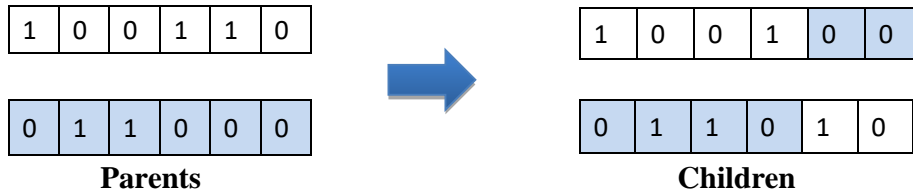


FIGURE 3.10: Crossing at a breakpoint

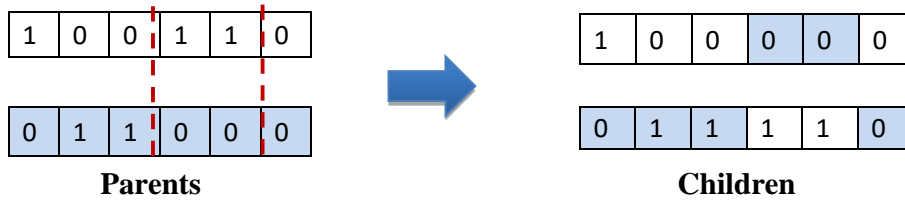


FIGURE 3.11: Crossing at two breakpoints

6. Mutation

This is a process where a minor change of genetic code is applied to an individual to introduce diversity and thus avoid falling into local optima with a very low probability P_m .

The mutation operator thus modifies in a completely random way the characteristics of a solution, which makes it possible to introduce and maintain diversity within our population of solutions. This operator plays the role of a disturbing element, it introduces noise in the population.

Mutation works as follows; for discrete problems, a gene on the chromosome is randomly drawn and its value is replaced by one of the other possible values, also randomly drawn. In the case of continuous problems, the gene is also randomly drawn, and replaced by a random value from the gene extension domain (state space). The following Figure 3.12 shows an example of a binary mutation:

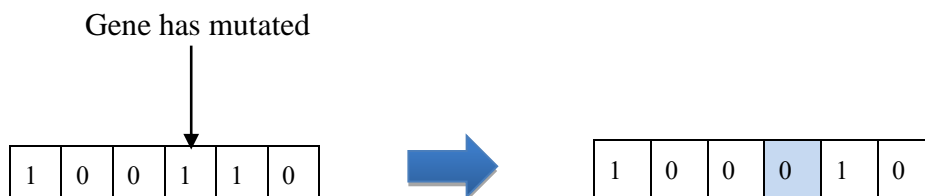


FIGURE 3.12: Example of a mutation in a binary string

In a simple genetic algorithm, mutation in binary coding is the occasional random change (of low probability) in the value of a character in the string.

Advantages and disadvantages of genetic algorithms

1. Advantages of GAs

- Potentially GAs explore all the point space at the same time, which limits the risks of falling into local optima
- GAs only use the values of the functional to optimize it, there is no need to perform expensive and sometimes very complex calculations
- GAs are very robust, i.e. they have a great capacity to find the global optimums of the optimization problems.

2. Drawbacks of GAs

- GAs are still not very efficient in terms of cost (or speed of convergence), compared to more classical optimization methods
- The respect of the domain constraint by the coded solution in the form of a bit string is sometimes a problem. It is necessary to choose the coding carefully, or even to modify the operators
- The use of a GA does not guarantee the success of the optimization
- In practice, the efficiency of a GA often depends on the nature of the optimization problem. Depending on the case, the choice of operators and parameters will often be critical, but no general theory allows us to know with certainty the right parameterization, it will be necessary to do several experiments to get closer to it.

3.4.6 Optimization criteria for a PID controller

In this study, the objective is to determine optimal gains for a PID controller to improve the performance of the four-quadrant converter based PMDC motor.

In this case, the objective is to minimize the error (e), for this purpose each individual in the population of solutions is sent to the evaluation unit and its fitness is calculated to determine its performance as a controller for the given process. The performance of the system is calculated using the criterion ITAE (Integral of Time Multiplied by Absolute Error).

$$ITAE = \int_0^{\infty} t |e(t)| dt \quad (3.37)$$

The performance criterion is related to the fitness function and the optimal PID parameters are derived by minimizing an objective.

The PID controller is used to minimize the error signals, or we can define more rigorously, in the term of error criteria: to minimize the value of performance indices mentioned above. And because the lower the value of the performance index of the chromosomes, the better the chromosomes will fit (perform), and vice versa, we define fitness of the chromosomes as [108]:

$$\text{Fitness value} = \frac{1}{\text{Performance index}} \quad (3.38)$$

3.5 SIMULATION RESULTS AND DISCUSSIONS

Four-quadrant chopper circuits have been simulated for the purposes of varying the speed of a DC motor using MATLAB/Simulink software.

A four-quadrant chopper was used to control the speed in both directions of rotation of a permanent magnet DC motor, the PMDC motor power circuit and four quadrant scheme are shown in figures (3.13 and 3.14) respectively.

The parameters of the PMDC motor, used to simulate the different quadrants of operation of the four quadrant chopper are as follows:

- Armature winding parameters: $R = 0.8 \Omega, L = 0.002 H$
- Moment of inertia of the machine: $J = 0.012 (Kg \cdot m^2)$.
- Viscous friction coefficient : $fr = 0.01 N \cdot m$.
- Coefficient of friction: $k = 0.002$.
- Proportional controller $K_p = 1.45$.
- Integrating controller $K_i = 15.76$.

In order to highlight the performances and constraints of the DC motor controlled in speed by a PI controller. The model shown in figure was simulated over a 16 seconds cycle during closed-loop operation with Speed and torque variations.

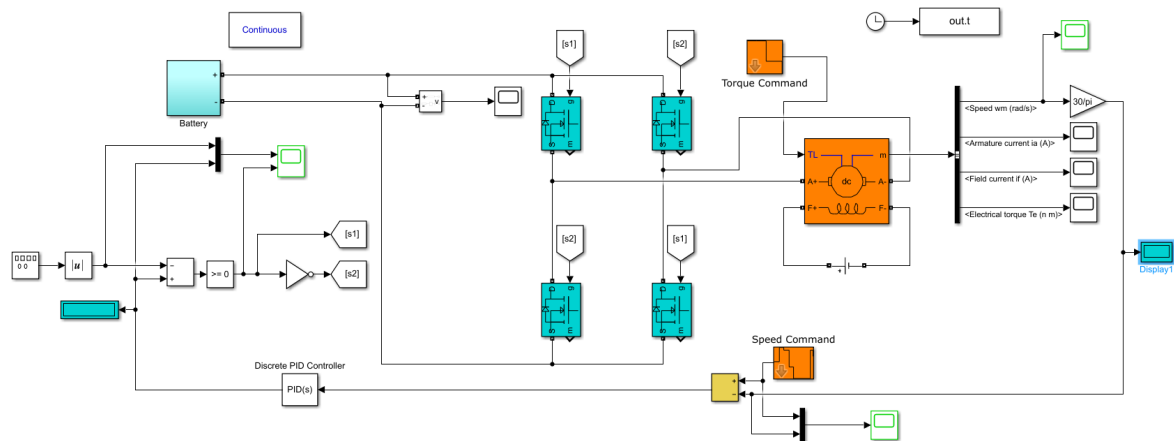


FIGURE 3.13: Global diagram of the simulation of a 4Q chopper driving a PMDC motor

Starting with the PWM control signal applied on the four quadrant DC-DC illustrated in Figure 3.15. Figure 3.16 shows the battery voltage, which contains a lot of disturbances. Figures (3.17 and 3.18) represent the armature current and the electrical torque of the PMDC motor respectively, since the current is the image of the torque it can be seen that these signals have similar dynamics. The following figure shows the field current of the motor where the variations are barely noticeable.

In an effort to improve the performances of the PI regulator, genetic algorithms have been trained to calculate the optimal gains for the controller. Figure 3.20 shows the control signal applied on the four-quadrant chopper based on the genetic algorithms optimization. Figure 3.21 shows the battery voltage, it can be seen that the perturbations in this signal are limited compared to the previous simulation (PI

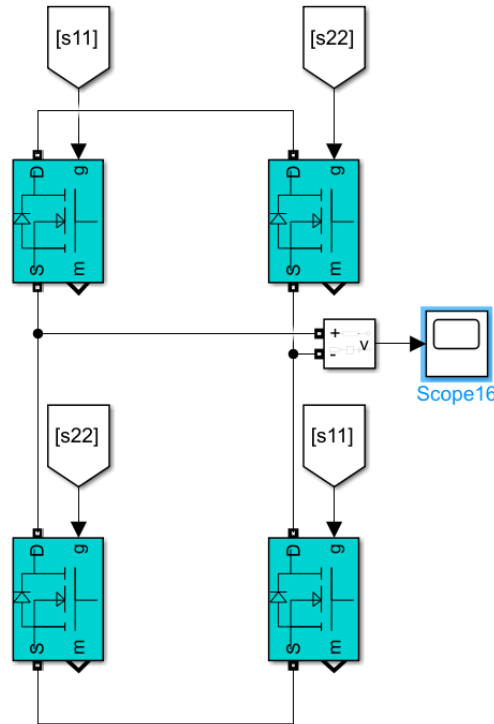


FIGURE 3.14: Block diagram of a four-quadrant chopper simulation

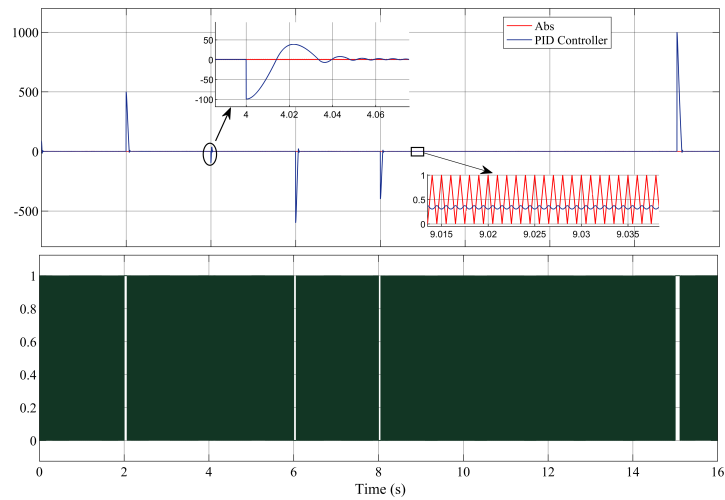


FIGURE 3.15: Control signal for the 4-Q chopper

controller). Same as the PI controller the armature current and the electrical torque variations shown in figures (3.22 and 3.23) have similar responses. Figure 3.24 is dedicated to the field current, where the variations are very small.

Figure 3.25 is a comparison between the motor’s speed responses to the variation in the reference speed between the PI controller and genetic algorithms based PI controller. Both of the control methods show good dynamics and efficient reference tracking proving the control strategy used for the PMDC motor. However, the signal of the PI controlled speed shows a variations in the sudden changes of the reference speed unlike the GA controlled speed where the signal is much smoother and shows less perturbations, which proves the effectiveness of the control technique applied to the system.

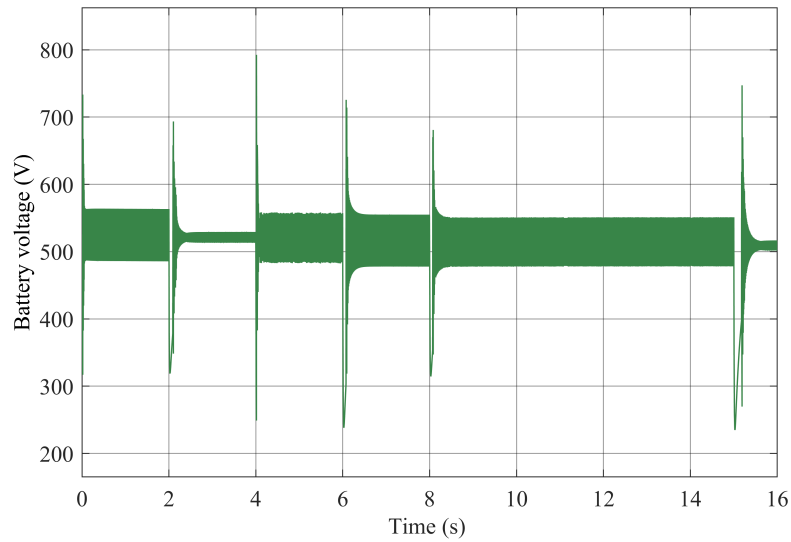


FIGURE 3.16: Battery voltage responses to the reference variation

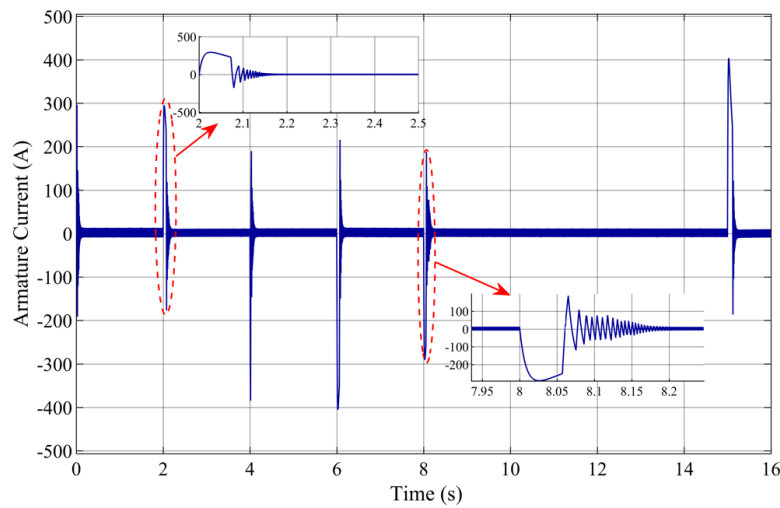


FIGURE 3.17: Armature current responses

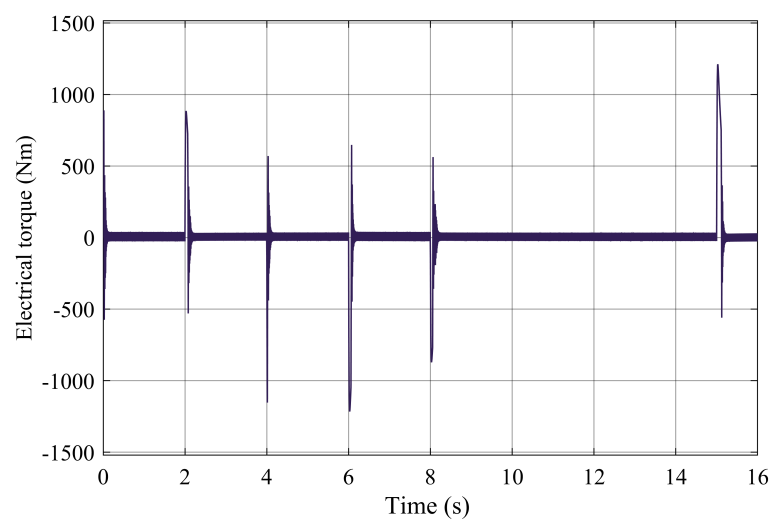


FIGURE 3.18: Electrical torque responses to load variations

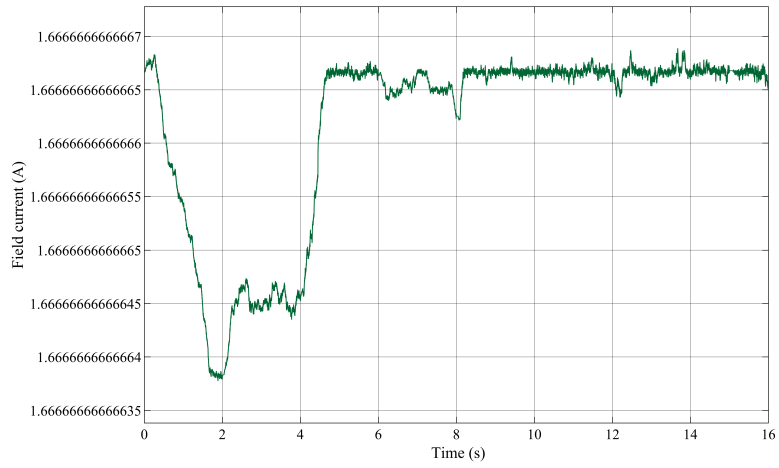


FIGURE 3.19: Field current of the PMDC motor

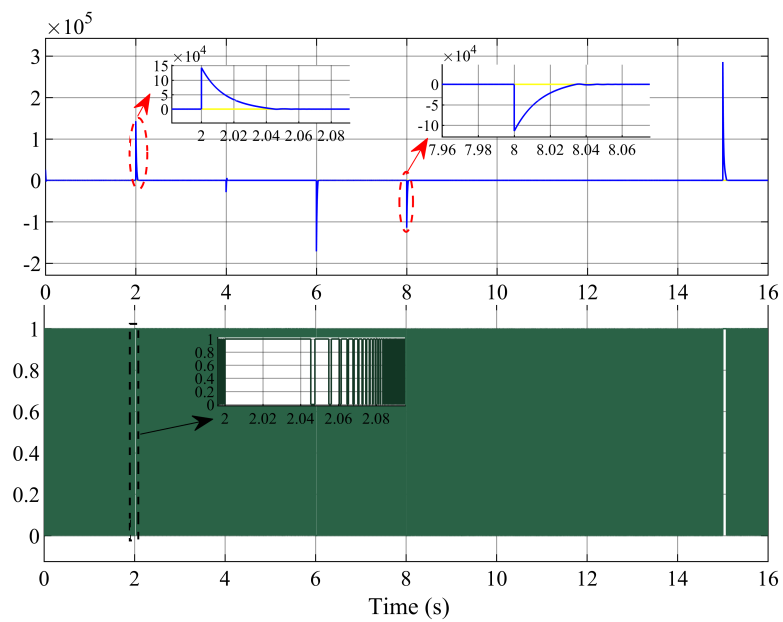


FIGURE 3.20: Four-quadrant control signals with genetic algorithms

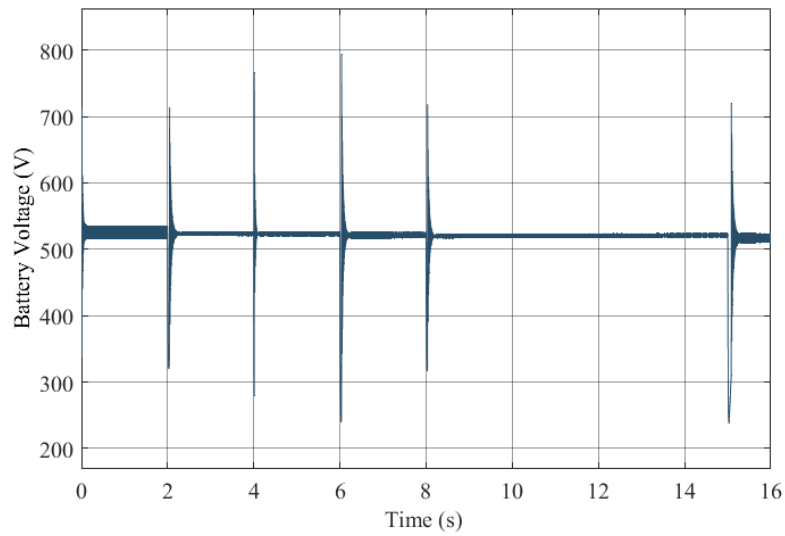


FIGURE 3.21: Battery Voltage in case of optimization with GA

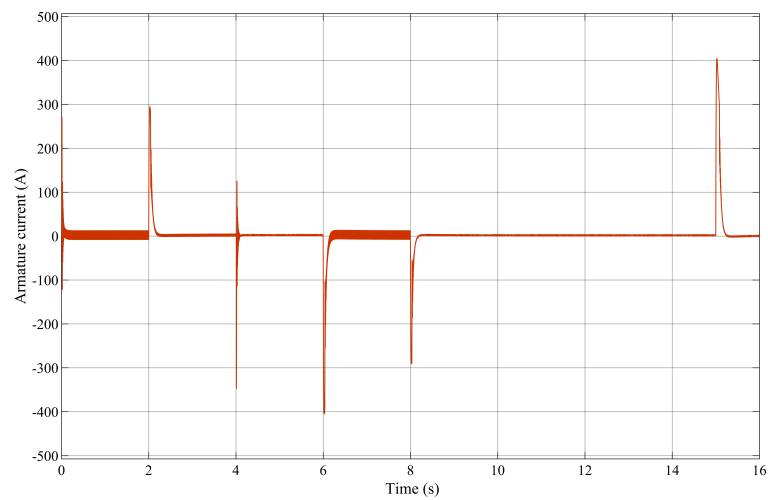


FIGURE 3.22: Armature current of the DC motor

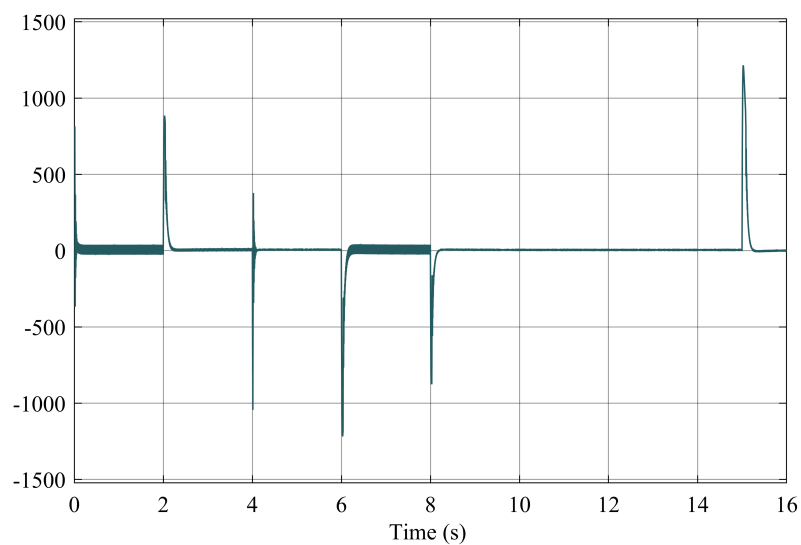


FIGURE 3.23: Electrical torque responses to the reference variations

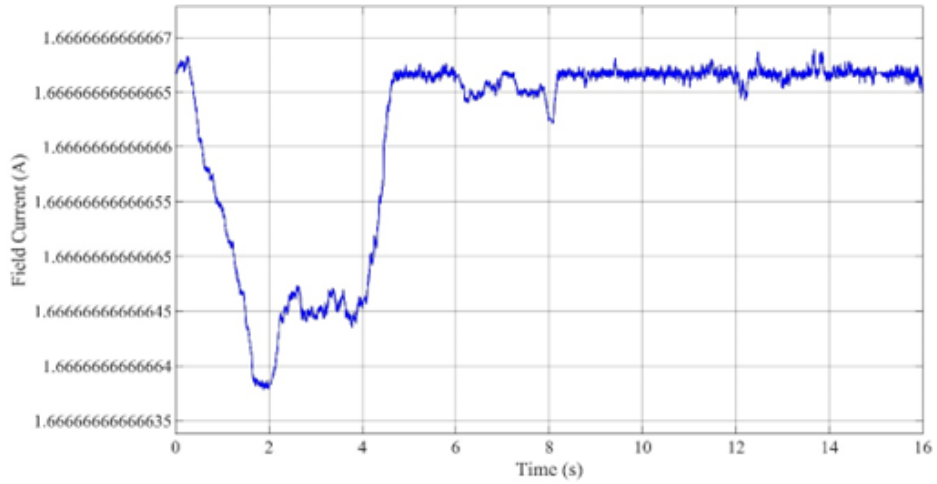


FIGURE 3.24: Field current of the PMDC motor

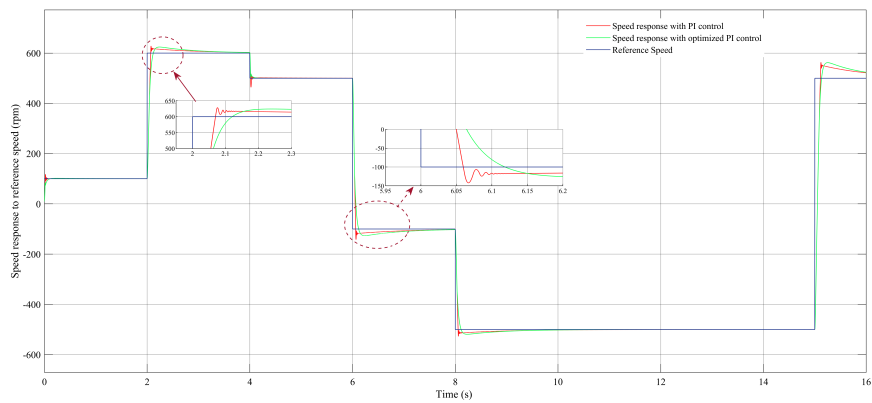


FIGURE 3.25: Comparison of the speed responses to the references in case of PI control and GA based optimized PI control

Chapter 4

Experimental design of a four-quadrant chopper for vehicular applications

In this chapter, we are interested in the practical realization of an identical prototype with a purely electric vehicle based on a four-quadrant chopper whose purpose is to analyze all the phenomena of energy flow (voltage, current, power...etc.) in the traction elements, as well as to control the static and dynamic evolution of the characteristics of the electric drive system. The data acquisition is ensured by an Arduino Uno microcontroller card. A PI corrector is used in the control loop of the DC bus voltage and the motor speed. Experimental tests have been performed in order to validate the proposed approach.

4.1 Main Diagram

Figure 4.1 depicts the basic control circuit of our application (the drive train of an electric vehicle). The four-quadrant chopper consists of two arms, each of which contains two MOSFET type switches with antiparallel diodes. This chopper is associated with a bidirectional DC-DC buck boost converter.

4.2 Synoptic Diagram

Figure 4.2 illustrates the studied system, it is composed of two main parts:

- A power block based on static switches.
- A control block consisting of three boards (Arduino uno board, isolation board and the driver control board).

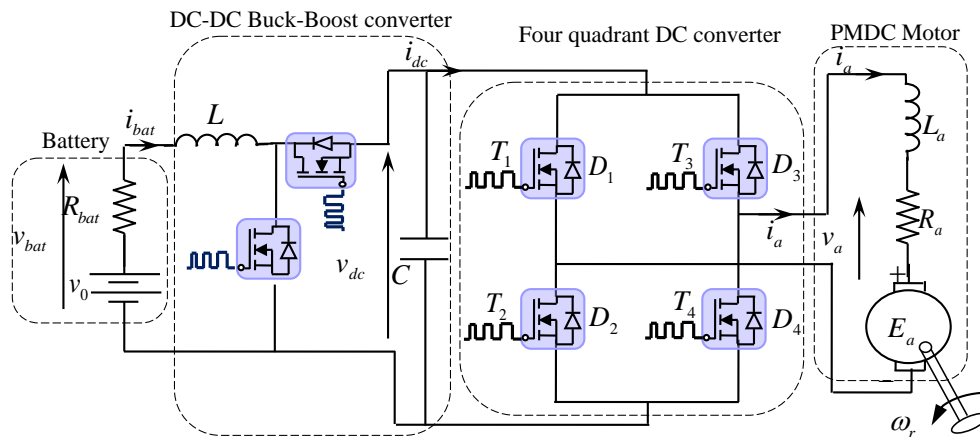


FIGURE 4.1: The drive train of an electric vehicle

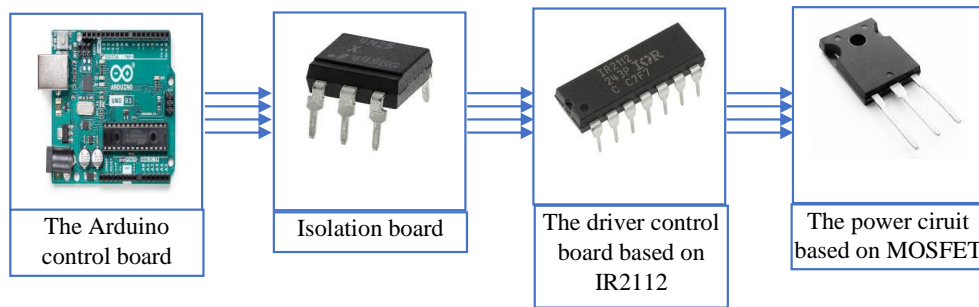


FIGURE 4.2: Synoptic scheme of the studied system

4.3 CONTROL BLOCK

The control block (Figure 4.3) is basically summarized by the use of the Arduino Uno module which will be detailed later in this chapter as well as the hardware part (optocoupler, drivers).

4.3.1 Arduino Board

The Arduino module is a free hardware board (control platform) whose plans of the board itself are published under a free license. Some components of the board, such as the microcontroller and additional components, are not under free license. A programmed microcontroller can analyze and produce electrical signals in order to perform a variety of tasks. The Arduino is used in many applications such as industrial and embedded electrical engineering, model making, home automation but also in different fields such as contemporary art and robot control, motor control and light shows, communication with the computer, mobile device control (model making). Each Arduino module has a +5 V voltage regulator and a 16 MHz quartz oscillator (or a ceramic resonator in some models). To program this board, we use the IDE (Integrated Development Environment) Arduino software.

Why Arduino Uno?

Many electronic boards are available with microcontroller-based platforms for programmed electronics. Each of these technologies acquire difficult programming information and incorporate them into an easy-to-use presentation. Similarly, the Arduino system makes working with microcontrollers easier.

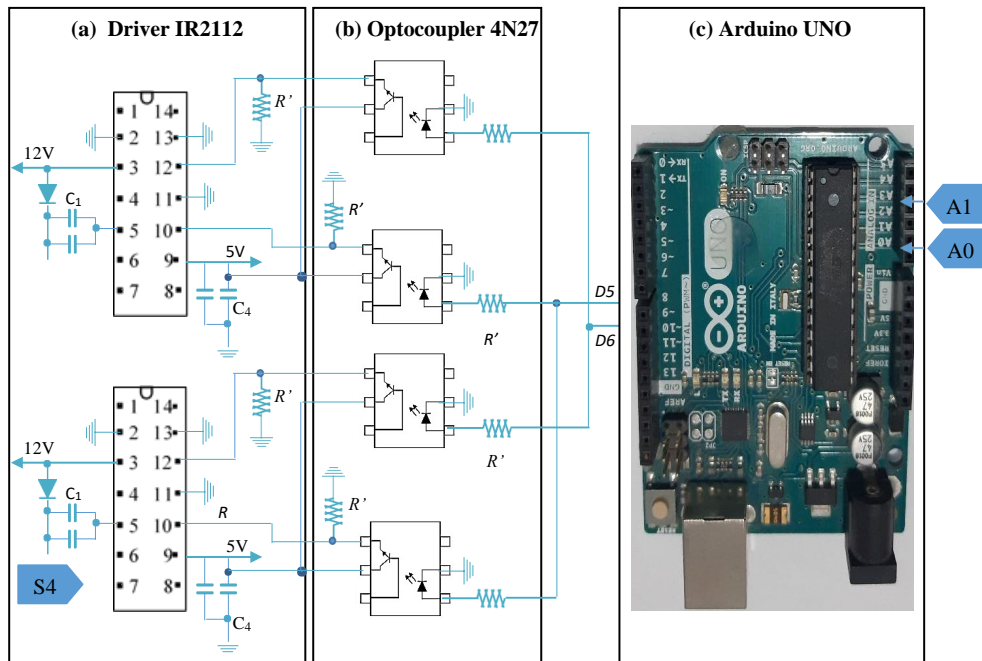


FIGURE 4.3: Control Block of the four-quadrant chopper



FIGURE 4.4: Arduino UNO board

While offering to potential customers several advantages as follows:

- Reduced price:**
 Arduino boards are relatively inexpensive compared to other hardware platforms. The cheapest version of the Arduino module can be assembled by hand, (pre-assembled Arduino boards cost less than 2500 Dinars).
- Multi-platform:**
 The Arduino software, written in JAVA, runs on Windows, Macintosh and Linux operating systems. Most microcontroller systems are limited to Windows.
- A clear and simple programming environment:**
 The Arduino programming environment (the Arduino IDE software) is easy to use for beginners while being flexible enough for advanced users to benefit as well.

- **Open source and extensible software:**

The Arduino software and the Arduino language are released under an open source license available for completion by experienced programmers. The Arduino module programming software is a cross-platform JAVA application (running on any operating system), serving as a code editor and compiler, and can transfer the program through the serial link (RS232, Bluetooth or USB depending on the module).

- **Open source and extensible hardware:**

Arduino boards are based on Atmel ATMEGA8, ATMEGA168, ATMEGA 328 microcontrollers, the schematics of the modules are published under a Creative Commons license, and experienced circuit designers can make their own version of Arduino boards, adding to and improving them. Even relatively inexperienced users can make the test board version of the Arduino board, the purpose of which is to understand how it works to save cost.

Constitution of the Arduino Uno board

An Arduino module is generally built around an ATMEL AVR microcontroller, and complementary components that facilitate programming and interfacing with other circuits. Each module has at least a 5V linear regulator and a 16 MHz quartz oscillator (or a ceramic resonator in some models). The microcontroller is pre-programmed with a boot loader so that a dedicated programmer is not required.

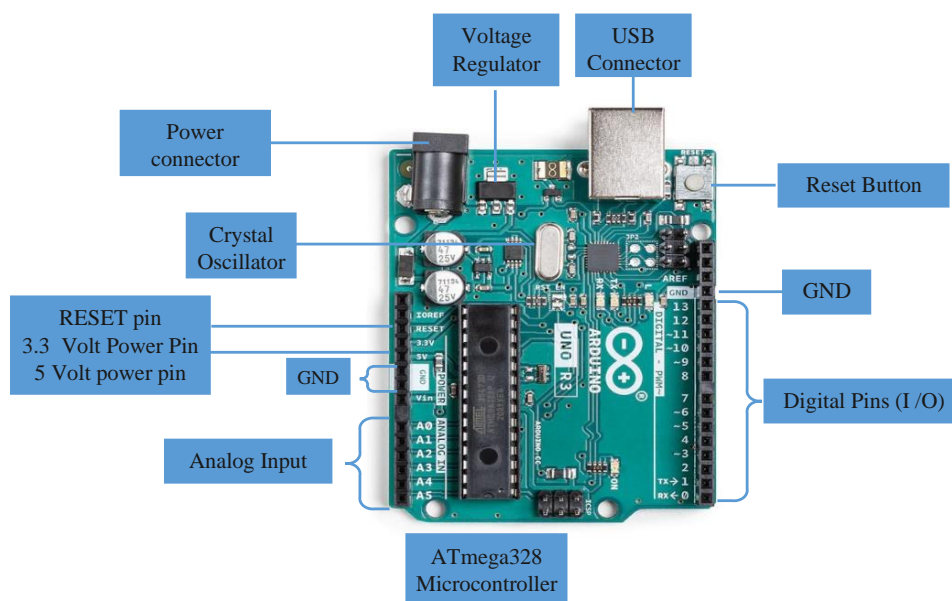


FIGURE 4.5: Constituents of the Arduino Uno board

The components of the Arduino board are :

- **Jack socket**

- Allows you to connect a power supply (battery, AC adaptor)
- USB connection. The USB port has two actions:
 - * Supply the card with electrical energy (5V)
 - * Download the program to the card

- **Microcontroller**
 - Allows to store the program and to execute it
- **6 analog inputs**
 - Allows the connection of analog sensors and detectors.
 - These six inputs can accept 1024 analog values between 0 and 5 Volts.
- **14 digital inputs and outputs**

Two actions of the connectors:

 - Connecting actuators
 - Connecting detectors
- **A 16 MHz crystal**
 - It is the Arduino's clock, which regulates its operation.
- **An ICSP header**
 - Allows the Arduino to communicate with external components via the SPI (Serial Peripheral Interface) protocol
- **Reset bouton**
 - Allows to reset the Arduino board.

4.3.2 Programming Framework

Arduino software

The programming software of the Arduino board serves as a code editor (a language similar to C). Once the program is typed or modified on the keyboard, it will be transferred and stored in the board through the USB link. The USB cable supplies both power to the board and also carries the information this program called Arduino IDE.



FIGURE 4.6: Communication with Arduino

Program download steps

A simple chained configuration must be followed in order to inject a code to the Arduino board via the USB port.

1. We design or open an existing program with the Arduino IDE software.

2. We check this program with the Arduino software (compilation).
3. If errors are reported, the program is modified.
4. We load the program on the board.
5. The electronic assembly is wired.
6. The execution of the program is automatic after a few seconds.
7. The card is powered either by the USB port or by an autonomous power source (9-volt battery for example).
8. We check that our assembly works.

Code injection

Prior to sending a program to the board, it is necessary to select the type of the board (Arduino Uno) and the number of the USB port (COM). The characteristics of the Arduino board are presented in Appendix B.

4.3.3 Galvanic isolation

Various problems are encountered when operating in a direct connection between the control circuit and the power circuit, such as ground returns, electrical noise and the risk of destruction of the control circuit by load current feedback. In order to avoid all such problems, the control circuit must be electrically isolated from the power circuit, this isolation is achieved by an optocoupler.

Isolation principle

Isolation is achieved by using two different power sources and two different grounds, so there is no electrical connection between the circuits mentioned. The galvanic isolation can be realized by an electromagnetic connection with a transformer, for example by a light connection or by an optocoupler. In our case we used the optocoupler type 4N25.

4N25 integrated circuit

An optocoupler (4N25) is a component of the control electronics that allows a galvanic isolation from the exchange (power circuits) or from a data transmission line. It is called an optical coupler or photocoupler (opto-isolation) and consists of a transmitter (LED: light-emitting diode) and a receiver (see Appendix C).

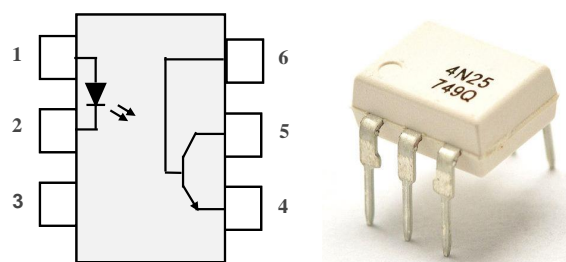


FIGURE 4.7: The internal structure of an opto-coupler

1. IR LED anode/ Positive Pin

2. IR LED cathode/Negative Pin
3. Not connected Pin
4. Base Pin of the photo transistor
5. Collector Pin of the photo Transistor
6. Emitter Pin of the photo transistor

The layout of the 4N25 integrated circuit (optocoupler) in the ISIS proteus software is shown in [Figure 4.8](#)

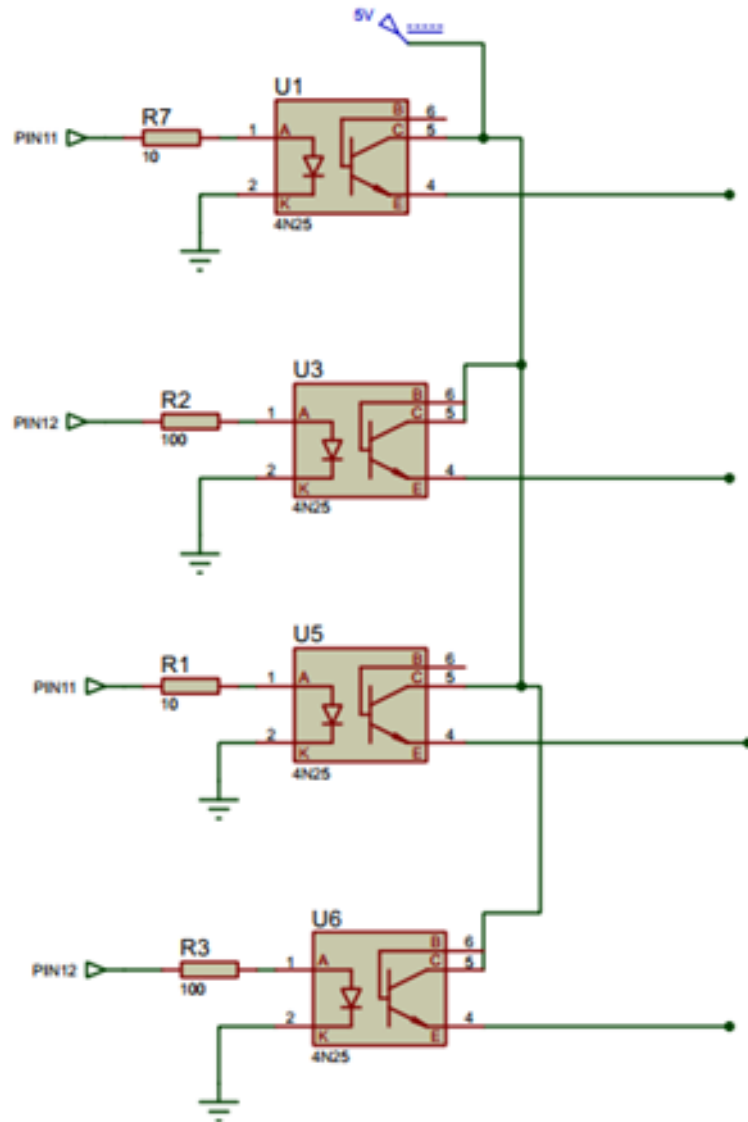


FIGURE 4.8: Mounting of optocoupler under ISIS Proteus

4.3.4 MOSFET Driver

The IR2112 is an integrated circuit that allows the high frequency control of two or one MOSFET, under voltages up to 600 V, ensuring the electrical isolation of the Arduino and our MOSFET (see Appendix C.)

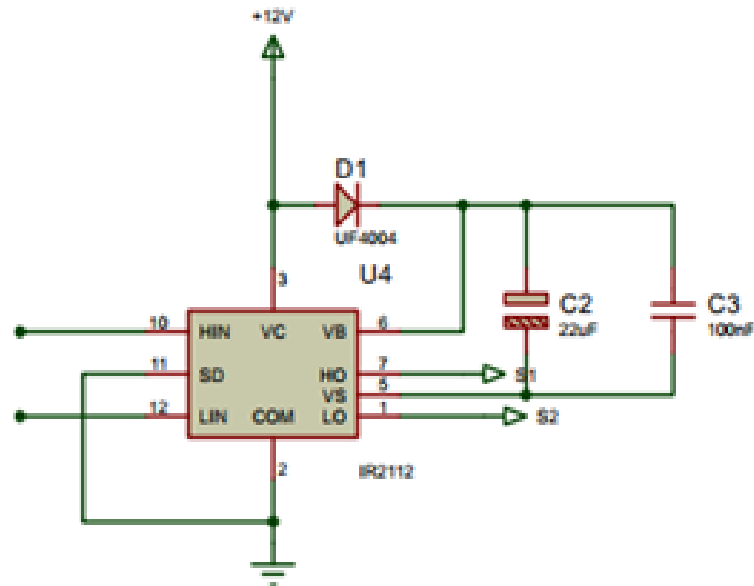


FIGURE 4.9: Driver implementation on Proteus software

4.4 POWER BLOCK

The power circuit consists mainly of two components: the four selected switches are MOSFET and the load (DC motor)

4.4.1 Static Solid State Switch

A MOSFET IRFP460 is used because of its simplicity of use, high switching frequency, sufficient characteristics and availability on the industrial market (see Figure. 5.10)

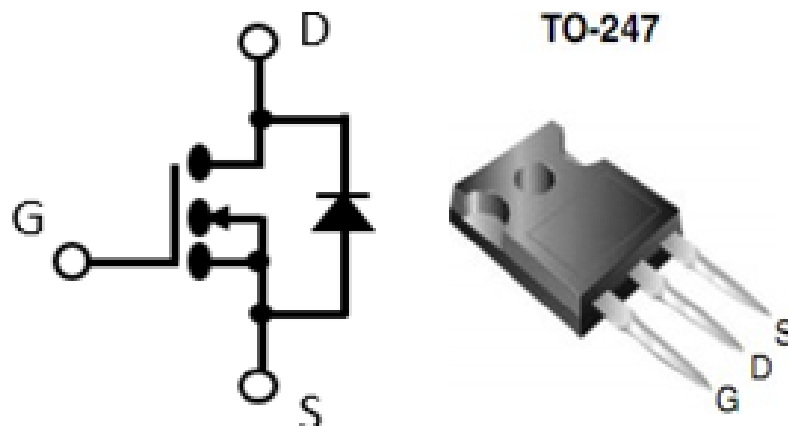


FIGURE 4.10: MOSFET Transistor IRFP460

4.4.2 Other Accessories

For the implementation of the control and power boards, the following elements are used (Table 4.1):

Diode	IN41
Capacity	$22\mu F$, $32\mu F$, $150nF$ and $3300\mu F$
Resistance	$1 k\Omega$
Load	120Ω

TABLE 4.1: Other accessories

4.5 PRACTICAL IMPLEMENTATION OF THE TEST BENCH

In this part, we present the practical realization of a chopper with four quadrants controlled by a conventional PI regulator.

4.5.1 Speed Sensor Output Conditioning

The output of the tachometric speed sensor gives a positive or a negative random value signal, but the analog input of the microcontroller (Arduino-Uno board) always requires a positive signal lower than 5 Volts. It is therefore essential to lower this output signal to be able to inject it into the Arduino board. This reduction must be equal to a quotient of (5/2) Volts (See figure 5.11).

Following the steps mentioned in figures 4.11 and 4.12 allows to guarantee a good calibration of the speed sensor and a good conditioning of the output signal of the acquisition chain (speed image) according to the parameters and physical constraints of the Arduino-Uno board. These steps are detailed as follows:

- The output of the speed sensor must be reduced by a voltage divider (potentiometer) (Of a ratio equal to $\frac{R_1}{100k\Omega}$ with $R_1 = 33 k\Omega$).
- We must add to our circuit an additional fixed positive voltage of about 2.5 Volts by reducing the voltage of 5 Volts by a potentiometer (with a ratio equal to $\frac{R_3}{100k\Omega}$ with $R_1 = 50 k\Omega$).

The addition of a filter capacitor of order $2\mu F$ improves the quality of the signal. Ultimately, we obtain at the input of the microcontroller a strictly positive signal $V \Omega$ and less than 5 volts according to the following scale:

4.5.2 Software Implementation

The Proteus software allows simulating the physical behavior of the component chosen for the realization of the four-quadrant DC-DC converter. Figure 4.13 represents the detailed diagram of the control of the parallel DC-DC converter by the Proportional-Integral controller under the Proteus software.

The simulated waveform of Arduino Uno board based DC motor speed control for the four quadrant modes of operation i.e. forward motoring and reverse motoring. Figures 4.14 and 4.15 represent the state of the switching devices during forward motoring movement and backward motoring movement respectively. Figures 4.16 and 4.17 show the output signal of the Arduino controlling the switching devices. These results are compatible with the before mentioned theory, as it can be seen that the switch S_1 and S_4 function simultaneously during forward motoring motion and S_2 and S_3 work together during backward motoring motion.

Figures 4.24 and 4.25 represent the motor speed response to references equivalent to 5.22 and 3.23 respectively. The adaptation of these equivalent values is explained in the previous section.

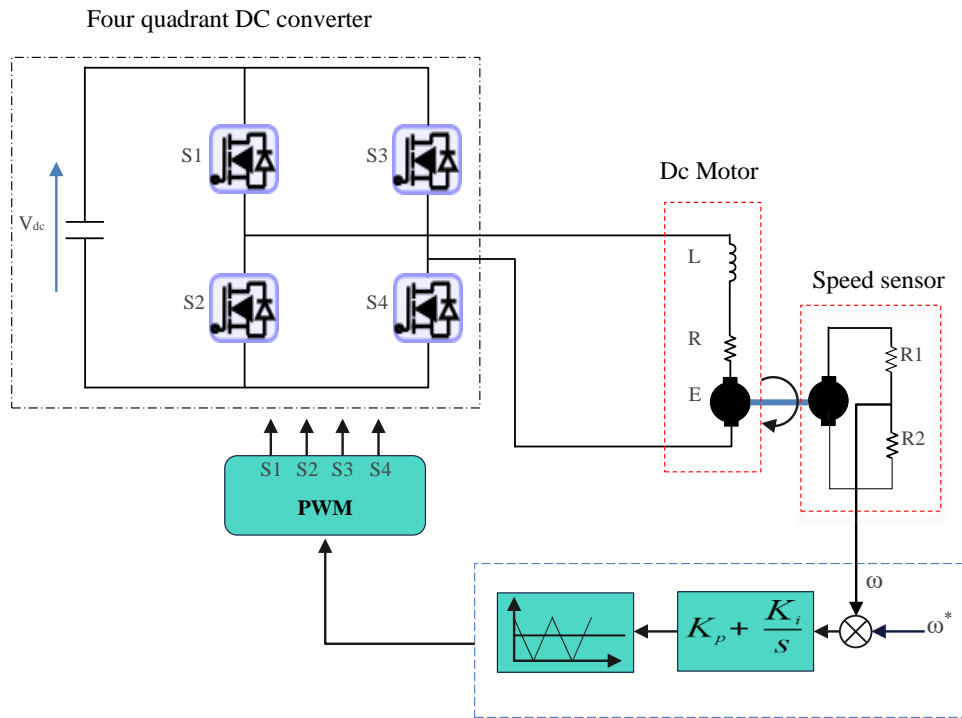


FIGURE 4.11: Speed sensor conditioning and calibration circuit

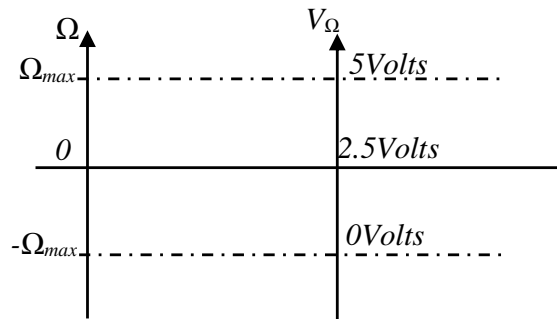


FIGURE 4.12: Conditioning scale

4.5.3 Global experimental bench

The practical global assembly of the drive train is developed and described in the previous diagrams. Such a prototype aims at reproducing the behavior of the electric drive train close to reality. The development of such a tool allows a considerable gain in terms of research cost, a minimal space requirement, a flexibility from the point of view of the characteristics of the car and especially a total control of the applied electrodynamic behavior. The test bench shown in Figure 4.26 is composed of the two physical processes (DC machine and battery) coupled by means of an electrical conversion bridge (four quadrant DC-DC boost-buck converter). The DC machine is always powered and self-driven by the DC-DC buck converter. The MOSFET module board (buck chopper) is equipped with passive current and voltage sensors. The control law is implemented on an Arduino-Uno microcontroller board.

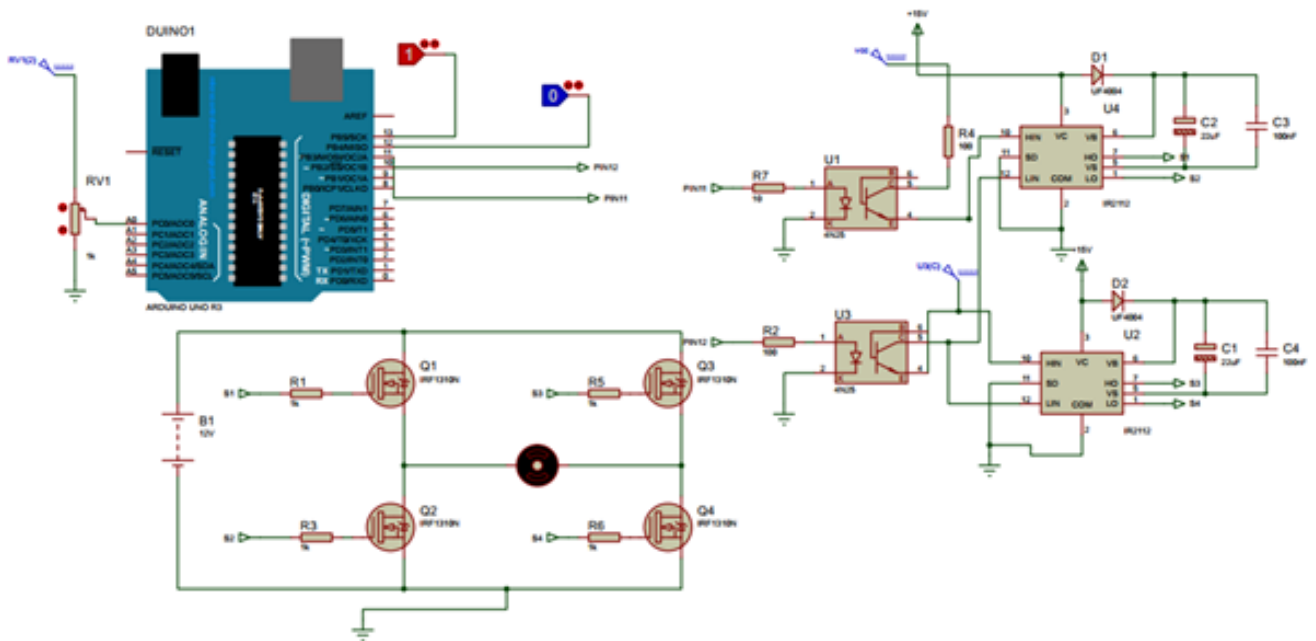


FIGURE 4.13: System tested on Proteus

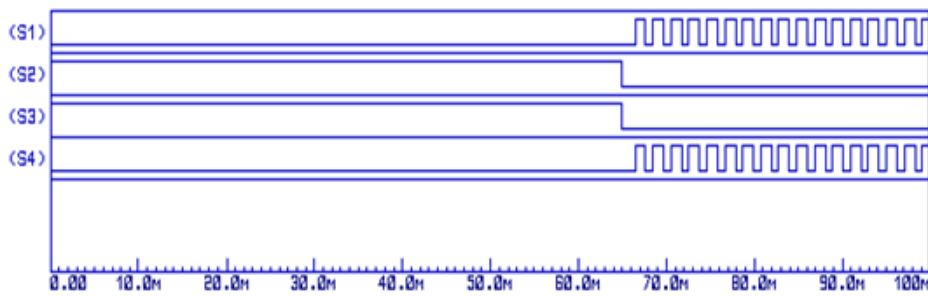


FIGURE 4.14: Control of the switches in forward motoring movement



FIGURE 4.15: Control of the switches in backward motoring movement

Detailed test bench

In the [Figure 4.27](#) it can be clearly seen that the main boards building the studied system to control a DC motor.

Experimental results

Figures [4.28](#) and [4.29](#) show the performance of the motor speed, DC voltage and current obtained without DC-DC converter. The experimental results confirm that the system loses its stability for a degraded

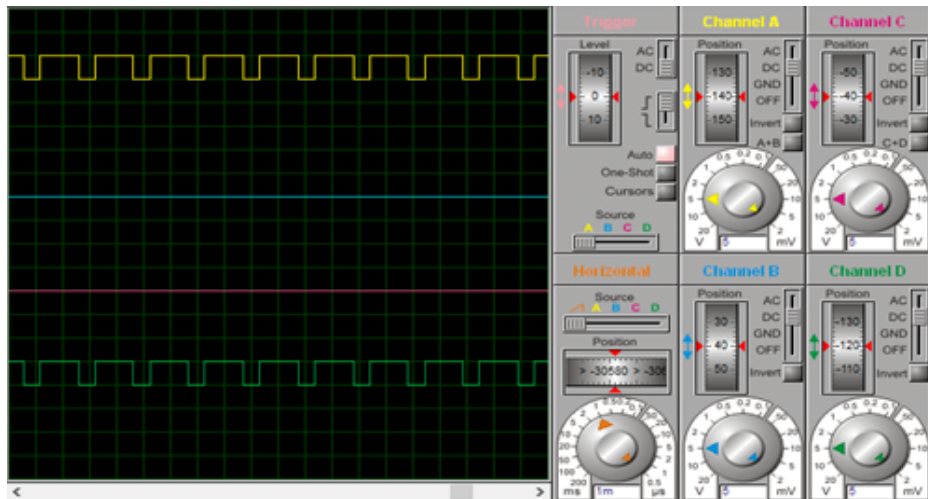


FIGURE 4.16: Output signals of the Arduino in forward motoring movement for duty cycle=0.8

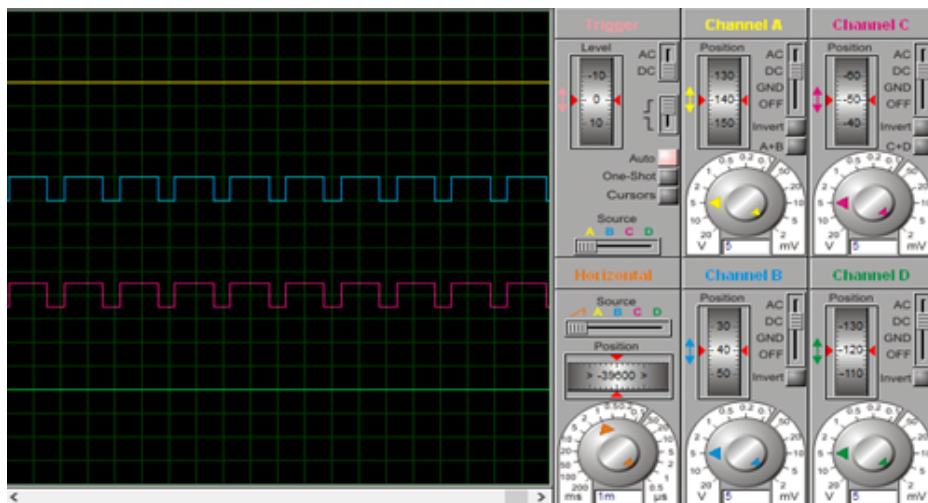


FIGURE 4.17: Output signals of the Arduino in backward motoring movement for duty cycle=0.8

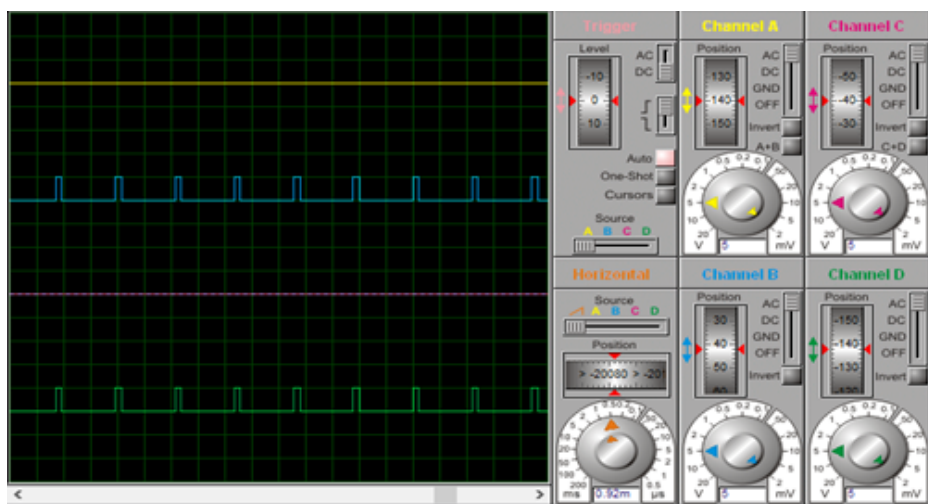


FIGURE 4.18: Output signals of the Arduino in forward motoring movement for duty cycle=0.15

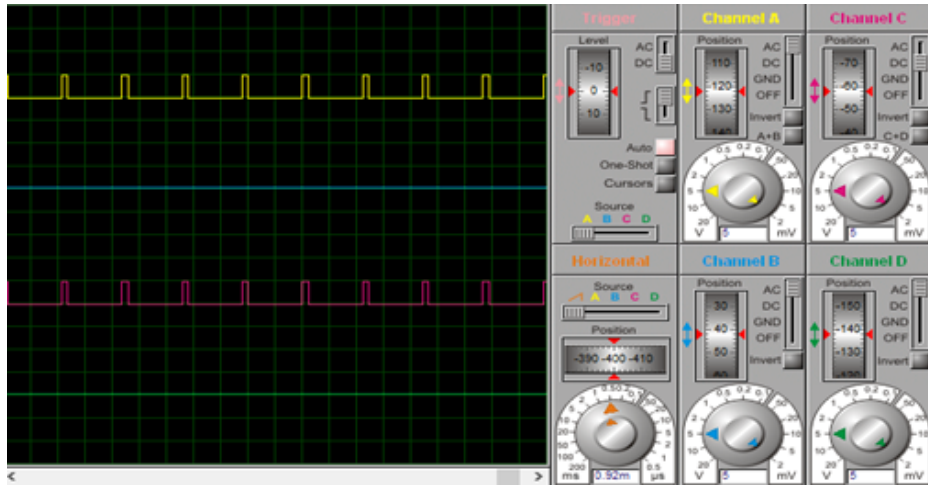


FIGURE 4.19: Output signals of the Arduino in backward motoring movement for duty cycle=0.15

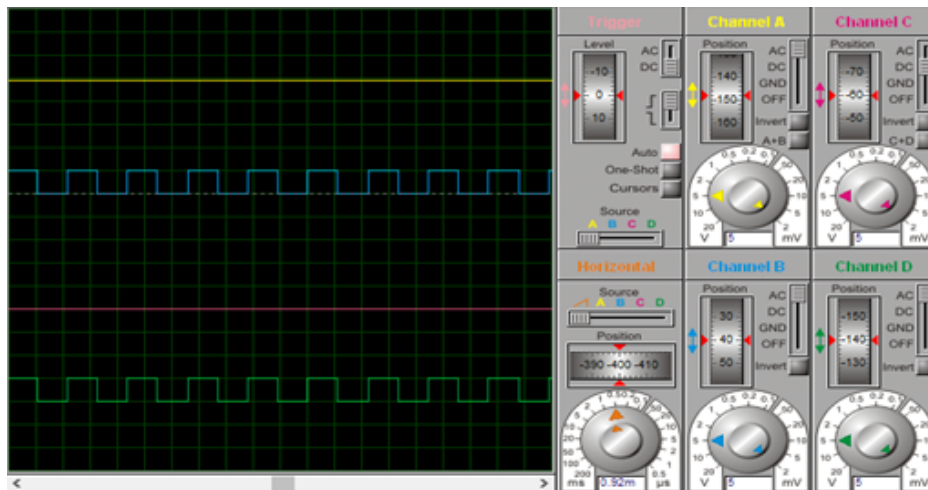


FIGURE 4.20: Output signals of the Arduino in forward motoring movement for duty cycle=0.5

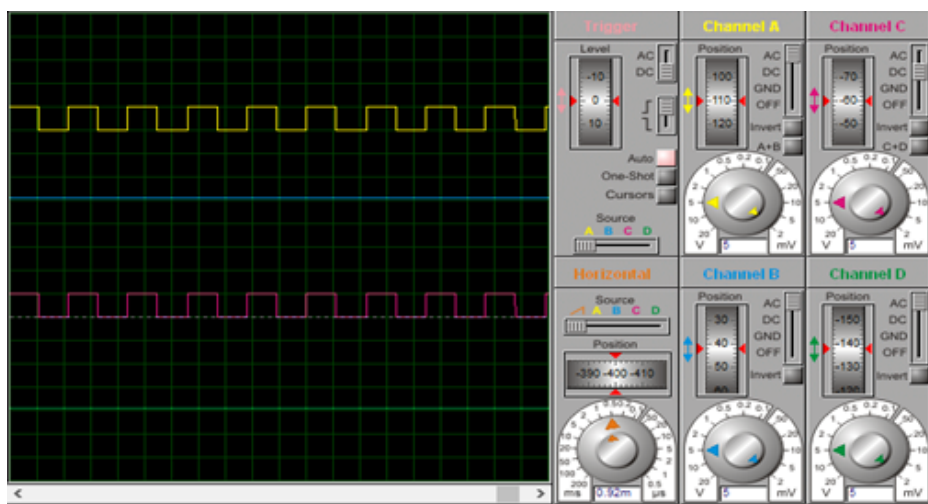


FIGURE 4.21: Output signals of the Arduino in backward motoring movement for duty cycle=0.5

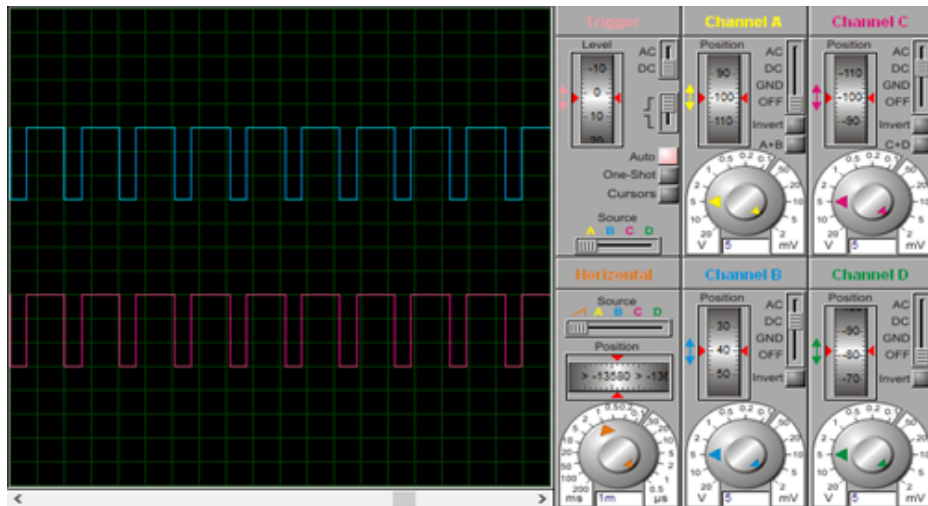


FIGURE 4.22: Output signals of the driver IR2112 in forward motoring movement (S1 and S2)

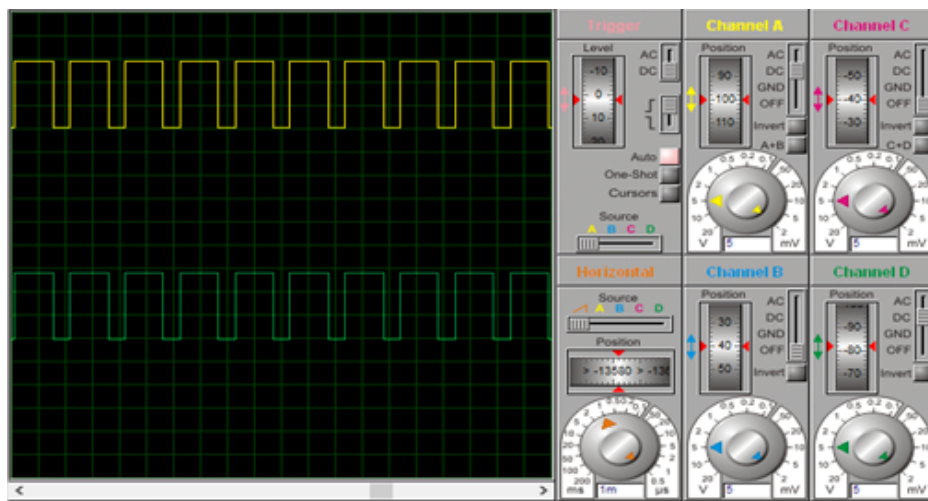


FIGURE 4.23: Output signals of the driver IR2112 in backward motoring movement (S2 and S3)

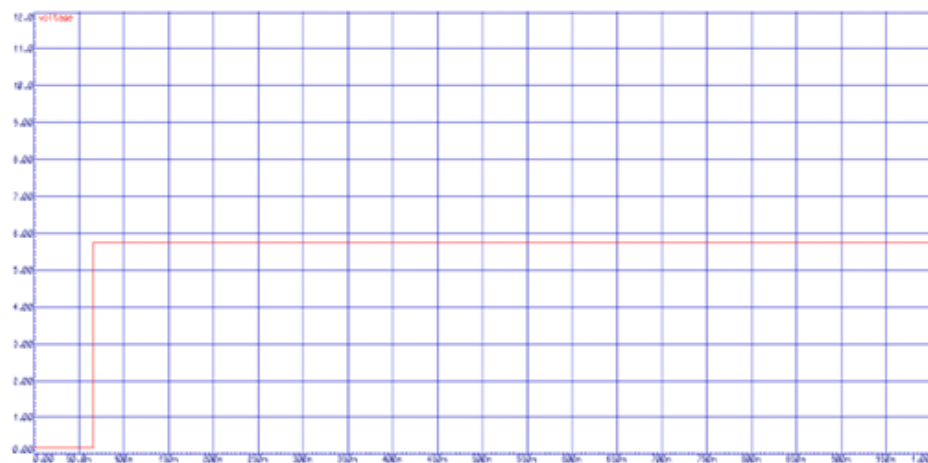


FIGURE 4.24: Motor speed response to a reference equivalent to 50rpm

battery voltage and no element of the conversion chain reacted to improve the situation.

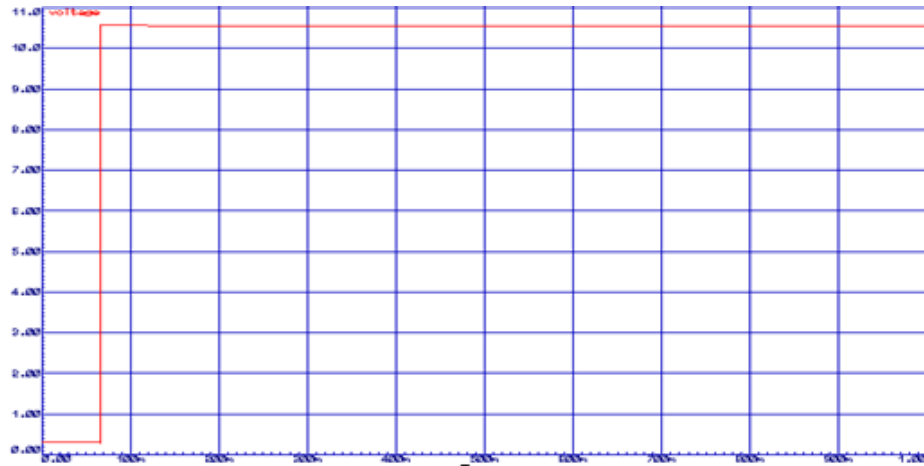


FIGURE 4.25: Motor speed response to a reference equivalent to 100rpm

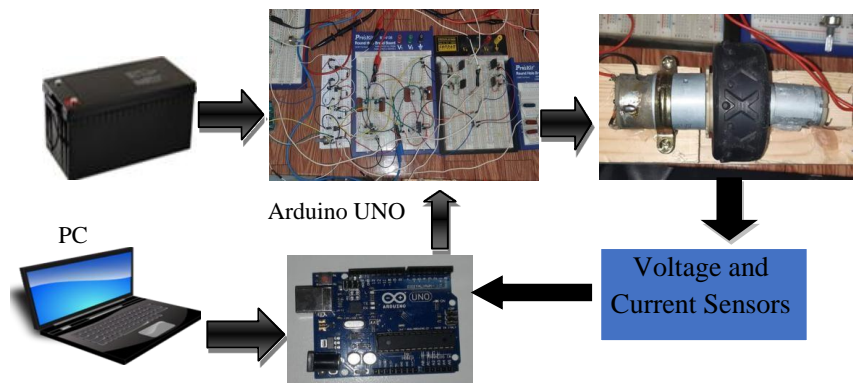


FIGURE 4.26: Experimental test bench

In the case of a decrease in the battery voltage (to 7 Volts) caused by a failure or over consumption, the dynamic characteristics of [Figure 4.30](#) below are obtained. Operation at low speed causes the presence of a considerable transient peak with better compliance with the order of the control in the steady state. On the other hand, in the event of a high speed caused by the control, there is a very large static error due to the limitation of the maximum electrical power generated by the battery.

[Figure 4.31](#) display the experimental result of a speed at free acceleration using the reference model adaptive control. Additionally, the real speed is measured and compared. It can be seen that there is a very good accordance between reference and real speed without any steady state error. On the same figure ([4.31](#)) appears the reference and measured DC voltage evolution, the controlled voltage is not affected by the transient starting regime and the change in the reference speed set point, which explains the correct intervention of the control algorithm.

[Figure 4.32](#) shows the speed responses when the DC voltage is equals to zero, it can be seen that the PMDC is still turning at a low speed with a lot of oscillation and that's when the regenerative braking takes role in charging the battery via the bidirectional DC-DC converter.

A test at different reference speed levels in the form of a staircase was applied. The speed control response is illustrated in the [Figure 4.33](#). These results made the drive remain stable and this condition can be maintained within the desired speed levels.

A benchmark reference is applied in ([4.34](#)) and ([4.35](#)), the reference speed varies from zero to different levels even at low speed. It is obvious from the obtained results that the measured speed follows its

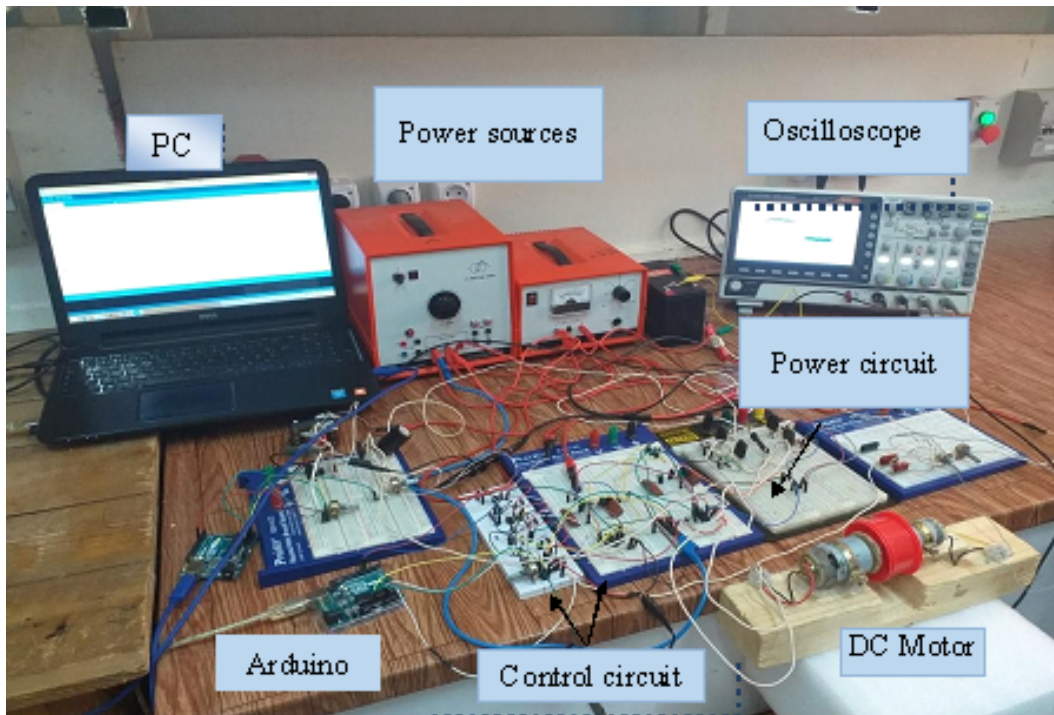
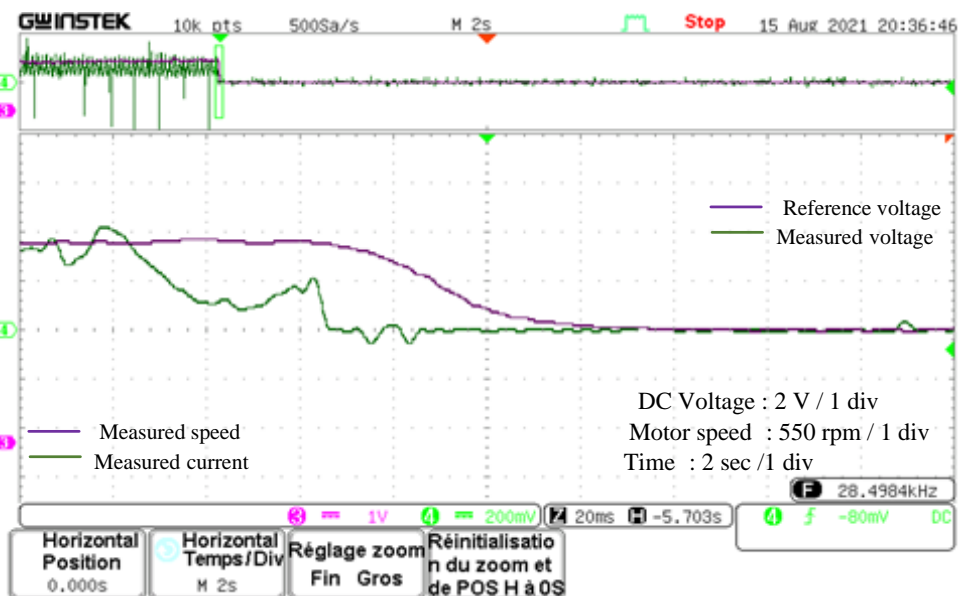


FIGURE 4.27: Experimental test bench

reference perfectly with a slight overshoot (Figure 4.36). Oscillations appear at the measured speed, these oscillations due to the measurement chain and the non-linearity of the electronic components used in the assembly.

FIGURE 4.28: Motor speed response and DC voltage response. $v_{bat} = 7V$ (without regulation).

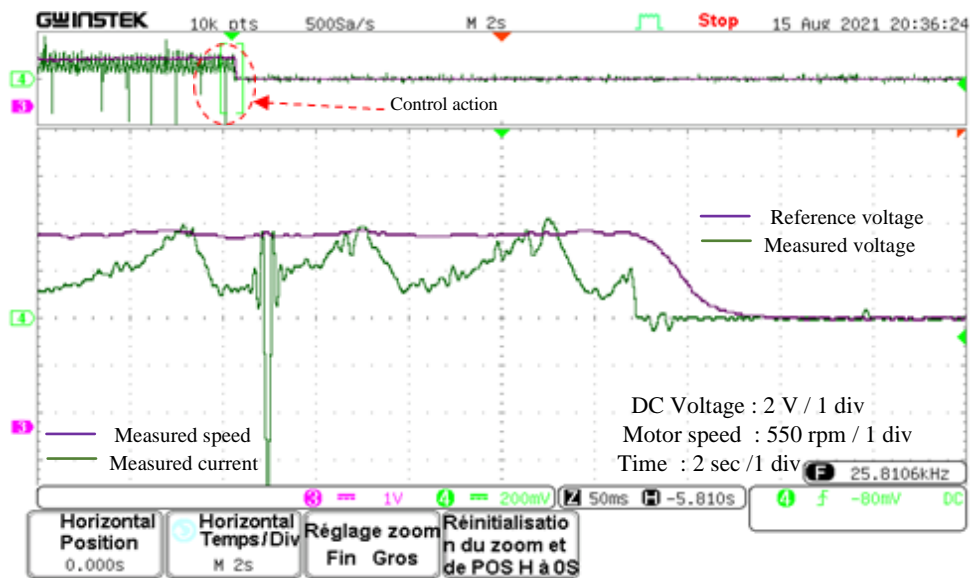


FIGURE 4.29: Motor speed response and DC voltage response in case of energy recovery.

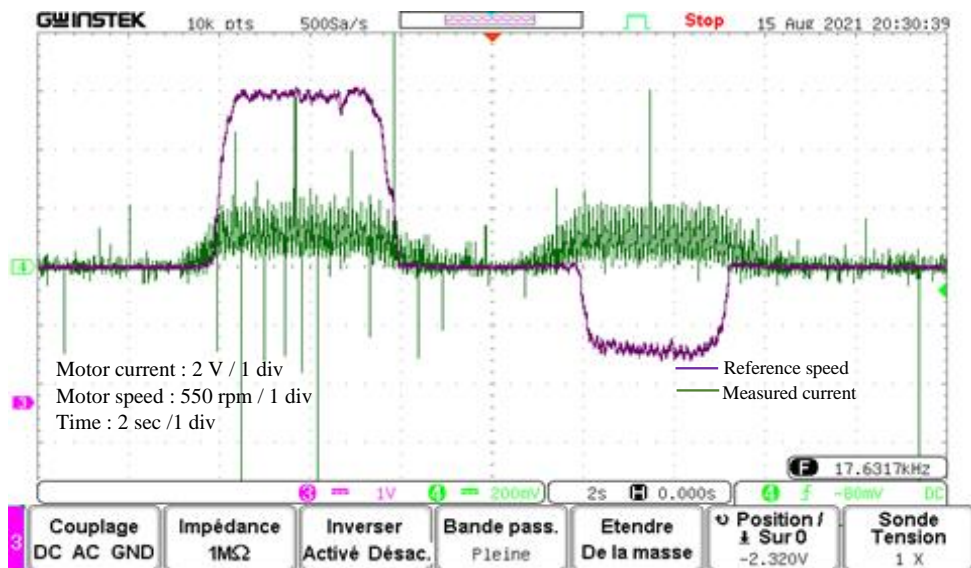


FIGURE 4.30: Speed response in case of backwards.

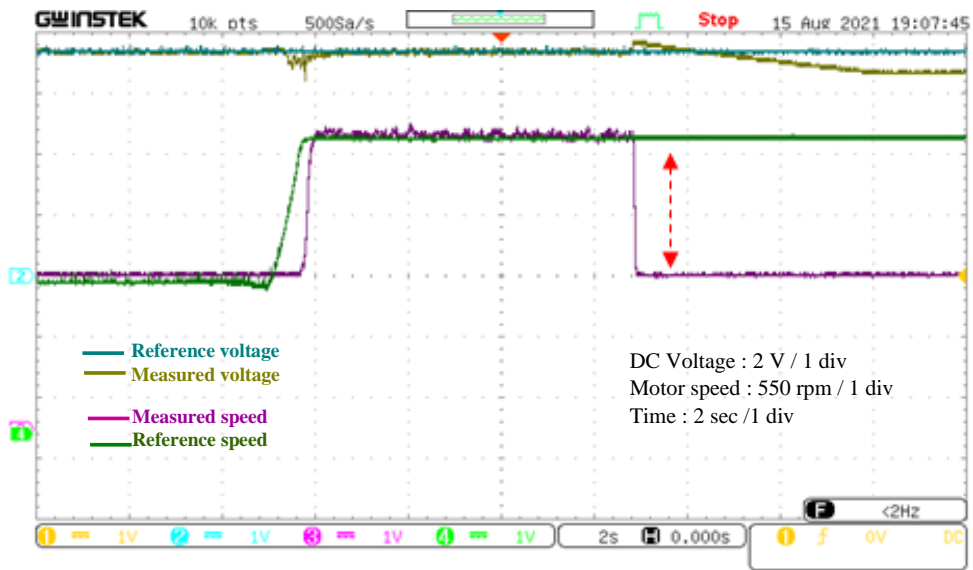


FIGURE 4.31: DC voltage regulation response with electric braking applied

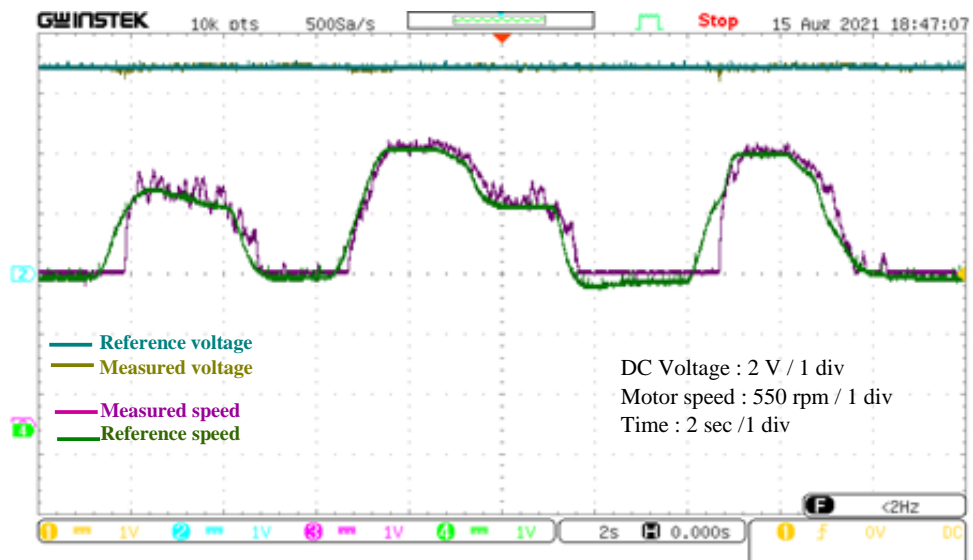


FIGURE 4.32: Performance tracking of motor speed regulation response for benchmark referenced

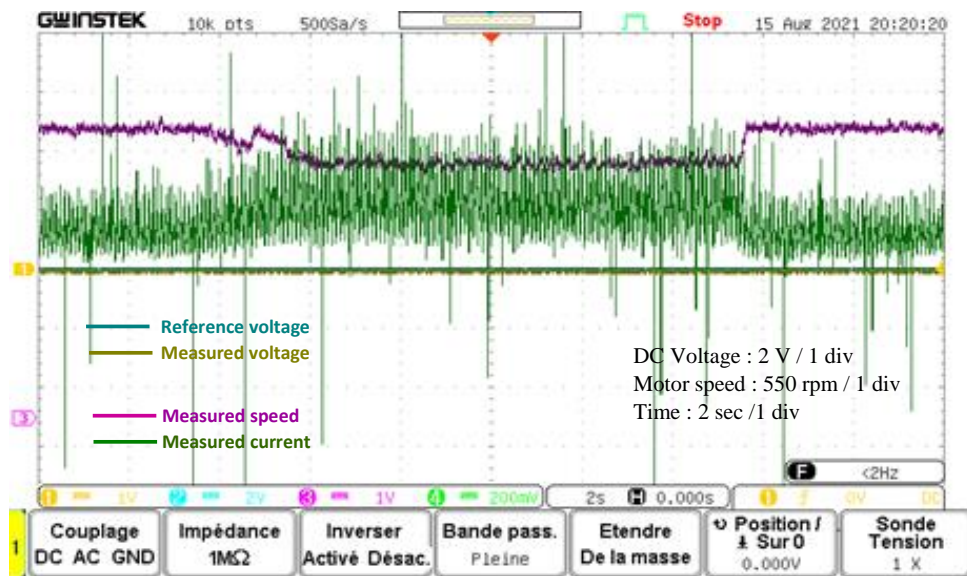


FIGURE 4.33: Speed response in the case of applied torque

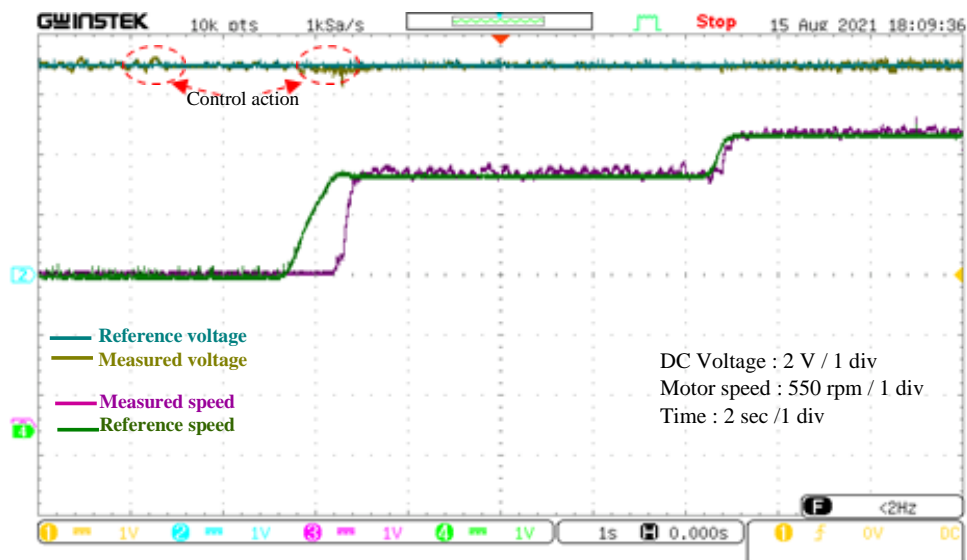


FIGURE 4.34: Speed response and DC voltage regulation with the DC-DC buck-Boost converter

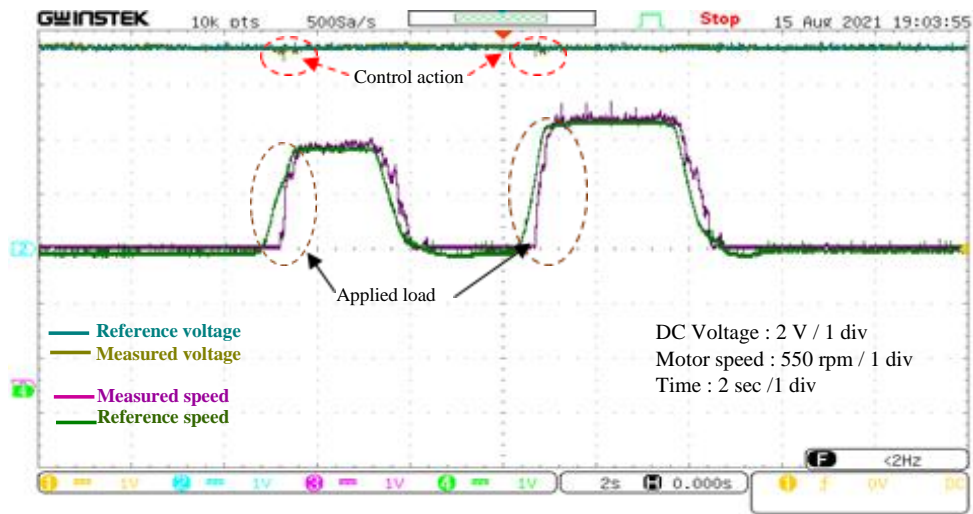


FIGURE 4.35: PMDC motor speed variation with sudden changes in the reference speed

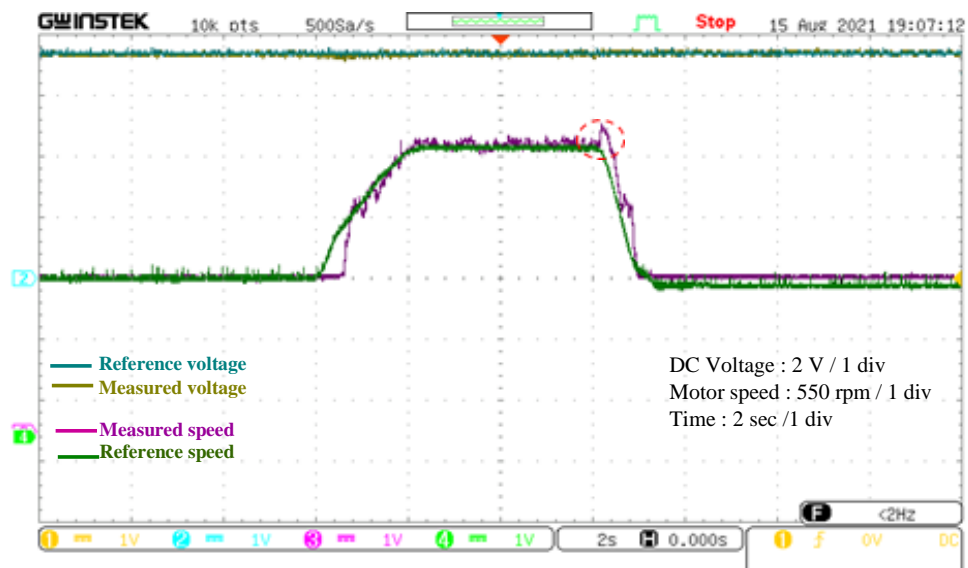


FIGURE 4.36: Motor speed regulation and voltage responses.

General conclusion and perspectives

The Final chapter of this thesis presents the general conclusion including the goal of work, contributions and limitation of this study. Along with the future trends in both academic and economic sectors in electric vehicle field, and to enclose the thesis personal perspectives are mentioned.

GENERAL CONCLUSION

Goal of Work

The electric vehicle is frequently regarded as a future technology that has the potential to end the problematic pollution of the atmosphere caused by the road transport sector by "cutting greenhouse gas emissions, improving air quality," but this is not the case. This failure is primarily due to competition from a well-established technology: the internal combustion engine, which has benefited from economies of scale, lower fuel costs, and government subsidies. After several readings, I became aware of the real gravity of the pollution caused by vehicles. I doubt that the electric car will make a significant contribution to solving the pollution problems facing our planet. The emissions of toxic gases occupy only a derisory place in the pollution in general and the real problems are in the production of electricity by polluting power plants. Solar or wind power plants seem to be a very promising future solution and I think that an evolution of the exploitation of these types of renewable energies in electricity production could bring real progress. Electric vehicles can be considered as much more than merely a pollution-reduction measure. Imagine a silent, light, fast and perfectly clean vehicle, as would be the transition from the combustion engine car to the electric car. My research has led me to conclude that the electric car can consciously become a replacement for the current cars. It is obvious that there is still a long way to go, the time and capacity of battery charging will play a very important role and practical aspects such as heating or defrosting will have to be solved efficiently. Besides, I remain optimistic and I think that other solutions such as bio-fuel, ethanol or hybrid cars are only transitory and have no real interest. I remain optimistic about the electric vehicles in Algerian roads according to the president's confirmation that energy transition is indeed the goal for the next five years.

The Goal of this thesis is to develop a control strategy in order to extend the limited driving range of an electric vehicle, which is primarily due to the use of the battery alone as an energy storage device. The Study of multiple power converters is also targeted in this work as a means to see their effect on the electric car's performances.

Used approach

In This work, a detailed dynamic model of an electric vehicle linked to a powertrain composed of PMDC motor along with a four-quadrant DC-DC converter associated with a DC-DC buck-boost converter. In this model, the motor was controlled with a conventional PI controller based control has the disadvantage of increasing peak overshoot, settling time, steady state error, and speed and torque variations with load step change and response time. In order to improve the performance of the drive system, another technique is introduced based on genetic algorithms (GA). The later uses artificial intelligence in order to calculate the optimal controller gains. The comparison between the two control techniques had led to the fact that genetic algorithms based PI controller improves the performances of speed response to the reference and showed the effectiveness of this approach compared to the classical control. This traction chain was later on modeled and implemented using only the PI controller, which is due to the lack of the necessary hardware.

Another power converter was studied in this thesis, which is the Z-source converter. The later was integrated in a traction system composed of a Fuel cell, battery, DC-DC converters and a PMSM controlled by a vector control that allows to have a torque proportional to the stator current. This leads to a direct control of the torque as in the case of a DC machine. The study of the control showed that the results are satisfactory and the coupling is perfect. The control of the machine by the intermediary of the current allowed to improve its tracking dynamics and an effective taking into account of the disturbances. The interest of such a control strategy is that it provides a partially simple control algorithm that can be integrated into a microprocessor where the only quantity measured by the sensors is the position.

Using multiple energy storage system in this model is a method to enhance the power quality and prolong the driving mileage and test the efficiency of the EV storage system. Thus, an efficient energy management strategy was used in order to guarantee the optimal power flow in the electric vehicle components in all the possible driving modes (High power generation, medium power generation , low power generation, braking and stop).

Contribution

In spite of all the limitations of our research, which we have attributed to the conditions in which we have worked, we believe that we have nevertheless contributed to introduce some novelties that we can summarize in the following points:

- The management of the battery and fuel cell power supply is applied to ensure a good operation of the system, especially the speed of the electric vehicle under different conditions and constraints.
- The curves and analysis of the performance characteristics were plotted by the proposed schemes and a detailed performance comparison was made between the advanced illustrations using the simulation results of the conventional PI and the Genetic algorithms based PI controller of the PMDC motor drive. The performance comparison shows that the proposed control GA
- The GA based controller provides better performance compared to the conventional PI controller. It reduces and minimizes the high torque ripple produced and appears in the electromagnetic torque.
- The energy management is carried out in relation to the estimated power in the vehicle and the power available in the two energy sources, namely the fuel cell and the energy storage system (battery). The expected electrical energy is correctly distributed through the components of this power supply stage, in order to guarantee the necessary power to the permanent magnet synchronous machine for the vehicle traction.

- After the practical realization of the conversion chain of the EV, some deductions have been made as follows: The battery provides a continuous voltage for a long period of time in case of degradation of battery performance. The studied system can be adapted to medium or high power. The effects of the DC voltage control by boost ensure it regardless of the battery behavior failures (voltage drop).
- Integrating new vehicle architectures that include the battery electric, fuel cell electric, and hybrid vehicles. Generally, hybrid vehicles are considered more fuel-efficient because the drive train allows us to recover kinetic energy when braking. Moreover, due to the presence of a second power source, the engine can be turned off or shifted to a more efficient operating point. With electric vehicles, the source of energy is flexible; any energy source can be used to generate the required electricity.
- Using advanced power electronics, namely the Z-source three level inverter, the four-quadrant DC-DC converter, the bidirectional buck-boost converter along with other converters in an effort to upgrade the traction system of the electric vehicle.
- Energy recovery from the regenerative braking, allowing the bidirectional power flow from the motor to the storage systems and the other way around.
- Advanced control methods used to control the traction system with the aim of achieving the reference speed in an optimum time.
- Implementation of a DC-DC 4-quadrant chopper associated with a buck-boost DC-DC converter in a PMDC motor based traction system. Note that the microcontroller (Arduino UNO board) used in these assemblies has advantages which are: moderate price, easy control program, inherent PWM signals (prerequisite) and not bulky and constraints which are: limited memory and can not support a high frequency and high power. It remains to be known that some signals emitted during the experimentation were disharmonious coming from the probes of the oscilloscope.

Limitations of this work

As with other study initiatives, various limitations were encountered during this work that prevented us from going further on this subject, such as:

- Electric vehicles do not exist in the Algerian roads, there was no prospect of visiting other countries due to time and economic constraints.
- Due to the lack of components, the experimental implementations did not meet with our expectation. Thus, we settled with a low budget prototype of an electric vehicle.
- Due to time constraints, our project's application of our realization on a genuine EV could not take place.
- Due to financial constraints, some converter topologies and management algorithms could not be investigated.

PERSPECTIVES AND FUTURE WORK

Future Trends and Technologies

- *Electric Motors & Power Electronics:*
The EV market has adopted several different motor design solutions in an effort to improve efficiency, including permanent magnet, induction, and wound rotor motors. The main emerging

motor technologies are axial flux motors and in-wheel motors. Axial flux motors use more magnetic material, making them more efficient and power dense, improving drive cycle efficiency through weight reduction. Similarly, if wheel-integrated motors require more motors per vehicle (one for each wheel), this allows for greater optimization. This also improves drive cycle efficiency. Major breakthroughs are being made in the field of automobile power electronics (inverters, on-board chargers, DC-DC converters) to enhance powertrain efficiency, which either reduces battery capacity or increases range. The move to silicon carbide MOSFETs and high-voltage (800 V or higher) vehicle platforms is one of the primary avenues for improving efficiency. Indeed, Renault, BYD, GM, Hyundai, and other automakers have indicated that their 800V vehicle platforms will use silicon carbide MOSFETs in their power electronics until 2025.

- *Battery trends:*

Solid-state batteries could be the next big thing in electric vehicles. Solid-state batteries, predictably, do not contain liquid and are less likely to catch fire. They can also carry up to three times as much energy as conventional EV batteries and function better in harsh settings. The issue is that these batteries are not yet mass-produced. Although NASA and certain automakers are working on solid-state batteries for automobiles, they will not be ready by 2023. When considering various next-generation battery technologies, a similar long-term time frame is useful. Batteries in future electric vehicles could become part of the vehicle structure, making them lighter while still providing a long range. Batteries with new chemistry, such as those that use a silicon anode or silicon produced from sand, could also see substantial changes by the end of the decade.

- *Expanding charging infrastructure:*

Governments and private businesses are developing their charging infrastructure. Luxury manufacturers are investing in networks that offer incentives to their vehicle owners, such as priority scheduling for charging reservations or connectors that only function with their own EVs. Furthermore, network providers that operate charging stations are constantly announcing expansions and new installations. Some of the places targeted by network operators for increased EV charging infrastructure in 2023.

- *Nuclear fusion energy breakthrough:*

In the longer term, the transition of our transportation to electric power opens up possibilities that were previously unthinkable. Nuclear fusion has yet to be proven as a viable technology. Nevertheless, the Department of the Environment announced in late 2022 that scientists had, for the first time, extracted more energy from the fusion process than they had injected. When we are finally able to use fusion to power the grid, our cars will be prepared for this potentially infinite energy source.

Research Trends in the EV Field

- *Green Hydrogen Production (Electrolyzer markets 2023-2033):*

Global hydrogen consumption is expected to grow through existing markets, such as refining and ammonia production, and new markets, such as methanol, green steel and transportation. In the later, hydrogen fuel cell electric vehicles (FCEVs) create power via a chemical reaction between hydrogen and oxygen in a fuel cell stack rather than extracting power from a battery. Apart from water, it is a procedure that produces no emissions. It takes less than five minutes to refuel the hydrogen tank with a pump. Once on the road, an FCEV provides a zero-emission travel that is just as safe, convenient, and pleasurable as any other car. The increase in hydrogen production and use is driven by the growing need to improve energy security and by decarbonization efforts.

- *Solid-State and Polymer batteries (2023-2033):*

Conventional lithium-ion batteries based on graphite anodes, layered oxide cathodes (LCO, NMC,

NCA) and liquid electrolyte have been adopted ubiquitously in our daily lives, from small consumer electronics to large electric vehicles and stationary energy storage systems. The demand for decarbonization has triggered electrification, leading to rapid growth in the electric vehicle market, which has spurred the development, manufacture and sale of batteries, especially lithium-ion batteries. Since their commercialization in 1991, lithium-ion batteries have held a dominant position in the battery market in various applications. Meanwhile, due to their limited performance, environmental considerations and supply chain constraints, new generation battery technologies are being researched, developed and commercialized. Among them, solid-state batteries have attracted the most attention from research institutes, materials suppliers, battery vendors, component suppliers, automotive OEMs, venture capitalists and investors. Popular discussions about solid-state batteries have sparked efforts in both academia and industry. A growing number of players are working in this area and some milestones have been reached.

- *Micro EVs (2023-2043):*

Microcars are intended for short travels of a few kilometers in length and travel at moderate speeds, often less than 80 kilometers per hour (with various regional exceptions). These tiny cars are inexpensive and developed for an urban context, providing greater space, power, and protection than two- or three-wheeled vehicles. The majority of car excursions are for one person. The majority of the energy is spent in supporting the vehicle's weight. Oversized vehicles are the principal source of urban congestion, pollution, and energy, material, and public space waste. As cities throughout the world transition to a high-density, low-speed, low-impact model, there is a demand for a new form of personal car that allows people to get around in a comfortable manner - this is where electric vehicles come in.

- *Thermal management for electric cars (2023-2033):*

Thermal management is still an important consideration in electric vehicle (EV) design. Early market trends were dominated by the introduction of active cooling for battery packs, which is now the industry standard. EV batteries, motors, and power electronics, on the other hand, continue to evolve, with the development of cell-to-block designs, direct oil-cooled motors, and silicon carbide power electronics, to name a few key trends that will impact the thermal management strategies of key EV powertrain components. Opportunities for materials makers, component suppliers, vehicle designers, and others in the fast increasing EV industry emerge as the thermal management business evolves.

Personal Perspectives

In perspective, this work can be continued and completed in order to improve the optimal functioning of a real prototype of an electric vehicle and this, by studying the following points:

- Practical study of energy management in an electric vehicle using different energy sources such as : a battery, a fuel cell and supercapacitors.
- Introduction of new structures of multilevel static converters such as the T-type converter and the multicellular converter. These converters can be equipped with intelligent control laws.
- Use of deep learning methods for the power management of the electric vehicle
- Integration of Hydrogen power generation system in the electric car.
- The approach proposed in this thesis can be adopted to a medium and high power experimental configuration by using easily platforms equipped with FPGA, DSP or Dspace boards.

Appendix A

The tables below show the different characteristics of the motor (MSAP,MI), battery and CAP.

Components	Rating values
PMSM parameters	
Power rating	57 kW
Stator resistance	$R_s = 0.0083\Omega$
frequency	$f = 50\text{Hz}$
Inductance	$L_d = 0.1741\text{mH}, L_q = 2.92\text{mH}$
Magnet induced flux	$\psi_f = 0.0711151\text{Wb}$
Number of pole pairs	$P = 4$
Asynchronous Motor Parameter Induction	
Power rating 38kW Stator resistance	$R_s = 0.01965\Omega$
Rotor resistance	$R_r = 0.01909\Omega$
Stator/rotor inductance	$L_s = L_r = 0.0397\text{H}$
Mutual inductance	$L_m = 1.354\text{H}$
Moment of inertia	$J = 0.09526\text{Kg} \cdot \text{m}^2$
Viscous friction	$f = 0.05479\text{N} \cdot \text{m}/\text{rad}/\text{sec}$
Number of pole pairs	$p = 2$

TABLE A.1: PMSM and IM parameters

Components	Rating values
Rated voltage	$V = 288\text{V}$
Capacity	$C_n = 678.260\text{Ah}$
Internal resistance	$R = 0.00384\Omega$

TABLE A.2: Battery parameters

Appendix B

Microcontroller	ATmega328
Clock Speed	16 MHz
Operating Voltage	5 V
Input Voltage (recommended)	7-12 V
Input Voltage (limits)	6 – 20V
Digital I/O pins	14 (6 provide PWM output)
Analog Input pins	6
DC current per I/O pin	40 mA
DC current for 3.3V pin	50 mA
Flash Memory	32 Kbits (0.5 Kbits used by bootloader)
SRAM	2 Kbits
EEPROM	1 Kbit

TABLE B.1: Parameters of the components used in the simulation

Appendix

C

- Data from the 4N25 optocoupler is available on the website.
<https://pdf1.alldatasheet.com/datasheet-pdf/view/2846/MOTOROLA/4N25.html>
accessed on 25/02/2023
- Data from the MOSFET Driver IR2112 is available on the website
<https://www.alldatasheet.com/datasheet-pdf/pdf/730334/IRF/IR2112.html>
accessed on 25/02/2023

Appendix D

Components	Rating values
Speed sensor (tachometer) parameters	
Rated power	68.7W
Voltage	(6, 12, 24)V
Rated speed	(30000, 6000, 14000) rpm
Rated current	0.8563A
Resistance, and inductance of rotor	$R_a = 0.8, L_a = 0.002H$
Battery parameters	
Voltage	12V
Capacity	6Ah
Static converter	
Capacitor	22 μ F, 32 μ F, 150nF and 3300 μ F
Inductance	$L = 3.6mH, r = 1.2\Omega$
Resistor	1k Ω
Potentiometer	10k Ω
MOSFET	IRFP460
Diode	IN41
Optocoupler	4N25
MOSFET Driver	IR2112

TABLE D.1: Parameters of the components used in the experimental part

Bibliography

- [1] A. Rabah, "Contribution à la modélisation et la commande d'un véhicule électrique hybride à architecture série/parallèle (étude théorique et expérimentale)," Ph.D. dissertation, Université Ibn Khaldoun-Tiaret-, 2020.
- [2] A. Daanoune, "Contribution à l'étude et à l'optimisation d'une machine synchrone à double excitation pour véhicules hybrides," Ph.D. dissertation, Université de Grenoble, 2012.
- [3] Z. Wu, "Conception optimale d'un entraînement électrique pour la chaîne de traction d'un véhicule hybride électrique: Co-conception des machines électriques, des convertisseurs de puissance et du réducteur planétaire," Ph.D. dissertation, Université de Franche-Comté, 2012.
- [4] K. Okba, "Control and energy management of an electrical vehicle," Ph.D. dissertation, 2015.
- [5] S. Akhegaonkar, "Development of a safe and efficient driving assistance system for electric vehicles," Ph.D. dissertation, Université Paris-Saclay (ComUE), 2015.
- [6] J. Aizarani. "Statista." (2023), [Online]. Available: <https://www.statista.com/statistics/262858/change-in-opec-crude-oil-prices-since-1960/>.
- [7] J. Aizarani. "Statista." (2023), [Online]. Available: <https://www.statista.com/statistics/265192/oil-production-in-algeria-in-barrels-per-day/>.
- [8] A. Ravey, "Conception et gestion de l'énergie des architectures pour véhicules hybrides électriques," Ph.D. dissertation, Belfort-Montbéliard, 2012.
- [9] H. Ritchie, M. Roser, and P. Rosado, "Co2 and greenhouse gas emissions," *Our World in Data*, 2020, <https://ourworldindata.org/co2-and-greenhouse-gas-emissions>.
- [10] A. quality in Algiers. "Iqair." (2023), [Online]. Available: <https://www.iqair.com/algeria/algiers>.
- [11] C. watch. "World bank data." (2023), [Online]. Available: <https://data.worldbank.org/indicator/EN.ATM.CO2E.KT?locations=DZ>.
- [12] L. D. Perlmutter and K. R. Cromar, "Comparing associations of respiratory risk for the epa air quality index and health-based air quality indices," *Atmospheric Environment*, vol. 202, pp. 1–7, 2019.
- [13] C. considers manufacturing of made-in-Algeria electric car. "Algeria press service." (2021), [Online]. Available: <https://www.aps.dz/en/economy/40126-cnese-considers-manufacturing-of-made-in-algeria-electric-car>.
- [14] a. o. t. g. o. o. t. d. o. h. The electric car. "Algeria press service." (2021), [Online]. Available: <https://www.aps.dz/economie/117341-la-voiture-electrique-une-option-pour-sortir-de-la-dependance-aux-hydrocarbures>.
- [15] C. C. Chan, "The state of the art of electric and hybrid vehicles," *Proceedings of the IEEE*, vol. 90, no. 2, pp. 247–275, 2002.
- [16] L. C. Rosario, "Power and energy management of multiple energy storage systems in electric vehicles," 2007.

- [17] F. Un-Noor, S. Padmanaban, L. Mihet-Popa, M. N. Mollah, and E. Hossain, "A comprehensive study of key electric vehicle (ev) components, technologies, challenges, impacts, and future direction of development," *Energies*, vol. 10, no. 8, p. 1217, 2017.
- [18] J. A. Sanguesa, V. Torres-Sanz, P. Garrido, F. J. Martinez, and J. M. Marquez-Barja, "A review on electric vehicles: Technologies and challenges," *Smart Cities*, vol. 4, no. 1, pp. 372–404, 2021.
- [19] R. R. Kumar and K. Alok, "Adoption of electric vehicle: A literature review and prospects for sustainability," *Journal of Cleaner Production*, vol. 253, p. 119911, 2020.
- [20] A. König, L. Nicoletti, D. Schröder, S. Wolff, A. Waclaw, and M. Lienkamp, "An overview of parameter and cost for battery electric vehicles," *World Electric Vehicle Journal*, vol. 12, no. 1, p. 21, 2021.
- [21] C. Liu, K. Chau, C. H. Lee, and Z. Song, "A critical review of advanced electric machines and control strategies for electric vehicles," *Proceedings of the IEEE*, vol. 109, no. 6, pp. 1004–1028, 2020.
- [22] S. S. Acharige, M. E. Haque, M. T. Arif, and N. Hosseinzadeh, "Review of electric vehicle charging technologies, configurations, and architectures," *arXiv preprint arXiv:2209.15242*, 2022.
- [23] SCOPUS. "Publications related to electric vehicles." (2023), [Online]. Available: <https://www.scopus.com/term/analyzer.uri?sid=c1a8ed3371f53a1461693e04bbbd3e44&origin=resultslist&src=s&s=TITLE-ABS-KEY%28electric+vehicle%29&sort=plf-f&sdt=b&sot=b&sl=31&count=141716&analyzeResults=Analyze+results&txGid=3454f2c98e6043b8fc52a912684f8299#compareJournal>.
- [24] Y. Zhang, Z. Chen, P. Li, H. Liu, Z. Zhou, and L. Yang, "Radiation influence model of electric vehicle charging station," in *2020 IEEE 4th Conference on Energy Internet and Energy System Integration (EI2)*, IEEE, 2020, pp. 914–917.
- [25] M. Alsayegh, B. Schmuelling, and M. Clemens, "Control signaling in wireless power transfer for electric vehicles through ultra-wideband," in *2019 Fourteenth International Conference on Ecological Vehicles and Renewable Energies (EVER)*, IEEE, 2019, pp. 1–5.
- [26] B. Haidar, "A techno-economic analysis of the electric vehicle transition: Policy, infrastructure, usage, and design," Ph.D. dissertation, Université Paris-Saclay, 2021.
- [27] O. M. F. Camacho, P. B. Nørgård, N. Rao, and L. Mihet-Popa, "Electrical vehicle batteries testing in a distribution network using sustainable energy," *IEEE Transactions on Smart Grid*, vol. 5, no. 2, pp. 1033–1042, 2014.
- [28] J. Deng, C. Bae, A. Denlinger, and T. Miller, "Electric vehicles batteries: Requirements and challenges," *Joule*, vol. 4, no. 3, pp. 511–515, 2020.
- [29] C. C. Chan, "The state of the art of electric and hybrid vehicles," *Proceedings of the IEEE*, vol. 90, no. 2, pp. 247–275, 2002.
- [30] E. A. Grunditz and T. Thiringer, "Performance analysis of current bevs based on a comprehensive review of specifications," *IEEE Transactions on Transportation Electrification*, vol. 2, no. 3, pp. 270–289, 2016.
- [31] J. Deng, C. Bae, A. Denlinger, and T. Miller, "Electric vehicles batteries: Requirements and challenges," *Joule*, vol. 4, no. 3, pp. 511–515, 2020, ISSN: 2542-4351. DOI: <https://doi.org/10.1016/j.joule.2020.01.013>. [Online]. Available: <https://www.sciencedirect.com/science/article/pii/S254243512030043X>.
- [32] M. Yilmaz and P. T. Krein, "Review of battery charger topologies, charging power levels, and infrastructure for plug-in electric and hybrid vehicles," *IEEE transactions on Power Electronics*, vol. 28, no. 5, pp. 2151–2169, 2012.
- [33] W. the Automotive Future Will be Dominated by Fuel Cells. "Ieee spectrum." (2023), [Online]. Available: <http://spectrum.ieee.org/green-tech/fuel-cells/why-the-automotive-future-will-be-dominated-by-fuel-cells>.
- [34] R. Rose, "Questions and answers about hydrogen and fuel cells," *US Dept. Energy*, 2005.
- [35] C. Thomas, "Fuel cell and battery electric vehicles compared," *international journal of hydrogen energy*, vol. 34, no. 15, pp. 6005–6020, 2009.

- [36] K. Rajashekara, "Present status and future trends in electric vehicle propulsion technologies," *IEEE journal of emerging and selected topics in power electronics*, vol. 1, no. 1, pp. 3–10, 2013.
- [37] R. Á. Silva, F. J. Pujatti, and I. A. Pires, "Nine-phase im for hybridisation of a compact vehicle by parallel ttr architecture," *IET Electric Power Applications*, vol. 12, no. 8, pp. 1134–1141, 2018.
- [38] M. Ehsani, Y. Gao, and J. M. Miller, "Hybrid electric vehicles: Architecture and motor drives," *Proceedings of the IEEE*, vol. 95, no. 4, pp. 719–728, 2007.
- [39] S. Sharma, A. K. Panwar, and M. Tripathi, "Storage technologies for electric vehicles," *Journal of traffic and transportation engineering (english edition)*, vol. 7, no. 3, pp. 340–361, 2020.
- [40] X. Sun, Z. Li, X. Wang, and C. Li, "Technology development of electric vehicles: A review," *Energies*, vol. 13, no. 1, p. 90, 2019.
- [41] Z. Li, A. Khajepour, and J. Song, "A comprehensive review of the key technologies for pure electric vehicles," *Energy*, vol. 182, pp. 824–839, 2019.
- [42] A. König, L. Nicoletti, D. Schröder, S. Wolff, A. Waclaw, and M. Lienkamp, "An overview of parameter and cost for battery electric vehicles," *World Electric Vehicle Journal*, vol. 12, no. 1, p. 21, 2021.
- [43] M. Iqbal, "Design and control of hybrid electric vehicle for efficient urban use.," Ph.D. dissertation, Université Bourgogne Franche-Comté, 2022.
- [44] M Kalantar *et al.*, "Dynamic behavior of a stand-alone hybrid power generation system of wind turbine, microturbine, solar array and battery storage," *Applied energy*, vol. 87, no. 10, pp. 3051–3064, 2010.
- [45] A. Louwen, W. G. Van Sark, A. P. Faaij, and R. E. Schropp, "Re-assessment of net energy production and greenhouse gas emissions avoidance after 40 years of photovoltaics development," *Nature Communications*, vol. 7, no. 1, p. 13 728, 2016.
- [46] L. Qi, X. Wu, X. Zeng, *et al.*, "An electro-mechanical braking energy recovery system based on coil springs for energy saving applications in electric vehicles," *Energy*, vol. 200, p. 117 472, 2020.
- [47] Z. Li, A. Khajepour, and J. Song, "A comprehensive review of the key technologies for pure electric vehicles," *Energy*, vol. 182, pp. 824–839, 2019.
- [48] V Krithika and C Subramani, "A comprehensive review on choice of hybrid vehicles and power converters, control strategies for hybrid electric vehicles," *International journal of energy research*, vol. 42, no. 5, pp. 1789–1812, 2018.
- [49] F. Mumtaz, N. Z. Yahaya, S. T. Meraj, B. Singh, R. Kannan, and O. Ibrahim, "Review on non-isolated dc-dc converters and their control techniques for renewable energy applications," *Ain Shams Engineering Journal*, vol. 12, no. 4, pp. 3747–3763, 2021.
- [50] M. Ehsani, K. V. Singh, H. O. Bansal, and R. T. Mehrjardi, "State of the art and trends in electric and hybrid electric vehicles," *Proceedings of the IEEE*, vol. 109, no. 6, pp. 967–984, 2021.
- [51] A. Janabi and B. Wang, "Switched-capacitor voltage boost converter for electric and hybrid electric vehicle drives," *IEEE Transactions on Power Electronics*, vol. 35, no. 6, pp. 5615–5624, 2019.
- [52] N Vázquez, H López, C Hernández, E Rodríguez, R Orosco, and J Arau, "A grid connected current source inverter.," in *2009 International Conference on Clean Electrical Power*, IEEE, 2009, pp. 439–442.
- [53] H. P. Vemuganti, D. Sreenivasarao, S. K. Ganjikunta, H. M. Suryawanshi, and H. Abu-Rub, "A survey on reduced switch count multilevel inverters," *IEEE Open Journal of the Industrial Electronics Society*, vol. 2, pp. 80–111, 2021.
- [54] N. Patel, A. K. Bhoi, S. Padmanaban, and J. B. Holm-Nielsen, *Electric vehicles: modern technologies and trends*. Springer, 2021.
- [55] J. R. García-Sánchez, E. Hernández-Márquez, J. Ramírez-Morales, *et al.*, "A robust differential flatness-based tracking control for the "mimo dc/dc boost converter–inverter–dc motor" system: Experimental results," *IEEE Access*, vol. 7, pp. 84 497–84 505, 2019.
- [56] S. Moussavi, M Alasvandi, and S. Javadi, "Speed control of permanent magnet dc motor by using combination of adaptive controller and fuzzy controller," *International Journal of Computer Applications*, vol. 52, no. 20, 2012.

- [57] S. M. Arif, T. T. Lie, B. C. Seet, S. Ayyadi, and K. Jensen, "Review of electric vehicle technologies, charging methods, standards and optimization techniques," *Electronics*, vol. 10, no. 16, p. 1910, 2021.
- [58] S Bouradi, K Negadi, R Araria, B Boumediene, and M Koulali, "Design and implementation of a four-quadrant dc-dc converter based adaptive fuzzy control for electric vehicle application.," *Mathematical Modelling of Engineering Problems*, vol. 9, no. 3, pp. 721–730, 2022.
- [59] S Bouradi, R Araria, K Negadi, and F Marignetti, "Nonlinear control of permanent magnet synchronous motor for high performances electric vehicle," *TECNICA ITALIANA-Italian Journal of Engineering Science*, pp. 317–324, 2020.
- [60] R. Araria, A. Berkani, K. Negadi, F. Marignetti, M. Boudiaf, *et al.*, "Performance analysis of dc-dc converter and dtc based fuzzy logic control for power management in electric vehicle application," *Journal Européen des Systèmes Automatisés*, vol. 53, no. 1, pp. 1–9, 2020.
- [61] T. A. T. Mohd, M. K. Hassan, and W. A. Aziz, "Mathematical modeling and simulation of an electric vehicle," *Journal of Mechanical Engineering and Sciences*, vol. 8, pp. 1312–1321, 2015.
- [62] S Lekshmi and L. P. PS, "Mathematical modeling of electric vehicles-a survey," *Control Engineering Practice*, vol. 92, p. 104 138, 2019.
- [63] E. Schaltz and S. Soylu, "Electrical vehicle design and modeling," *Electric vehicles-modelling and simulations*, vol. 1, pp. 1–24, 2011.
- [64] J. C. Amphlett, R. M. Baumert, R. F. Mann, B. A. Peppley, P. R. Roberge, and T. J. Harris, "Performance modeling of the ballard mark iv solid polymer electrolyte fuel cell: I. mechanistic model development," *Journal of the Electrochemical Society*, vol. 142, no. 1, p. 1, 1995.
- [65] T. Zhou and B. Francois, "Modeling and control design of hydrogen production process for an active hydrogen/wind hybrid power system," *International journal of hydrogen energy*, vol. 34, no. 1, pp. 21–30, 2009.
- [66] A. A. Elbaset, "Design, modeling and control strategy of pv /fc hybrid power system," *J. Electrical Systems*, vol. 7, no. 2, pp. 270–286, 2011.
- [67] P. Thounthong, A. Luksanasakul, P. Koseeyaporn, and B. Davat, "Intelligent model-based control of a standalone photovoltaic/fuel cell power plant with supercapacitor energy storage," *IEEE Transactions on Sustainable Energy*, vol. 4, no. 1, pp. 240–249, 2012.
- [68] Z Mokrani, D Rekioua, N Mebarki, T Rekioua, and S Bacha, "Proposed energy management strategy in electric vehicle for recovering power excess produced by fuel cells," *International Journal of Hydrogen Energy*, vol. 42, no. 30, pp. 19 556–19 575, 2017.
- [69] P. Sharma and T. Bhatti, "A review on electrochemical double-layer capacitors," *Energy conversion and management*, vol. 51, no. 12, pp. 2901–2912, 2010.
- [70] T. Zhou, "Control and energy management of a hybrid active wing generator including energy storage system with super-capacitors and hydrogen technologies for microgrid application," Ph.D. dissertation, Ecole Centrale de Lille, 2009.
- [71] B. BOUMEDIENE, "Commande non linéaire d'un système hybride éolien-photovoltaïque à base de nouvelles structures en électronique de puissance," Ph.D. dissertation, Université Ibn Khaldoun-Tiaret-, 2022.
- [72] Q. Fei, Y. Deng, H. Li, J. Liu, and M. Shao, "Speed ripple minimization of permanent magnet synchronous motor based on model predictive and iterative learning controls," *IEEE Access*, vol. 7, pp. 31 791–31 800, 2019. DOI: [10.1109/ACCESS.2019.2902888](https://doi.org/10.1109/ACCESS.2019.2902888).
- [73] R. Araria, K. Negadi, F. Marignetti, *et al.*, "Design and analysis of the speed and torque control of im with dtc based ann strategy for electric vehicle application," *TECNICA ITALIANA*, vol. 63, no. 2-4, pp. 181–188, 2019.
- [74] L. Chen, H. Xu, X. Sun, and Y. Cai, "Three-vector-based model predictive torque control for a permanent magnet synchronous motor of evs," *IEEE Transactions on Transportation Electrification*, vol. 7, no. 3, pp. 1454–1465, 2021. DOI: [10.1109/TTE.2021.3053256](https://doi.org/10.1109/TTE.2021.3053256).

- [75] S. G. Petkar, K. Eshwar, and V. K. Thippiripati, "A modified model predictive current control of permanent magnet synchronous motor drive," *IEEE Transactions on Industrial Electronics*, vol. 68, no. 2, pp. 1025–1034, 2021. DOI: [10.1109/TIE.2020.2970671](https://doi.org/10.1109/TIE.2020.2970671).
- [76] J. Singh, B. Singh, S. P. Singh, and M. Naim, "Investigation of performance parameters of pmsm drives using dtc-svpwm technique," in *2012 Students Conference on Engineering and Systems, 2012*, pp. 1–6. DOI: [10.1109/SCES.2012.6199092](https://doi.org/10.1109/SCES.2012.6199092).
- [77] Y. Wang, D. Gao, D. Tannir, *et al.*, "Multiharmonic small-signal modeling of low-power pwm dc-dc converters," *ACM Transactions on Design Automation of Electronic Systems (TODAES)*, vol. 22, no. 4, pp. 1–16, 2017.
- [78] J. Liu, J. Yang, J. Zhang, Z. Nan, and Q. Zheng, "Voltage balance control based on dual active bridge dc/dc converters in a power electronic traction transformer," *IEEE Transactions on Power Electronics*, vol. 33, no. 2, pp. 1696–1714, 2017.
- [79] F. Wu, S. Fan, X. Li, and S. Luo, "Bidirectional buck-boost current-fed isolated dc-dc converter and its modulation," *IEEE Transactions on Power Electronics*, vol. 35, no. 5, pp. 5506–5516, 2019.
- [80] R. H. Tan and L. Y. Hoo, "Dc-dc converter modeling and simulation using state space approach," in *2015 IEEE Conference on Energy Conversion (CENCON)*, IEEE, 2015, pp. 42–47.
- [81] M.-T. Latreche, "Commande floue de la machine synchrone à aimant permanent (msap) utilisée dans un système éolien," Ph.D. dissertation, Université Ferhat Abbas-Setif, 2018.
- [82] M. LOUCIF, "Synthèse de lois de commande non-linéaires pour le contrôle d'une machine asynchrone à double alimentation dédiée à un système aérogénérateur," Ph.D. dissertation, Université Aboubakr Belkaid-Tlemcen, 2016.
- [83] P. C. Loh and F. Blaabjerg, "Magnetically coupled impedance-source inverters," *IEEE Transactions on Industry Applications*, vol. 49, no. 5, pp. 2177–2187, 2013.
- [84] S. kumar Vishwakarma and M. Rahman, "Speed control of pv array-based z-source inverter fed brushless dc motor using dynamic duty cycle control," in *2022 2nd International Conference on Emerging Frontiers in Electrical and Electronic Technologies (ICEFEET)*, IEEE, 2022, pp. 1–6.
- [85] P. C. Loh, D. M. Vilathgamuwa, Y. S. Lai, G. T. Chua, and Y. Li, "Pulse-width modulation of z-source inverters," in *Conference Record of the 2004 IEEE Industry Applications Conference, 2004. 39th IAS Annual Meeting.*, IEEE, vol. 1, 2004.
- [86] F. Z. Peng, "Z-source inverter," *IEEE Transactions on Industry Applications*, vol. 39, no. 2, pp. 504–510, 2003. DOI: [10.1109/TIA.2003.808920](https://doi.org/10.1109/TIA.2003.808920).
- [87] M. Bakar, N. Rahim, K. Ghazali, and A. Hanafi, "Z-source inverter pulse width modulation: A survey," in *International Conference on Electrical, Control and Computer Engineering 2011 (InECCE)*, IEEE, 2011, pp. 313–316.
- [88] M Hanif, M. Basu, and K Gaughan, "Understanding the operation of a z-source inverter for photovoltaic application with a design example," *IET Power Electronics*, vol. 4, no. 3, pp. 278–287, 2011.
- [89] M. Shen and F. Z. Peng, "Operation modes and characteristics of the z-source inverter with small inductance or low power factor," *IEEE Transactions on Industrial Electronics*, vol. 55, no. 1, pp. 89–96, 2008.
- [90] T. Matsumoto, N. Watanabe, H. Sugiura, and T. Ishikawa, "Development of fuel-cell hybrid vehicle," *SAE TRANSACTIONS*, vol. 111, no. 3, pp. 376–382, 2002.
- [91] S. Ben-Yaakov, Y. Hadad, and N. Diamantstein, "A four quadrants hf ac chopper with no dead-time," in *Twenty-First Annual IEEE Applied Power Electronics Conference and Exposition, 2006. APEC'06.*, IEEE, 2006, 5–pp.
- [92] H. K. Nunna, Y. Amanbek, B. Satuyeva, and S. Doolla, "A decentralized transactive energy trading framework for prosumers in a microgrid cluster," in *2019 IEEE PES GTD Grand International Conference and Exposition Asia (GTD Asia)*, IEEE, 2019, pp. 824–830.
- [93] J. R. García-Sánchez, E. Hernández-Márquez, J. Ramírez-Morales, *et al.*, "A robust differential flatness-based tracking control for the "mimo dc/dc boost converter-inverter-dc motor" system: Experimental results," *IEEE Access*, vol. 7, pp. 84 497–84 505, 2019.

- [94] C. S. Joice, S. Paranjothi, and V. J. S. Kumar, "Digital control strategy for four quadrant operation of three phase bldc motor with load variations," *IEEE transactions on industrial informatics*, vol. 9, no. 2, pp. 974–982, 2012.
- [95] S. Tiwari and S Rajendran, "Four quadrant operation and control of three phase bldc motor for electric vehicles," in *2019 IEEE PES GTD grand international conference and exposition Asia (GTD Asia)*, IEEE, 2019, pp. 577–582.
- [96] B. Mohamed, "Impact d'une combinaison smes-ipfc sur le comportement d'un réseau électrique multi-machines," Ph.D. dissertation, Université Ibn Khaldoun-Tiaret-, 2018.
- [97] A Rangel-Merino, J. López-Bonilla, and R. L. y Miranda, "Optimization method based on genetic algorithms," *Apeiron*, vol. 12, no. 4, pp. 393–408, 2005.
- [98] J.-K. Hao, P. Galinier, and M. Habib, "Métaheuristiques pour l'optimisation combinatoire et l'affectation sous contraintes," *Revue d'intelligence artificielle*, vol. 13, no. 2, pp. 283–324, 1999.
- [99] F. Héliodore, A. Nakib, B. Ismail, S. Ouchraa, and L. Schmitt, *Métaheuristiques pour les réseaux électriques intelligents*. ISTE Group, 2017, vol. 3.
- [100] H. Jh, "Adaptation in natural and artificial systems," *Ann Arbor*, 1975.
- [101] A. Król and G. Sierpiński, "Application of a genetic algorithm with a fuzzy objective function for optimized siting of electric vehicle charging devices in urban road networks," *IEEE Transactions on Intelligent Transportation Systems*, vol. 23, no. 7, pp. 8680–8691, 2022. DOI: [10.1109/TITS.2021.3085103](https://doi.org/10.1109/TITS.2021.3085103).
- [102] N. Benahmed, *Optimisation de réseaux de neurones pour la reconnaissance de chiffres manuscrits isolés: Sélection et pondération des primitives par algorithmes génétiques*. école de technologie supérieure, 2002.
- [103] H.-B. Yuan, W.-J. Zou, S. Jung, and Y.-B. Kim, "A real-time rule-based energy management strategy with multi-objective optimization for a fuel cell hybrid electric vehicle," *IEEE Access*, vol. 10, pp. 102 618–102 628, 2022. DOI: [10.1109/ACCESS.2022.3208365](https://doi.org/10.1109/ACCESS.2022.3208365).
- [104] M. J. Mayer, A. Szilágyi, and G. Gróf, "Environmental and economic multi-objective optimization of a household level hybrid renewable energy system by genetic algorithm," *Applied Energy*, vol. 269, p. 115 058, 2020.
- [105] H. M. El-Helw, A. Magdy, and M. I. Marei, "A hybrid maximum power point tracking technique for partially shaded photovoltaic arrays," *IEEE access*, vol. 5, pp. 11 900–11 908, 2017.
- [106] O. Cordon, F. Herrera, and P. Villar, "Generating the knowledge base of a fuzzy rule-based system by the genetic learning of the data base," *IEEE Transactions on fuzzy systems*, vol. 9, no. 4, pp. 667–674, 2001.
- [107] S. Hadji, "Optimisation de la conversion énergétique pour les systèmes à énergie photovoltaïque," Ph.D. dissertation, Université Ferhat Abbas-Setif, 2018.
- [108] A. Mirzal, S. Yoshii, and M. Furukawa, "Pid parameters optimization by using genetic algorithm," *arXiv preprint arXiv:1204.0885*, 2012.

Abstract: This thesis aims to address the limited driving range and high costs of electric vehicles by developing a control strategy to extend their autonomy, especially in the Algerian context. The study focuses on the modeling and control of an electric vehicle containing an electric motor powered by two energy sources. The primary energy source consists in the fuel cell and the secondary source comprises the battery with static power converters (chopper and two-level voltage inverter). A simulation tests have been conducted on a PMSM to test the performance of the power management strategy with the use of a Z-source inverter. Another series of simulation tests have also been carried out on a permanent magnet DC motor controlled by PI control and genetic algorithm based optimized PI control with the use of a four-quadrant DC-DC converter. The latter was then exploited on an experimental realization of a four-quadrant DC-DC along with bidirectional DC-DC buck-boost converter in the propulsion chain of an electric vehicle based on a permanent magnet DC motor powered by a battery. The obtained performances show that the proposed system leads to a better energy management of an electric vehicle and exhibits ideal control in different operating conditions, mainly in nominal operation in the presence of a load torque and even in case of battery failure. The entire system was experimentally tested using two microcontrollers and the results were comprehensively analyzed and demonstrated to be highly satisfactory.

Key words: electric vehicles, power management strategy, four-quadrant DC-DC chopper, DC-DC buck-boost converter.

ملخص: تهدف هذه الأطروحة إلى معالجة الاستقلالية المحدودة والتكاليف المرتفعة للسيارات الكهربائية من خلال تطوير استراتيجية تحكم لتوسيع نطاق استقلاليته، لا سيما في السياق الجزائري. تركز الدراسة على النمذجة والتحكم في سيارة كهربائية تحتوي على محرك كهربائي يعمل بمصدرين للطاقة. مصدر الطاقة الأساسي هو خلية الوقود والمصدر الثانوي هو البطارية التي تحتوي على اختبار أداء استراتيجية إدارة PMSM محولات طاقة ثابتة (قاطع جهد ثنائي المستوى وعاكس). تم إجراء اختبارات المحاكاة على كما تم إجراء سلسلة أخرى من اختبارات المحاكاة على محرك بمغناطيس دائم تيار مباشر يتم Z-source الطاقة باستخدام عاكس رباعي. بطارية تُظهر DC-DC يعتمد على خوارزمية جينية باستخدام محول PI وتحسينه تحكم PI التحكم فيه عن طريق التحكم في العروض التي تم الحصول عليها أن النظام المقترح يسمح بإدارة أفضل للطاقة في السيارة الكهربائية ويقدم تحكماً مثالياً في ظروف التشغيل المختلفة، خاصة في التشغيل الاسمي في ظل وجود عزم تحميل وحتى في حالة حدوث عطل. تم اختبار النظام بالكامل بشكل تجريبي باستخدام متحكمين دقيقين وتم تحليل النتائج بالتفصيل ووجدت أنها مرضية للغاية.

الكلمات المفتاحية: السيارات الكهربائية، استراتيجية إدارة الطاقة، الكلمات المفتاحية: السيارات الكهربائية، استراتيجية إدارة الطاقة ، DC-DC Boost. رباعي الأرباع ، محول DC-DC محول

Resumé : Cette thèse vise à répondre à l'autonomie limitée et aux coûts élevés des véhicules électriques en développant une stratégie de contrôle pour étendre leur autonomie, en particulier dans le contexte algérien. L'étude se concentre sur la modélisation et le contrôle d'un véhicule électrique contenant un moteur électrique alimenté par deux sources d'énergie. La source d'énergie primaire est la pile à combustible et la source secondaire est la batterie avec des convertisseurs de puissance statiques (hacheur et onduleur de tension à deux niveaux). Des tests de simulation ont été effectués sur un PMSM pour tester les performances de la stratégie de gestion de la puissance avec l'utilisation d'un onduleur à source Z. Une autre série d'essais de simulation a également été réalisée sur un moteur à courant continu à aimant permanent contrôlé par une commande PI et une commande PI optimisée basée sur un algorithme génétique avec l'utilisation d'un convertisseur CC-CD à quatre quadrants. Ce dernier a ensuite été exploité sur une réalisation expérimentale d'un convertisseur DC-DC à quatre quadrants avec un convertisseur DC-DC buck-boost bidirectionnel dans la chaîne de propulsion d'un véhicule électrique basé sur un moteur DC à aimant permanent alimenté par une batterie. Les performances obtenues montrent que le système proposé permet une meilleure gestion de l'énergie d'un véhicule électrique et présente un contrôle idéal dans différentes conditions de fonctionnement, principalement en fonctionnement nominal en présence d'un couple de charge et même en cas de défaillance de la batterie. L'ensemble du système a été testé expérimentalement à l'aide de deux microcontrôleurs et les résultats ont été analysés en détail et se sont révélés très satisfaisants.

Mots clés : véhicules électriques, stratégie de gestion de l'énergie, hacheur DC-DC à quatre quadrants, convertisseur DC-DC buck-boost.